

**SONOCHEMICAL REMEDIATION OF FRESHWATER  
SEDIMENTS CONTAMINATED WITH POLYCYCLIC AROMATIC  
HYDROCARBONS**

DISSERTATION

Presented in Partial Fulfillment of the Requirements for the Degree Doctor of Philosophy  
in the Graduate School of The Ohio State University

By

Gim-Yang Pee, B.S., M.S.

\*\*\*\*\*

The Ohio State University

2008

Dissertation Committee:

Professor Linda K. Weavers, Adviser

Professor Yu-Ping Chin

Professor John J. Lenhart

Professor Nicholas Basta

Approved by:

\_\_\_\_\_  
Adviser

Civil Engineering Graduate Program

## **ABSTRACT**

The objective of this study was to promote desorption, degradation and switching of polycyclic aromatic hydrocarbons (PAHs) to powdered activated carbon, thus decreasing the bioaccessibility of PAHs (i.e., naphthalene, phenanthrene and pyrene) in three creosote contaminated sediments (Little Scioto, Ohio (LS); Gary, Indiana (GI) and Eagle Harbor, Washington (EH)) using sonication.

Firstly, the ability of sonication to degrade these PAHs (naphthalene, phenanthrene and pyrene) in aqueous solution was investigated. Pyrene had the fastest sonolytic degradation rate compared to naphthalene and phenanthrene, a trend opposite to Henry's law and diffusion coefficients for these three compounds. Based on the degradation trend, pyrene appeared to accumulate to a greater extent at the gas/solution interface of the cavitation bubbles compared to naphthalene and phenanthrene. Once on the interface, pyrene reacts more efficiently with OH radicals compared to reactions in bulk solution, which is dependent on the diffusion of OH radicals from cavitation bubbles to bulk solution. Decreased formation of hydroxyterephthalate, a measure of bulk solution OH radical, during sonolysis in the presence of pyrene but not in the presence of naphthalene or phenanthrene was consistent with pyrene accumulation on cavitation bubble interfaces. In addition, increased bulk solution temperature and naphthalene solution concentration increased the degradation rates of naphthalene. These two

operating parameters increased the amount of naphthalene diffusing into cavitation bubbles available for pyrolysis. Finally, sonolytic degradation rate constants with 0.5  $\mu\text{M}$  each of these PAHs in a mixture were lower compared to sonolysis of aqueous solutions containing these compounds individually. Naphthalene and phenanthrene, which diffused faster than pyrene, inhibited the accumulation of pyrene at the interface. Conversely, pyrene on cavitation bubble interfaces reacted with interfacial  $\bullet\text{OH}$  decreasing  $[\bullet\text{OH}]$  in bulk solution available for reaction with naphthalene and phenanthrene.

Secondly, the application of ultrasound for remediation of PAHs in freshwater sediments was examined with the aim of exploiting the ability of ultrasound to promote desorption of contaminants from sediments for sonolytic degradation and understanding the effect of sonolysis on bioaccessibility of the sediment. After 60 min sonolysis of 12.5  $\text{g L}^{-1}$  of natural sediment suspended in MilliQ water, the combined solution and sediment concentrations of naphthalene, phenanthrene and pyrene extracted were reduced by 23 %, 15 %, and 23 %, respectively. This reduction in concentration is a result of sonodegradation and/or occlusion of PAHs into the particles. Decrease in solid-liquid ratio below 12.5  $\text{g L}^{-1}$  resulted in reduction in the rate of sonodegradation and/or occlusion of the PAHs due to low particle concentration resulting in decrease particle-particle collisions and microjets formation which facilitated mass transfer of PAHs desorption. An increase in the solid-liquid ratio above 12.5  $\text{g L}^{-1}$  resulted in a decrease in the rates of sonodegradation and/or occlusion of the PAHs. This decrease was attributed

to reduced ultrasonic intensity as a result of sound attenuation in the presence of excess sediment particles and/or limitations in the solubility of PAHs.

In addition to sonodegradation, the fast desorbing fraction of pyrene, which has been related to bioaccessibility, was found to increase with sonication time of 20min followed by a plateau of a slight decrease at 120 min. Sonolysis of particles facilitated the desorption of PAHs through localized turbulent liquid movement, microjets formation and particles fragmentation, exposing new surfaces to the aqueous phase, thus decreasing the slow fraction of Phenanthrene and pyrene. This result suggested that ultrasound irradiation of natural sediment can release the PAHs on the slow desorbing sites. Although PAHs on these slow sites are less accessible, they are potential source for PAHs release and are difficult to treat using bioremediation due to limitation on their desorption rates. Thus the potential of decreasing these fractions using sonolysis is important.

Lastly, the use of powdered activated carbon (PAC) amendment and sonication was employed to reduce the bioaccessibility of PAHs in these three creosote contaminated sediments. For these three sediments, sonochemically induced switching of phenanthrene and pyrene from sediment to PAC was more effective than mechanical mixing in decreasing the fast desorbing fraction ( $F_{Fast}$ ) (i.e., % reduction in  $F_{Fast}$ ; ultrasound: EH=  $91 \pm 3$  %, GI =  $67 \pm 3$  %, and LS =  $67 \pm 3$  %, mixing: EH=  $81 \pm 3$  %, GI =  $42 \pm 3$  %, and LS =  $53 \pm 3$  %). The enhancement effect observed for sediment

treated with sonication was attributed to the facilitation of desorption of PAHs through localized turbulent liquid movement, microjets formation and particles fragmentation, exposing new surfaces to the aqueous phase.

**Dedicated to my parents and sisters,  
my husband Chee Guan,  
and my two lovely daughters Hannah and Abby**

## **ACKNOWLEDGMENTS**

First of all, I would like to express my sincere gratitude to my advisor, Dr. Linda K. Weavers, for her understanding, encouragement, and support throughout my study and research. Dr. Weavers has been instrumental in providing great ideas and guidance for my research. She has shown me qualities to be a good researcher and advisor. I would also like to thank her for all the advice and help in my career pursuit. Without her, completion of my PhD would have been impossible.

I would like to acknowledge Dr. John J. Lenhart, Dr. Yu-Ping Chin, and Dr. Nicholas T. Basta for serving as my committee in my candidate exam and final defense. I would also like to thank Dr. Harold W. Walker and Dr. Joe Z. Sostaric for their valuable comments and suggestions. This study was supported by NOAA/Ohio Sea Grant College Program and the NSF Environmental Molecular Science Institute (EMSI) at The Ohio State University.

Special thanks to Dr. Ziqi He for his flexibility and help in using freeze drying, BET surface analyses and review of my manuscript. Many thanks to former and current labmates: Mustafa Bob, Dong Chen, Jason Cheng, Liang-Hiong Chia, Dawn Deojay, Allison Burcham, Aaron Frim, Ziqi He, Yusik Hwang, Laura Jacobs, Mikko Lamminen, June Ju Lee, Ryan Mackos, Corin Marron, Eric Onderak, Daniel Petrarca, Krishnakumar Raman, Ping Sun, Mike Scullion, Panuwat Taerakul, Xueming Tang, Sindhu Tatimatla,

Vibhash Vaidya, Limei Yang, and Yaning Yang for their friendship and the wonderful time we had together in lab, office and during Group Meeting.

I would like to dedicate this work to my parents and sisters for their unconditional support and understanding. I would like to express my outmost gratitude to my sister, Gim-Nee Pee, for the time she dedicated in helping me with my children. Special thanks to my husband, Chee Guan Koh, for his love, support, encouragement and companionship. Lastly but not least, this is dedicated to my two lovely daughters, Hannah and Abby, who are my pride and joy.



## VITA

23 February, 1975 .....Born – Johor, Malaysia

June 1998 ..... B.S., Chemical Engineering  
The Ohio State University

December 2000 ..... M.S., Chemical Engineering  
The Ohio State University

March 2004 – Present ..... Graduate Research Associate,  
The Ohio State University

## PUBLICATIONS

### Research Publications

1. Weavers L. K.; Pee GY.; Frim J. A.; Yang LM.; Rathman J. F. Ultrasonic destruction of surfactants: Application to industrial wastewaters. *Water Environment Research* **2005**, 77, 259-265.
2. Pee GY.; Rathman J. F.; Weavers L.K. Effects of surface active properties on the cavitation degradation of surfactant contaminants. *Industrial & Engineering Chemistry Research* **2004**, 43, 5049-5056.

## FIELDS OF STUDY

Major Field: Civil Engineering

## TABLE OF CONTENTS

<b>ABSTRACT.....</b>	<b>Page ii</b>
<b>ACKNOWLEDGMENTS .....</b>	<b>vii</b>
<b>VITA.....</b>	<b>ix</b>
<b>LIST OF TABLES .....</b>	<b>xiii</b>
<b>LIST OF FIGURES .....</b>	<b>xiv</b>

### Chapters :

<b>INTRODUCTION AND BACKGROUND.....</b>	<b>1</b>
1.1 Introduction and source of polycyclic aromatic hydrocarbons.....	1
1.2. Traditional treatment methods .....	3
1.3. Sonochemistry: The Chemical Effects of Ultrasound .....	6
1.4. Physical/chemical properties of reactant affecting its sonochemical degradation rate in aqueous solution .....	8
1.4.a. Volatile compounds .....	8
1.4.b. Semi-volatile compounds.....	10
1.4.c. Non-volatile compounds .....	11
1.5. Ultrasound: Physical Effects.....	12
1.6. Carbon amendments.....	14
1.7. The effects of sonication on mass transfer.....	16
1.8. Partitioning of Hydrophobic organic contaminants in Sediment.....	17
1.9. Determining Bioaccessibility.....	19
1.10. Objectives and Outline of the dissertation .....	21

<b>SONOCHEMICAL DEGRADATION OF NAPHTHALENE, PHENANTHRENE AND PYRENE IN AQUEOUS SOLUTION .....</b>	<b>29</b>
2.1. Abstract .....	29
2.3. Experimental Methods .....	35
2.4. Results and Discussion .....	37
<b>SONOCHEMICAL TREATMENT OF POLYCYCLIC AROMATIC HYDROCARBON IN FRESHWATER SEDIMENTS .....</b>	<b>57</b>
3.1. Abstract .....	57
3.2. Introduction.....	58
3.3. Materials and Methods.....	61
3.4. Results and Discussion .....	66
<b>EFFECT OF ULTRASOUND ON THE BIOACCESSIBILITY OF PAHS ON SEDIMENT .....</b>	<b>91</b>
4.1. Abstract .....	91
4.2. Introduction.....	92
4.3. Materials and Methods.....	94
4.4. Result and Discussion .....	99
<b>REMEDIATION OF POLYCYCLIC AROMATIC HYDROCARBON CONTAMINATED FRESHWATER SEDIMENTS USING AN ACTIVATED CARBON AMENDMENT ENHANCED BY ULTRASOUND.....</b>	<b>120</b>
5.1. Abstract .....	120
5.2. Introduction.....	121
5.3. Experimental Methods .....	124
5.4. Results and Discussion .....	129
<b>CONCLUSION AND FUTURE WORK .....</b>	<b>145</b>

6.1. Conclusion .....	145
6.2. Future work.....	147
<b>BIBLIOGRAPHY .....</b>	<b>149</b>

## LIST OF TABLES

	Page
Table 2.1: Physical properties of NAP, PHEN and PYR. ....	48
Table 3.1: Properties: % dry weight, surface area (BET), particle diameter and concentration of PAHs of Little Scioto (LS) and Gary, Indiana (GI).....	81
Table 4. 1: Properties: % dry weight, surface area (BET), particle diameter and concentration of PAHs of Little Scioto.....	108
Table 5. 1: Properties of Little Scioto (LS), Eagle Harbor (EH), and Gary (GI) Sediments. .....	137

## LIST OF FIGURES

	Page
Figure 1. 1: PAHs representatives and their chemical structures. ....	23
Figure 1. 2: Atmospheric sources of PAH in the United States. Data is taken from Technical Report of the Sources, Pathways and Loadings Workgroup by Jay A.Davis <sup>6</sup> .....	24
Figure 1. 3: Atmospheric PAH cycling in San Francisco Bay <sup>6</sup> .....	25
Figure 1. 4: Bubble growth through many ultrasound cycles.....	26
Figure 1. 5: Reactive zones in collapsing cavitation bubble.....	27
Figure 1. 6: Graph of fraction of contaminant remaining on sediment with respect to Tenax mixing time. ....	28
Figure 2. 1: The first-order sonolytic degradation rate constants of NAP, PHEN and PYR at 34 °C. (Sonication power = 430 W L <sup>-1</sup> , Sonicating volume = 85 mL, [C] <sub>0</sub> = 0.5 μM, error bar represents 95% confidence interval, n = 3). Inset is the 1 <sup>st</sup> order plot for PYR at 34 °C. ....	49
Figure 2. 2: HTA formation @ solution temperature of 34 °C with and without PAHs. (Sonication power = 430 W L <sup>-1</sup> , Sonicating volume = 85 ml, Reactor volume = 100 mL, [TA] = 2.2 mM, pH = 7.4, error bar represents 95% confidence interval, n = 3). The concentration of the HTA with time was quantified by Shimadzu Spectrofluorophotometer at 426 nm. ....	50

Figure 2. 3: Effect on degradation rate constants of 0.5  $\mu\text{M}$  of PAH with varying solution temperatures. (Sonication power =  $430 \text{ W L}^{-1}$ , Sonicating volume = 85 ml, Reactor volume = 100 mL,  $[\text{C}]_0 = 0.5 \mu\text{M}$  error bar represents 95% confidence interval,  $n = 3$ ). ..... 51

Figure 2. 4: Effect of degradation rate constants of PYR, PHEN and NAP at 80% solubility limit with varying solution temperature (Sonication power =  $430 \text{ W L}^{-1}$ , Sonicating volume = 85 ml, Reactor volume = 100 mL,  $[\text{C}]_0 = 0.80 [\text{C}]_{\text{solubility limit}}$ , error bar represents 95% confidence interval,  $n = 3$ ). ..... 52

Figure 2. 5: Concentration Effect on degradation of NAP (Sonication power =  $430 \text{ W L}^{-1}$ , Sonicating volume = 85 ml, Reactor volume = 100 mL,  $T = 34^\circ\text{C}$ , error bar represents 95% confidence interval,  $n = 3$ ). (a) Degradation rate constants, (b) Rate of degradation with respect to concentration (c) Langmuir-Hinshelwood model. ... 53

Figure 2. 6: Degradation rate constants for PAHs in a mixture and individually (Sonication power =  $430 \text{ W L}^{-1}$ , Sonicating volume = 85 ml, Reactor volume = 100 mL,  $[\text{C}]_{0,i} = 0.5 \mu\text{M}$ ,  $T = 34^\circ\text{C}$ , error bar represents 95% confidence interval,  $n = 356$

Figure 3. 1: Fraction of pyrene in aqueous phase and sediment as a function of sonication time, determined using liquid-liquid hexane extraction and microwave extraction, respectively (LS sediment,  $T = 20^\circ\text{C}$ ,  $[\text{particle}] = 12.5 \text{ g L}^{-1}$ ,  $[\text{Pyrene}]_{\text{initial on particle}} = 0.319 \mu\text{mol g}^{-1}$ ,  $D_0 = 75 \mu\text{m}$ ). 82

Figure 3. 2: Rate of sonodegradation of PAHs  $\left( \left( \frac{d(n_{\text{PAH},\text{sed},t} + n_{\text{PAH},\text{sol},t})}{dt} \right)_{\text{combined}} \right)$  for varying solid-liquid ratio for LS (Little Scioto, Marion, OH) and GI (Gary, Indiana) sediments. Solid-liquid ratios represent LS sediment particle concentrations unless otherwise noted. ( $T = 20^\circ\text{C}$ , sonication power  $430 \text{ W L}^{-1}$ , Sonication time = 60 min,  $D_0$  for LS =  $75 \mu\text{m}$ ,  $D_0$  for GI =  $303 \mu\text{m}$ ). 83

Figure 3. 3: TOC released into the aqueous phase during sonication of: (i)  $5.0 \text{ g L}^{-1}$ , (ii)  $8.75 \text{ g L}^{-1}$ , (iii)  $12.5 \text{ g L}^{-1}$ , (iv)  $18.75 \text{ g L}^{-1}$ , and (v)  $25.0 \text{ g L}^{-1}$  solid-liquid ratio of LS sediment. The aqueous solution (8 ml) was removed from sonicated mixture after 10 min centrifugation. 84

Figure 3. 4: % volume of sediment with particle diameter, measured by Malvern Mastersizer, for sediment treated with different sonication time ( $T = 20\text{ }^{\circ}\text{C}$ ,  $[\text{particle}] = 12.5\text{ g L}^{-1}$ , sonication power  $430\text{ W L}^{-1}$ ,  $D_0 = 75\text{ }\mu\text{m}$ ). 85

Figure 3. 5: % volume of sediment with particle diameter, measured by Malvern Mastersizer, after 80 mins sonication for various solid-liquid ratios ( $T = 20\text{ }^{\circ}\text{C}$ , sonication power  $430\text{ W L}^{-1}$ ,  $D_0 = 75\text{ }\mu\text{m}$ ). 86

Figure 3. 6: Particle morphology from SEM images (a) before sonication (size  $> 75\mu\text{m}$ ), (b) after 80 min sonication (size  $> 75\mu\text{m}$ ), (c) before sonication (size  $\sim 5 - 10\text{ }\mu\text{m}$ ), and (d) after 80 min sonication (size  $\sim 5 - 10\text{ }\mu\text{m}$ ). ( $T = 20\text{ }^{\circ}\text{C}$ ,  $t = 80\text{ min}$ , sonication power =  $430\text{ W L}^{-1}$ ,  $D_0 = 75\text{ }\mu\text{m}$ ). 87

Figure 4. 1: (a) Naphthalene (nmol) in aqueous solution and on sediment after selected ultrasonic exposure time; (b) the fraction of naphthalene in aqueous phase and sediment as a function of US time, determined using liquid-liquid hexane extraction and microwave extraction, respectively (LS sediment,  $T = 20\text{ }^{\circ}\text{C}$ ,  $[\text{particle}] = 12.5\text{ g L}^{-1}$ ,  $[\text{Naphthalene}]_{\text{initial on particle}} = 167\text{ nmol g}^{-1}$ ,  $D_0 = 75\text{ }\mu\text{m}$ ). The fraction of naphthalene is calculated through dividing total nmol of naphthalene in aqueous or sediment after sonolysis by total nmol of naphthalene in  $0.50\text{ g}$  LS sediment before sonication. 109

Figure 4. 2: Phenanthrene (nmol) in aqueous solution and on sediment after selected ultrasonic exposure time; (b) the fraction of phenanthrene in aqueous phase and sediment as a function of US time (LS sediment,  $T = 20\text{ }^{\circ}\text{C}$ ,  $[\text{particle}] = 12.5\text{ g L}^{-1}$ ,  $[\text{Phenanthrene}]_{\text{initial on particle}} = 446\text{ nmol g}^{-1}$ ,  $D_0 = 75\text{ }\mu\text{m}$ ). 111

Figure 4. 3: (a) Pyrene (nmol) in aqueous solution and on sediment after selected ultrasonic exposure time (b) the fraction of pyrene in aqueous phase and sediment as a function of US time (LS sediment,  $T = 20\text{ }^{\circ}\text{C}$ ,  $[\text{particle}] = 12.5\text{ g L}^{-1}$ ,  $[\text{Pyrene}]_{\text{initial on particle}} = 0.319\text{ nmol g}^{-1}$ ,  $D_0 = 75\text{ }\mu\text{m}$ ). 113

Figure 4. 4:  $F_{\text{fast}}$  of naphthalene, phenanthrene and pyrene in the absence of sonication and respective  $\log K_{\text{ow}}$ . 115

Figure 4. 5: (a) Amount of phenanthrene (nmol) in fast and slow desorbing LS sediment sites in the presence and absence of sonication and sonolytically degraded; (b) the fraction of phenanthrene on fast desorbing sites ( $F_{\text{fast}}$ ), slow desorbing sites ( $F_{\text{slow}}$ ),



and sonolytically degraded ( $F_{degraded}$ ), after sonolysis on Little Scioto (LS) sediment. The sum of these fractions is equal to 1 (Sonication power = 430 W L<sup>-1</sup>, Sonicating volume = 40 mL, Sonicating mass = 0.50 g sediment, Tenax mass = 1.0 g, T = 20 °C, Tenax adsorption time = 6 hr). 116

Figure 4. 6: (a) Amount of pyrene (nmol) in fast and slow desorbing LS sediment sites in the presence and absence of sonication and sonolytically degraded; (b) the fraction of pyrene on fast desorbing sites ( $F_{fast}$ ), slow desorbing sites ( $F_{slow}$ ), and sonolytically degraded ( $F_{degraded}$ ), after sonolysis on Little Scioto (LS) sediment. (Sonication power = 430 W L<sup>-1</sup>, Sonicating volume = 40 mL, Sonicating mass = 0.50 g sediment, Tenax mass = 1.0 g, T = 20 °C, Tenax adsorption time = 6 hr). 118

Figure 5. 1: Effect of addition of 3% PAC by mass to LS sediment on  $F_{fast}$ ,  $F_{degraded}$ , and  $F_{slow}$  for phenanthrene as a function of treatment time on LS sediment (Sonication power = 430 W L<sup>-1</sup>, Sonicating volume = 40 mL, Sonicating mass = 0.50 g sediment, [PAC] = 3% by weight, Tenax mass = 1.0g, T = 20 °C, mechanical mixing = 300 rpm, duplicate were performed for selected points). 138

Figure 5. 2: Effect of addition of 3% PAC by mass to LS sediment on  $F_{fast}$ ,  $F_{degraded}$ , and  $F_{slow}$  for pyrene as a function of treatment time (Sonication power = 430 W L<sup>-1</sup>, Sonicating volume = 40 mL, Sonicating mass = 0.50 g sediment, [PAC] = 3% by weight, Tenax mass = 1.0g, T = 20 °C, mechanical mixing = 300 rpm, duplicate were performed for selected points). 139

Figure 5. 3: % volume of LS sediment with particle diameter for selected sonication time (T = 20 °C, Sonication power = 430 W L<sup>-1</sup>, [particle] = 12.5 g L<sup>-1</sup>, Sonicating time = 80 min,  $D_0 = 75.411 \mu\text{m}$ ). 140

Figure 5. 4: The effect of adding 3% PAC on  $F_{fast}$  for phenanthrene and pyrene as a function of treatment time on Eagle Harbor (EH) sediment (Sonication power = 430 W L<sup>-1</sup>, Sonicating volume = 40 mL, Sonicating mass = 0.50 g sediment, [PAC] = 3% by weight, Tenax mass = 1.0g, T = 20 °C, Tenax adsorption time = 24 hr, error bar represents 95% confidence interval, n = 2). 141

Figure 5. 5: The effect of adding 6% PAC and 3% PAC on  $F_{fast}$  of phenanthrene and pyrene on EH sediment (Sonication power = 430 W L<sup>-1</sup>, Sonicating volume = 40 mL, Sonicating mass = 0.50 g sediment, [PAC] = 3% by weight, Tenax mass = 1.0g, T = 20 °C, Tenax adsorption time = 24 hr, error bar represents 95% confidence interval, n = 2). 142

Figure 5. 6: The effect of adding 3% PAC and treating with ultrasound or mixing on  $F_{fast}$  of pyrene on Gary, Indiana (GI) sediment. Unless otherwise stated, 3 % PAC by sediment weight was added to sediment slurry. (Sonication power = 430 W L<sup>-1</sup>, Sonicating volume = 40 mL, Sonicating mass = 0.50 g sediment, Tenax mass = 1.0g, T = 20 °C, Tenax adsorption time = 24 hr, error bar represents 95% confidence interval, n = 2).

143

Figure 5. 7: Comparison of organic carbon content to % decrease in  $F_{fast}$  for EH, GI, and LS sediment.

144

## **CHAPTER 1**

### **INTRODUCTION AND BACKGROUND**

#### **1.1 Introduction and source of polycyclic aromatic hydrocarbons**

Soils and sediment contaminated by organic pollutants are of environmental concern. Polycyclic aromatic hydrocarbons (PAHs) are among the most common contaminants in aquatic sediment<sup>1</sup>. PAHs are fused benzene ring compounds (see Figure 1.1 for PAH structures) that are highly resistant to biodegradation under normal conditions because of their strong molecular bonds. Many compounds in this group are suspected human carcinogens<sup>2</sup>. Human maybe exposed to PAHs through air, soil and food<sup>3</sup>. The US EPA has classified 16 PAHs as priority pollutants based on their toxicity, potential for human exposure, and on the frequency of occurrence at hazardous waste sites<sup>4</sup>.

PAHs occur naturally through forest fires and volcanic activity<sup>5</sup>. However, human activities have led to a great increase the concentration of PAHs in the environment<sup>6</sup>. These activities include industrial emissions from aluminum smelting and coke production, vehicle emissions, and residential wood and agricultural burning<sup>6,7</sup>. In the United States., motor vehicles are the major source of PAHs, accounting for 36% of the annual total mass of PAHs released<sup>6</sup>. Aluminum production (17%), forest fires (17%),

residential wood burning<sup>7-9</sup> (12%), coke manufacturing (11%), power generation (7%), and incineration (3%) are other sources for atmospheric discharge of PAHs<sup>6</sup> (Figure 1.2). PAHs released to the atmosphere will undergo short- and long-range transport followed by removal by wet and dry deposition onto soil, water, and vegetation<sup>5</sup>. Most of the mass of these emitted PAHs are deposited on land or water surfaces near the site of emission.

Motor vehicles emissions have a relatively large impact on aquatic ecosystems in urban areas because a high proportion of these emissions are transported to water bodies in runoff<sup>6</sup>. Another significant source of PAHs in aquatic environment is from creosotes. Coal tar creosotes are distillation products of coal tar (which is rich in PAHs<sup>10</sup>) used to preserve wood in both aquatic and terrestrial applications<sup>7,11</sup>. The PAHs from these treated woods desorb into solution and are then dispersed in water bodies<sup>7</sup>.

The accidental spill of crude oil is also a significant source that results in the direct release of PAHs to water bodies. Bojes and Pope report that petroleum refinery processes such as catalytic cracking and delayed coker units, and bitumen processing units contained 10  $\mu\text{g}/\text{m}^3$  and 1 to 40  $\mu\text{g}/\text{m}^3$  total PAHs<sup>12</sup>. A spill occurred in 1988 when approximately 400,000 gallons of crude oil was released into Suisun Bay due to an accident at the Shell Oil Company refinery in Martinez<sup>5</sup> killing wildlife.

Once released to aquatic environments, PAHs in surface water can volatilize, abiotically degrade (i.e., through photolysis or oxidation), biodegrade, bind to suspended particles or sediments, or accumulate in aquatic organisms<sup>12</sup> (Figure 1.3). PAHs adsorbed onto sediments can also volatilize, undergo degradation (e.g., photolysis and oxidation), biodegrade, or accumulate in biota. PAHs in soil can be released back into groundwater and be transported within an aquifer resulting in a significant source for drinking water

contamination. The elimination of PAHs by natural attenuation is limited in part due to the low solubility of PAHs and their high affinity to the organic rich sediments<sup>13</sup>.

## **1.2. Traditional treatment methods**

Traditional field-scale technologies such as capping, dredging for direct incineration, and bioremediation of the contaminated soil have been used to destroy organic contaminants but are usually not cost effective and/or are time consuming when treating a large volume of contaminated soil<sup>14</sup>. Moreover, there are drawbacks for each of these technologies.

In-situ capping is the method of placing a subaqueous covering or cap of clean material over contaminated sediments<sup>15</sup>. Capping materials used are typically granular material, such as clean sediment, sand, or gravel<sup>15</sup>. A more complex cap design involves geotextiles, liners, and other permeable or impermeable materials in multilayers<sup>15</sup>. These capping materials act to isolate and stabilize the contaminated sediments<sup>15</sup>. The principle functions of capping materials are to reduce: 1) direct contact between sediment and organisms, 2) re-suspension, 3) transport of sediment to other sites, and 4) exposure of the environment to dissolved and colloidally bound contaminants transported into the water column<sup>15</sup>. As of 2004, in-situ capping has been used in fifteen superfund sites either as the primary approach or in combination with sediment removal and/or monitored natural recovery<sup>15</sup>.

Two advantages of capping are that it can quickly reduce exposure of the environment to contaminants and that it requires less infrastructure in terms of material handling, dewatering, treatment and disposal compared to dredging or excavation<sup>15</sup>.

However, a major limitation of in-situ capping is that the contaminated sediment remain in the aquatic environment. These contaminants can become exposed or be dispersed if the cap is significantly disturbed or if contaminants leach through the cap in significant amounts<sup>15</sup>. In addition to this, during compaction and disruption of the underlying sediment, significant contaminant losses can occur<sup>15</sup>. Furthermore, in shallow water bodies, the cap may experience disturbances from boat anchoring, keel drag<sup>15</sup>, storms and shipping activity. Yet another potential limitation of in-situ capping is that a preferred habitat may not be provided by the surficial cap materials. For example, as a protection against erosion and to limit bioturbation, coarse materials that are different from native soft bottom materials and materials that discourage colonization may be used<sup>15</sup> thus altering the sediment conditions.

Dredging involves the removal of contaminated sediment for treatment or disposal. This method allows removal of contaminated soil to a more desirable level, has less uncertainty about long-term effectiveness of the cleanup, particularly regarding future environmental exposure to contaminated sediment and allows for treatment and/or beneficial reuse of dredged or excavated material<sup>15</sup>.

Dredging in itself is an expensive alternative. The combined cost of dredging and incineration of the removed soil is much higher than dredging alone, although a combination of these processes can potentially eliminate 99.99% of the contaminants. For example, the operation of an incinerator to meet the required 99.9999 % removal efficiency of PCBs and dioxins costs \$1,650 to \$6,600 per metric ton (\$1,500 to \$6,000 per ton) to incinerate<sup>16</sup>. In addition to the cost associated with dredging, during the implementation of this process, small soil particles may be suspended. These suspended

particles are not removed by the dredging process. The concentration of PAHs on these light particles (i.e. coal/wood derived particles) far exceeded the concentration of PAHs on heavy particles (i.e. clay, silt and sand)<sup>17</sup>. Therefore, the dredging process may mobilize these light particles causing them to be more accessible to organisms and accumulation in the food web.

A less costly and relatively green technology compared to capping and dredging is bioremediation. This method, however, requires the contaminant to be in the aqueous phase for degradation. Direct application of this technology to contaminated sediment is limited by strong sorption and slow degradation<sup>18</sup> hence often requiring months or years for complete remediation. Additional constraints of bioremediation are the correct selection of microbes, appropriate solution conditions, recalcitrance of pollutants to biodegradation, and formation of metabolites which maybe more toxic than the parent contaminant<sup>19</sup>. For example, studies by Heitkamp and Cerniglia<sup>20</sup>, Sim et al.<sup>21</sup> and Reynaud and Deschaux<sup>22</sup> showed that high molecular weight PAHs are difficult to biodegrade and is affected by site-specific environmental factors.

A relatively innovative technique that uses ultrasound to produce sonochemical effects for the desorption of mercury and polychlorinated biphenyl (PCBs) from synthetic particles has been reported<sup>23,24</sup>. The application of ultrasound was shown to desorb mercury and a representative PCB (4-chlorobiphenyl) from the particles very quickly<sup>23,24</sup>. In addition to ultrasound-induced desorption of 4-chlorobiphenyl from particles, the subsequent sonochemical degradation of 4-chlorobiphenyl released into the aqueous phase was also observed<sup>23</sup>. The ability of sonication to enhance desorption of organics

from sediment to aqueous phase for treatment suggests that ultrasound is a promising remediation technology.

### 1.3. Sonochemistry: The Chemical Effects of Ultrasound

The exposure of homogenous and heterogenous aqueous solutions to high intensity ultrasound can initiate chemical reactions (i.e., sonochemistry) and mechanical effects through a process known as acoustic cavitation. When sound waves above 16 kHz are applied to an aqueous solution, bubbles are created from nucleation sites (i.e., weak spots such as trapped gas on particles) in solution<sup>25,26</sup>. The bubbles, known as cavitation bubbles, absorb energy from the wave and grow in size with each acoustic cycle. Upon reaching a certain critical size ( $R_{\max}$ ), cavitation bubbles collapse almost adiabatically to produce localized “hot spots”<sup>27</sup> (Figure 1.4). Studies have shown that the temperature and pressure of a hot spot can reach 5200 K and 1000 atm within the collapsing bubble and 1900 K in the interfacial area surrounding the hot spot<sup>27</sup>. These extreme conditions result in the thermolysis of contaminants within or in close proximity to the collapsing bubble. During the growth cycle of the bubble, water vapor and volatile organics partition into the cavity. The thermolysis of water vapor yields OH radicals and hydrogen atoms as shown in equation 1.1. These OH and H radicals are very reactive and non-selective towards organic solutes.



When an aqueous solution is exposed to ultrasound, the existence of three different reaction sites has been postulated (Figure 1.5): (i) High temperature and pressure (up to and above 5000 K and 1000 atmospheres, respectively) within the



gaseous interiors of collapsing cavitation bubbles causes thermolysis of vaporized compounds such as water and volatile solutes<sup>28</sup>; (ii) the interfacial region between the core of the hot spot and the bulk solution with high temperatures (ca. 1000-2000 K), high hydroxyl radical concentration, and high temperature gradients induces destruction via pyrolysis and radical reaction; (iii) the bulk solution at ambient temperature where secondary radicals and peroxide, formed during collapse of cavitation bubbles can diffuse to react with organic contaminants. These three regions act simultaneously to result in sonochemical degradation of reactants in solution.

Relatively high concentrations of peroxide (e.g. hydrogen peroxide ( $H_2O_2$ )) can also form in solution following the recombination of two hydroxyl radical as shown in equation 1.2<sup>29</sup>.



For example, rates of production of  $H_2O_2$  and  $\bullet OH$  at 20.2 kHz were measured to be 0.204  $\mu M/min$  and 0.07  $\mu M/min$ , respectively, for an ultrasound probe operating at 20 kHz<sup>30</sup>.

As thermolysis and radical reactions occur in parallel during sonolysis, the reaction rate equation can be written as<sup>31</sup>

$$-\frac{d[C]}{dt} = k_{\bullet OH}[\bullet OH][C] + k_{pyrolysis}[C] \quad (1.3)$$

where  $[C]$  is the bulk concentration of reactant,  $k_{pyrolysis}$  is the reaction rate constant for pyrolysis within the bubble,  $k_{\bullet OH}$  is the second-order rate constant for reaction with OH, and  $[\bullet OH]$  is the concentration at the region (i.e. interface or bulk) where the reaction occurs.

When a steady-state has been reached in the system, the concentration of the OH on the interface and the bulk are constant with time and equation (1.3) can be rewritten as a first-order rate reaction describe as<sup>31</sup>

$$-\frac{d[C]}{dt} = k'[C] + k_{pyrolysis}[C] = k[C] \quad (1.4)$$

where  $k'$  is  $k_{\bullet OH}[\bullet OH]$  and  $k$  is the pseudo first-order rate constant of the process.

#### **1.4. Physical/chemical properties of reactant affecting its sonochemical degradation rate in aqueous solution**

Sonochemical degradation of various organic reactants has been extensively studied<sup>25,32-37</sup>. Physicochemical properties of organic compounds have been identified to be important in determining the site and rate of sonochemical reaction<sup>38</sup>. Organic compounds are often classified by their volatility into three categories: (a) volatile, (b) semi-volatile and (c) non-volatile.

##### **1.4.a. Volatile compounds**

For volatile compounds, such as trichloroethylene (TCE) and tetrachloromethane, studies have shown that they react primarily inside the collapsing cavitation bubbles<sup>25,34,35,39,40</sup> thus yielding primarily thermal decomposition or combustion byproducts<sup>28,41-44</sup>. In particular, Jiang et al. applied ultrasound to chlorobenzene and reported the formation of brown carbonaceous particles throughout the ultrasonic irradiation process, consistent with soot formation under pyrolytic conditions<sup>44</sup>, Petrier and Francony reported that n-butanol, an OH radical scavenger, did not affect the degradation of carbon tetrachloride, which reacted inside the cavitation bubble<sup>45</sup>. Thus,

for these volatile compounds that react primarily by thermolysis, the rate of degradation can be simplified to

$$-\frac{d[C]}{dt} \approx k_{pyrolysis} [C]_{bubble} \quad (1.5)$$

where  $[C]_{bubble}$  is the concentration of the solute in the bubble during collapse of the cavitation bubble. The concentration of the solute in the bubble ( $[C]_{bubble}$ ) was approximated by Ayyildiz et al.<sup>46</sup> from a mass balance between liquid and gas phases as

$$V_B \frac{d[C]_{bubble}}{dt_{lifetime}} = A_B K_L ([C] - [C]^*) \quad (1.6)$$

where  $V_B$  is the volume of an individual bubble,  $A_B$  is the surface area of the bubble,  $K_L$  is the overall liquid phase mass transfer coefficient, and  $[C]^*$  is the hypothetical liquid phase solute concentration if the system was in equilibrium :

$$[C]^* = \frac{[C]_{bubble}}{K_H} \quad (1.7)$$

where  $K_H$  is the Henry's law coefficient. Equation 1.8 assumes that the volume of the cavitation bubble is constant<sup>46</sup>. Ayyildiz et al.<sup>46</sup> reported that the Henry's law coefficient seemed to exert a greater influence on the sonochemical degradation rate of TCE and ethylene dibromide (EDB) compared to the diffusion coefficient of these solutes. Henry's law coefficient and diffusion can be used to calculate partitioning of solute into the cavitation bubble (i.e.,  $[C]_{bubble}$ ) but they cannot be used for hydrophilic compounds because the dominant sonolytic degradation pathway of these compounds may include hydroxyl radical reactions<sup>46</sup> in the bulk solution. The dependence of sonolytic degradation of volatile compounds on Henry's law coefficient and diffusivity was also reported by Colussi et al.<sup>32</sup>, and Drijvers et al.<sup>36</sup> and DeVisscher et al.<sup>34</sup>, respectively.

#### 1.4.b. Semi-volatile compounds

PAHs consist of a group of hydrophobic and semi-volatile compounds, and therefore have a wide range of volatility ( $K_H < 10^{-3} \text{ atm-m}^3 \text{ mol}^{-1}$ <sup>47</sup>). Their sonochemical degradation in aqueous solution and the byproducts formed have been investigated in a number of studies<sup>48-50</sup>. Psillakis et al. showed that complete sonochemical degradation of naphthalene, acenaphthylene and phenanthrene was achieved in up to 120 min sonolysis<sup>50</sup>. They also found that sonochemical treatment was capable of destroying a variety of lower molecular weight PAHs (naphthalene, acenaphthylene, acenaphthene, fluorine, phenanthrene, anthracene, fluoranthene and pyrene) but that the higher molecular weight PAHs were more recalcitrant to ultrasound treatment<sup>49</sup>. The byproduct from sonolysis of phenanthrene was phenanthrene diol suggesting that the reaction pathway to involved hydrogen abstraction reactions from the hydrocarbon skeleton<sup>28,51</sup>. In another study by Little et al.<sup>48</sup>, the byproduct of sonochemical degradation of phenanthrene was found to have reduced aromaticity or conjugation, consistent with free radical reactions.

Semi-volatile compounds (including certain PAHs, Polychlorinated dibenzo-p-dioxins (PCDDs) and polychlorinated biphenyl (PCB)), which can exhibit some partitioning into the bubble, may not be preferentially degraded in any of the three sonochemical reaction sites. Zhang and Hua<sup>52</sup> reported that both thermolysis and bulk free radical attack are important pathways for PCB destruction<sup>52</sup> and from the resulted reported, the sonochemical degradation rates of 2-PCB, 4-PCB and 2,4,5-PCB appeared to be correlated to log  $K_{ow}$  of the PCBs. Katsumata et al.<sup>53</sup> reported that the sonochemical degradation of 2,3,7,8-tetrachlorodibenzo-p-dioxins at 20 kHz was diffusion-controlled

and the destruction of methyl tert-butyl ether (MTBE) was hypothesized to be dependent on the concentration of solute, partition of the solute inside cavitation bubbles, and hydrophobic effects<sup>54</sup>. The degradation rate of MTBE was represented by<sup>55</sup>

$$-\frac{d[MTBE]}{dt} = (k_{pyrolysis} + k_{MTBE, \bullet OH} [\bullet OH]) [MTBE] = k [MTBE] \quad (1.8)$$

Therefore, the rate of degradation should incorporate reactions in all sonochemical reaction three sites and can be written as

$$-\frac{d[C]}{dt} = k_{\bullet OH} [\bullet OH]_{interface} [C]_{interface} + k_{\bullet OH} [\bullet OH]_{bulk} [C] + k_{pyrolysis} [C]_{bubble} \quad (1.9)$$

where  $[\bullet OH]_{interface}$ ,  $[C]_{interface}$  and  $[\bullet OH]_{bulk}$  are the concentrations of  $\bullet OH$  or reactant at the interface of cavitation bubbles or in the bulk solution.

#### 1.4.c. Non-volatile compounds

Sonochemical reaction for non-volatile and hydrophobic or surface-active compounds occurs primarily with  $\bullet OH$ <sup>38</sup> at the interfacial or via  $\bullet OH$  pathway in the bulk solution<sup>28,56</sup> for hydrophilic compounds. Henglein and Kormann found that solutes with different hydrophobicity resulted in radical scavenging occurring in different phases<sup>38</sup>. Hydrophobic enrichment of the solute<sup>38,57</sup> at the interface is a term used to represent the accumulation of the solute at the air-water interface of cavitation bubbles. The importance of partitioning of the contaminants to the interface of cavitation bubbles was illustrated by studies of sonochemical degradation rates of phenol and substituted phenol<sup>57,58</sup>. The sonochemical degradation rate constants of 4-nitrophenol (protonated species) appeared to be much faster than the 4-nitrophenolate ion (deprotonated species)<sup>57</sup>. The authors suggested that the difference in behavior is due to a hydrophobic

enrichment of 4-nitrophenol at the interface of the cavitation bubble by a factor of about 80<sup>57</sup>.

In some studies<sup>46,59</sup>, octanol-water partitioning coefficient of the solute was used to predict hydrophobicity<sup>46</sup>. Compounds with higher octanol-water partition coefficient representing greater hydrophobicity tend to degrade faster than compounds with lower octanol-water partition coefficient<sup>59</sup>, suggesting these compounds more readily accumulated at the gas/solution interface of cavitation bubbles.

The Gibbs surface excess, a measure the amount of solute that accumulates at the gas/solution interface has also been used to describe the accumulation and sonochemical degradation of surfactant at the gas/solution interface of cavitation bubbles<sup>60</sup>. Decreased in surface tension can potentially affect the bubble growth and collapse dynamic<sup>61</sup>.

For non-volatile and hydrophilic compounds, that do not partition into the cavitation bubble or accumulate on the interface, it is believed that degradation occurs via •OH pathway in the bulk solution<sup>28,56</sup>.

### **1.5. Ultrasound: Physical Effects**

In addition to producing sonochemistry, cavitation bubbles produced three main physical effects. At the point of critical radius, cavitation bubbles collapse resulting in the dissipation of energy in the form of acoustic shockwaves. The second physical effect is microstreaming from bubble oscillation creating eddy motion in the immediate adjoining liquid of the cavitation bubble<sup>62</sup>. A microjet occurs during asymmetric collapse of a bubble on any surface larger than the bubbles itself resulting in the formation of a liquid jet through the bubble. At an ultrasonic frequency of 20 kHz, the jet moves with such

speed (up to 400 km/hr) that it can readily result in the pitting and erosion of the solid surface<sup>63,64</sup>.

When particles are added to the solution, the collapse of bubbles may occur symmetrically or asymmetrically depending on the proximity and size of the particles compared to the cavitation bubbles. Shockwaves generated during cavitation collapse in close vicinity to sediment particles cause nearby particles to move away from the cavitation event in a radial direction with great speed<sup>65</sup> resulting in particle-particle collisions ( $> 500 \text{ kmhr}^{-1}$ <sup>66</sup>). These collisions between the particles have been shown to produce interparticle melting<sup>67</sup> and agglomeration of zinc particles<sup>66</sup>. The second effect, acoustic microstreaming enhances the mass and heat transfer at interfacial films surrounding nearby adsorbent particles and within the pores<sup>62</sup>. The third effect microjets when occur on the surfaces of solid particles that are several orders of magnitude larger than the bubble<sup>65</sup> result in pitting and surface cleaning. For a 20 kHz system, Doktycz and Suslick noted that at the start of cavitation collapse, the collapsing bubble will have a diameter of 150  $\mu\text{m}$  and particles smaller than this cannot cause microjet formation<sup>67</sup>.

The presence of particles in solution has various effects on cavitation. It is known that particles with different acoustic impedances than water act to attenuate (i.e., scatter and adsorb) sound waves<sup>68,69</sup>, affect the shape of cavitation bubbles<sup>70</sup> (i.e., the surfaces of particles much larger than a collapsing cavitation bubble, 100-150  $\mu\text{m}$ <sup>66,67</sup>, allow for the formation of microjet while particles smaller than the cavitation bubble has no effect on the bubble collapse), and create solid-liquid interface with lower tensile strength than bulk solution thus allowing more bubbles to grow into active cavitation bubbles<sup>69</sup>. These two opposing factors (i.e., sound attenuation and additional solid-liquid interface) coexist

in sonication systems in the presence of particles. Sound attenuation acts to dissipate sound waves resulting in decreased ultrasonic intensity while additional active cavitation bubbles may allow for more cavitation collapse compared to a system in the absence of particles.

These three mechanical effects (i.e., shockwaves, microstreaming, and microjets) were shown to have the ability to increase the mass-transfer coefficient<sup>26</sup>, enhance dissolution of solids<sup>26,71</sup>, induce the supersaturation of a sparingly soluble solid in a liquid system<sup>65</sup>, change particle size and surface properties<sup>26,69</sup> strip un-reactive coatings from surfaces<sup>66</sup>, and modify material structure<sup>26,72</sup>. The physical effects coupled with chemical effects of ultrasound have been exploited for the remediation of metal and organics from sediments<sup>23,73-80</sup>. For example, Feng and Aldrich showed that sonolytic treatment of sand contaminated with diesel reduced the diesel content on the sand<sup>78</sup>, Koparal et al. showed that ultrasound is more effective than the simple mechanical stirring in tar removal from tar-contaminated sand<sup>79</sup>, Hamdaoui et al. showed that sonication significantly increase the rate of desorption of p-chlorophenol from granular activated carbon<sup>81</sup> and Meegoda et al. showed that sonication effectively removed p-terphenyl from synthetic dredged sediments<sup>77</sup>. The results obtained from these studies<sup>23,73-80</sup> suggest that ultrasound is a viable technology for the remediation of contaminated sediment.

## **1.6. Carbon amendments**

The complete sonochemical destruction of contaminants on sediments may require a large energy input. Therefore a more practical approach may be the use of sonication to reduce the bioavailability (i.e., the proportion of a chemical in the system



which is available for uptake by biota) of contaminants in natural sediments. Bioaccumulation (or bioavailability) of hydrophobic organic contaminant (HOC) is a measure of the three phase equilibrium relationship between sediment, pore water and organism lipids<sup>82</sup>.

Recent studies have shown that by amending sediments with activated carbon for persistent organic pollutants; minerals such as apatite, zeolites, bauxite, and alumina for metals or metalloids; ion exchange resins for metals or other inorganic contaminants; or lime for pH control or nitroaromatics degradation, the binding and assimilation capacity of natural sediments<sup>83</sup> are modified and the contaminant transport pathways (i.e., out of the sediment) are interrupted<sup>83</sup>.

For example, a number of studies have shown that the bioavailability of organics (i.e., PCBs and PAHs) in natural sediment was shown to decrease by the addition of 2 % PAC<sup>18,84-86</sup>. Addition of carbon particles to the sediment provides strong sorption sites for these HOCs and reduces the freely dissolved HOC concentrations; thus, reducing the amount available for organism intake. In results presented by Millward et al.<sup>18</sup>, for sediment in contact with activated carbon for 1 month, the bioavailability of PCB was reduced by 70 to 82% for *Neanthes arenaceodentata* (worm) and *Leptocheirus plumulosus* (amphipod), respectively. With 6 months contact time, bioavailability of PCB was further reduced by 75% and 87% from 70% and 82%, respectively. Although carbon amendments seem promising by decreasing bioavailability of HOCs, this method is dependent on the desorption rate of HOCs from the sediment, which can be slow. Hence in this study, ultrasound was evaluated as a possible technology for enhancing desorption

of PAHs from three freshwater sediments to the aqueous phase for re-adsorption onto activated carbon.

### **1.7. The effects of sonication on mass transfer**

Remediation of contaminated sediments involves a 2 step process: desorption of contaminants from the particles to the aqueous phase and the degradation/removal of the contaminants. For hydrophobic organic carbons (HOCs), the rate of desorption of is often the rate limiting step since they are increasingly sequestered with residence time in soil<sup>87-90</sup> and sediment.

It has been shown that ultrasound can produce supersaturated solutions of solute, enhance the rate of mass transfer and enhance dissolution of sparingly soluble solid have been demonstrated in previous studies<sup>26,65,71</sup>. The enhancement in rate of mass transfer for dissolution is a result of increased localized turbulence from microstreaming, increased interfacial area through interparticle collisions and pitting as a result of microjets, and enhanced solution concentration through increased solubility in supercritical fluid at cavitation site<sup>65</sup>.

In addition to enhancement in rate of mass transfer for dissolution of sparingly soluble solid, Koparal et al. showed that ultrasound is more effective than mechanical stirring in tar removal from tar-contaminated sand<sup>79</sup>, Hamdaoui et al. showed that sonication significantly increase the rate of desorption of p-chlorophenol from granular activated carbon<sup>81</sup> and Meegoda et al. showed that sonication effectively removed p-terphenyl from synthetic dredged sediments<sup>77</sup>. Thus, when sonication is applied to HOC-contaminated sediment, increases in microstreaming, interfacial area and solution

concentration may lead to enhanced desorption of HOCs from sediment particles for degradation or removal.

### **1.8. Partitioning of Hydrophobic organic contaminants in Sediment**

Sediment is composed of a continuum of pores ranging in size from micropores < 0.1  $\mu\text{m}$  in diameter through to macropores >20  $\mu\text{m}$ <sup>91</sup>, continuum of compartments (i.e., rubbery (loose, flexible) to glassy (condensed, rigid) organic matter<sup>92,93</sup>) ordered by their desorption rate constants<sup>94</sup> and degree of sorption<sup>95</sup>. The release of contaminants from these sites is often considered to occur in biphasic stages: a fast desorbing contaminant fraction in equilibrium with contaminant in solution and a slow desorbing contaminant fraction that is not in equilibrium with the contaminant in solution<sup>93,96-98</sup>. There is also a third fraction of non-desorbable, (possibly) non-extractable covalently, electrostatically bound or physically entrapped contaminants<sup>99</sup>, which is considered “nonlabile”.

The fast desorbing fraction is assumed to be associated with amorphous materials, such as partly degraded and/or reconstituted biopolymers (e.g., polysaccharides, lignins), lipoproteins, amino acids, lipids, and humic/fulvic substances<sup>100,101</sup>. This fast desorbing fraction is often related to bioavailability<sup>97,102-104</sup>. Bioavailability is defined as the amount of contaminants freely available to cross an organism’s (cellular) membrane from the medium the organism inhabits at a given point in time<sup>105</sup>.

The slow desorbing fraction can account for a large percentage of contaminants in the sediment. For example, Pignatello and Xing found that the apparent sorption distribution coefficient can be increased by 30% to as much as 10-fold for long contact times compared to short contact (1-3 day)<sup>94</sup>. Therefore, ignoring the slow desorbing fraction in

fate, transport, and risk assessment models can lead to an underestimation of the true extent of sorption, false predictions about the mobility and bioavailability of contaminants<sup>94</sup>.

The importance of this slow desorbing fraction of contaminants in bioremediation is currently unclear<sup>101</sup>. This slow desorbing fraction may not be degraded once the easily available contaminants are exhausted or are degraded over long time spans (>years)<sup>101</sup> because release of contaminants can occur over a time scale of weeks to years<sup>93,101,106,107</sup>. White et al.<sup>108</sup> suggested that although the contaminant is not destroyed during sequestration, this process decreases the exposure of susceptible organisms to the harmful effects of the contaminant with time<sup>98</sup>. Conversely, if the availability of such aged contaminants is increased, they will be more susceptible to bioremediation or treatment, leading to a lower final concentration of the contaminants of concern<sup>108</sup>.

The slow desorbing fraction is associated with carbonaceous particles. For example, it was hypothesized by Pignatello and Xing that slow diffusion in, or extensive sorption to, rigid parts of the carbonaceous geosorbents could be responsible for slow desorption<sup>94</sup>. Furthermore, PAHs sorbed on carbonaceous particles (i.e., black carbon, coal, and kerogen)<sup>101</sup> in sediments were found to be strongly bound and unavailable for biological treatment or for uptake in earthworms<sup>17,109,110</sup>. This fraction was found to increase with HOCs interaction with sediment<sup>111-114</sup>. It was proposed that as sediment aged, there is more time for the HOCs to be sequestered into the interior sites of the sediment particles<sup>115</sup> consequently increasing the sorption-desorption hysteresis, which is the non-coincidence of adsorption and desorption isotherms<sup>116</sup>.

Based on the three fractions contaminants are adsorbed to in sediment, the mass balance of the contaminants on the sediment can be written as

$$n_{Total} = n_{fast} + n_{slow} + n_{nonlabile} \quad (1.7)$$

where  $n_{Total}$  is the total amount ( $\mu\text{mol}$ ) of contaminant on sediment,  $n_{fast}$  is the amount of contaminant in the fast desorbing fraction ( $\mu\text{mol}$ ),  $n_{slow}$  is the slow desorbing fraction that represents the contaminant that is more strongly bound to the sediment ( $\mu\text{mol}$ ) but can be release to the aqueous phase slowly, and  $n_{nonlabile}$  which is the amount of contaminant that are non-desorbable, (possibly) non-extractable fraction comprising of covalently and electrostatically bound contaminant, as well as physically entrapped contaminant<sup>99,117</sup>.

Extraction methods (i.e., microwave extraction, soxhlet extraction) used to determine the amount of contaminant on the sediment are likely going to underestimate  $n_{Total}$  because they cannot extract contaminant that are covalently, electrostatically bound and entrapped. Thus the above equation can be written as

$$n_{extracted} = n_{fast} + n_{slow} \quad (1.8)$$

where  $n_{extracted}$  is the number of moles of contaminants extracted by organic solvent techniques.

## 1.9. Determining Bioaccessibility

The sorption of contaminants on the sediment is important for determining the environmental fate of these contaminants. Several techniques has been used to attempt to reliably predict the bioavailability of organic compounds<sup>97,102,104,117</sup> to catabolically active microbes that control the rate of microbial degradation<sup>117,118</sup> without using bioassays (i.e.,

bioaccessibility). A common technique is chemical extraction to assess hydrophobic organic carbon (HOC) contamination<sup>104</sup> and microbial degradation of organic contaminants in soil<sup>117,118</sup>. There are two types of chemical extraction method: “non-exhaustive” extraction method (e.g., organic solvent shake extraction<sup>119,120</sup>), which removes the rapid and part of slow desorbing fraction, and “exhaustive” extraction method (e.g., pressurized liquid extraction), which offers quantitative recovery of the contaminants<sup>117</sup>. A limitation for “non-exhaustive” extraction method is its sensitivity to ageing. The extractability of contaminants was found declines with ageing and for the higher molecular weight PAHs, there was poor or no correlation to bioavailability<sup>117</sup>. A limitation for “exhaustive” method is it may overestimate the bioaccessibility (i.e., that which is available to cross an organisms<sup>105</sup>) of the contaminants.

The desorption of contaminants from sediment particles is a major process in the bioaccumulation of contaminants by benthic organisms<sup>121</sup>. Thus “aqueous based extraction method” has gained more attention as a tool to evaluate bioaccessibility. This method uses water to carry the contaminants to “hydrophobic sinks” that scavenge the contaminants from the aqueous phase following desorption from the sediment<sup>117</sup>. Examples of these hydrophobic sinks are Tenax TA and C-18-membrane<sup>117</sup>.

Tenax TA is a solid porous polymer based on 2,6-diphenyl-pphenylene oxide. Greenberg et al. showed that Tenax TA shows triphasic adsorption kinetics namely, fast, slow, and very slow phases as shown in Figure 1.6. Tenax TA was chosen for our experiments because it has been demonstrated to have an approximately similar affinity for PAHs as organic matter<sup>97,106,117</sup> and has been correlated to bioavailability<sup>102,104,121,122</sup>.

### **1.10. Objectives and Outline of the dissertation**

In this study, our first objective was to compare the sonochemical degradation rate constant of naphthalene, phenanthrene and pyrene and relate the trends observed to their respective physical/chemical properties. Some of the physical/chemical properties examined were Henry's law coefficient, diffusivity, second order rate constants with OH radicals and partitioning to the interface.

Secondly, the feasibility of using sonochemistry to degrade PAHs sorbed on natural sediments was investigated. The use of sonication has been shown to degrade organic contaminants such as PCBs and PAHs in aqueous solution<sup>23,37,50</sup> in a period of hours. Coupled with the ability of sonication to increase mass-transfer<sup>26</sup>, we hypothesized that ultrasound will be a viable technology for the desorption and remediation of PAH contaminated sediments.

Our third objective was to determine if sonolysis of sediment field-contaminated with PAHs will result in decreased bioaccessibility of PAHs similar to the mercury occlusion He et al. observed during sonication of mercury-laden alumina particles<sup>76</sup>. For natural sediment, occlusion may not occur as readily since natural sediments have a continuum of compartments consisting of rubbery (loose, flexible) to glassy (condensed, rigid) organic matter<sup>92,93</sup>. Thus formation of a saturated solution of aluminum leading to aluminum precipitation occluding contaminants may not occur as readily as was observed by He et al.<sup>76</sup>. However, the bioaccessibility of PAHs in natural sediment can be decreased if there is selective desorption of PAHs from bioaccessible sites allowing for sonodegradation or readsorption on sites that tightly bind PAHs.

Finally, carbon was added as a sink for PAHs desorbed during sonication. Recent work by McLeod et al.<sup>84</sup>, Werner et al.<sup>85</sup>, Zimmerman et al.<sup>86</sup> and Millward et al.<sup>18</sup> focused on the use of activated carbon amendments to lower contaminant bioavailability. Bioaccumulation of HOCs is a measure of the three phase equilibrium relationship between sediment, pore water and organism lipids<sup>82</sup>. The addition of carbon to the sediment provides strong sorption sites for these HOCs and reduces the freely dissolved HOC concentrations; thus, the amount available for organism intake is reduced. However, in results presented by Millward et al.<sup>18</sup>, sediment needs to be in contact with activated carbon for 1 month to reduce bioavailability of polychlorinated biphenyl (PCB) by 70 to 82% for *Neanthes arenaceodentata* (worm) and *Leptocheirus plumulosus* (amphipod), respectively. With a 6 month contact time, bioavailability of PCB was only further reduced to 75% and 87%, respectively. We hypothesized that the bioaccessibility of PAHs in natural sediments can be decreased faster through the use of ultrasound coupled with carbon amendments compared to mechanical mixing because ultrasound can facilitate the desorption of PAHs from sediment allowing for readsorption to PAC.




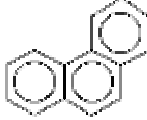


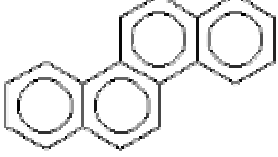
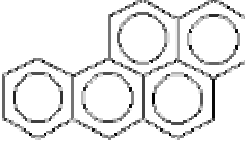
Compound Name	Structure
Naphthalene	
Phenanthrene	
Anthracene	
Pyrene	
Chrysene	
Benzo(a)pyrene	

Figure 1. 1: PAHs representatives and their chemical structures.

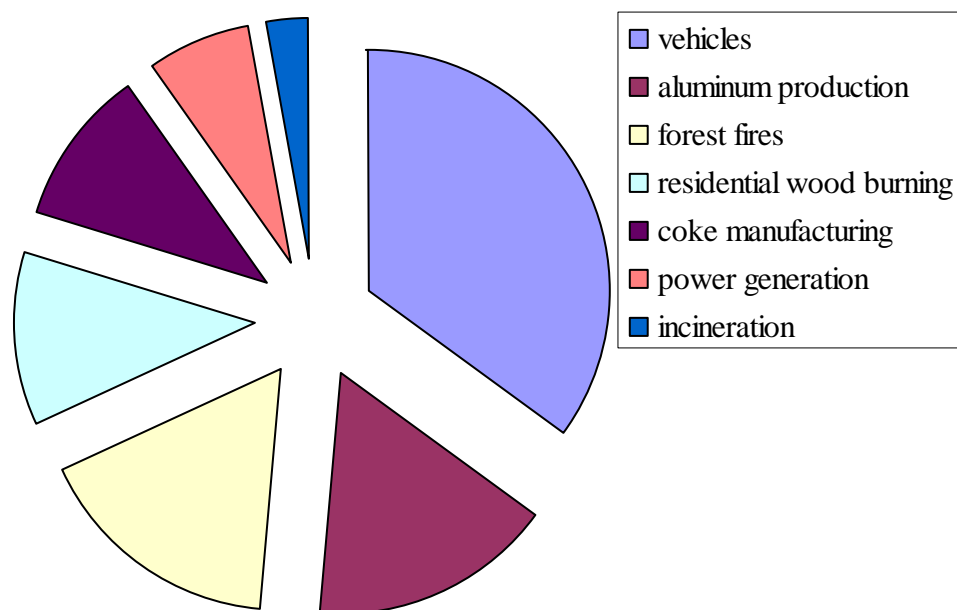


Figure 1. 2: Atmospheric sources of PAH in the United States. Data is taken from Technical Report of the Sources, Pathways and Loadings Workgroup by Jay A.Davis<sup>6</sup>.

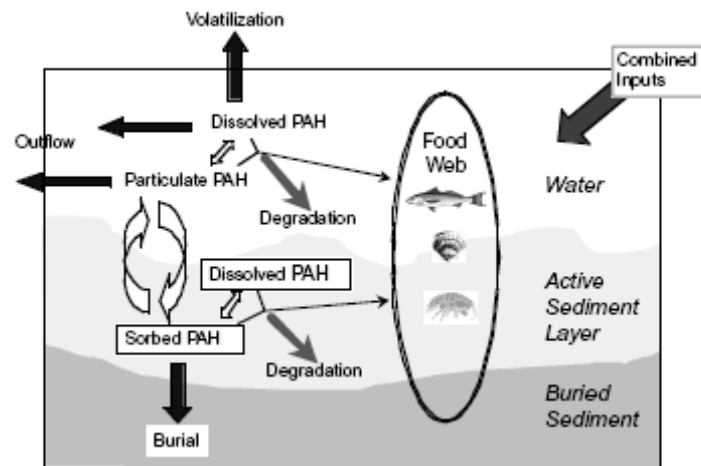


Figure 1. 3: Atmospheric PAH cycling in San Francisco Bay <sup>6</sup>.

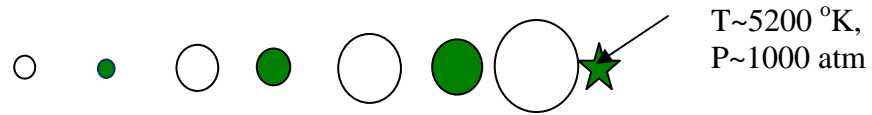


Figure 1. 4: Bubble growth through many ultrasound cycles.

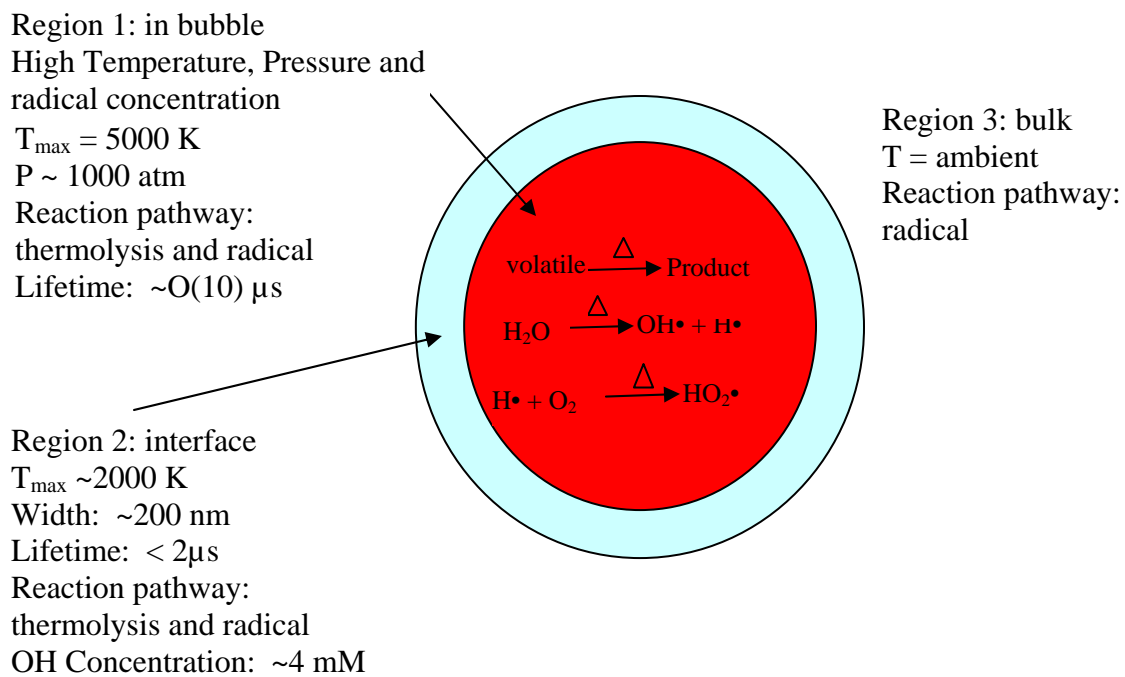


Figure 1. 5: Reactive zones in collapsing cavitation bubble

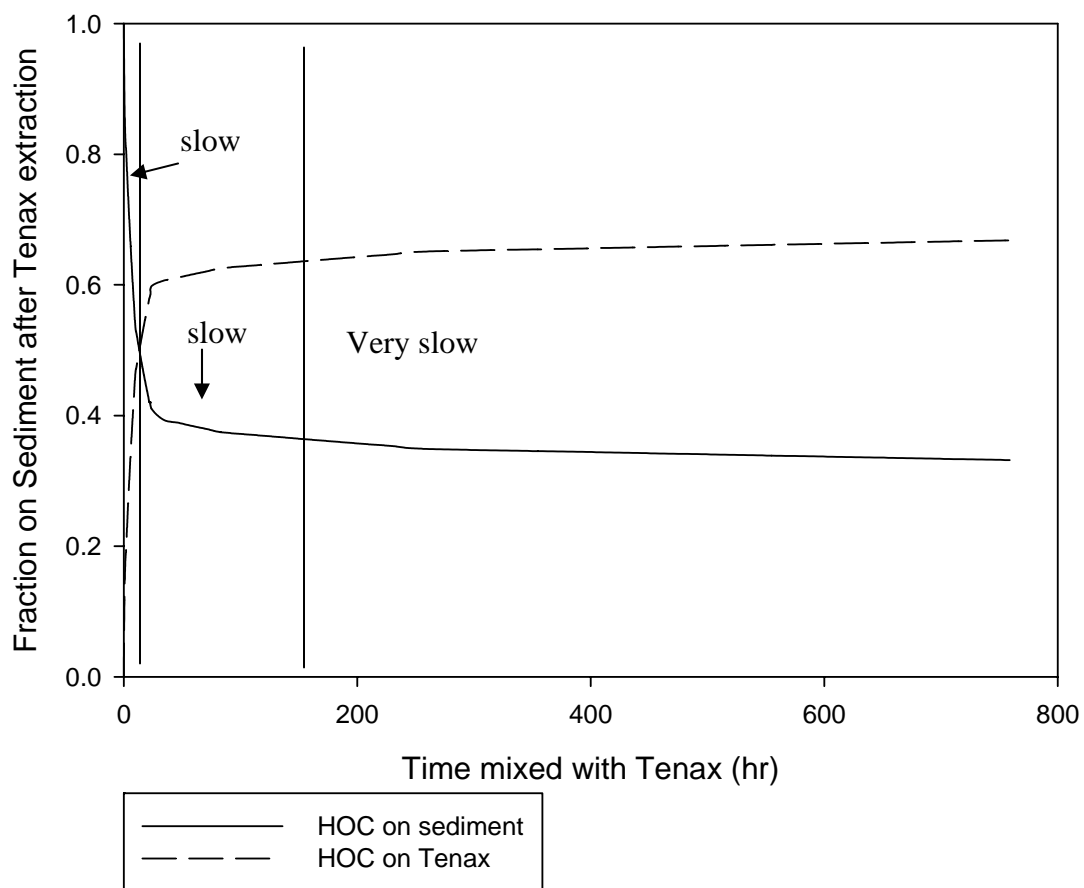


Figure 1. 6: Graph of fraction of contaminant remaining on sediment with respect to Tenax mixing time.

## **CHAPTER 2**

### **SONOCHEMICAL DEGRADATION OF NAPHTHALENE, PHENANTHRENE AND PYRENE IN AQUEOUS SOLUTION**

#### **2.1. Abstract**

The sonochemical degradation of three polycyclic aromatic hydrocarbons (PAHs), naphthalene, phenanthrene and pyrene, were investigated. Pyrene had the fastest sonolytic degradation rate compared to naphthalene and phenanthrene, a trend opposite to Henry's law and diffusion coefficients for these three compounds. Based on the degradation trend, pyrene appeared to accumulate to a greater extent at the gas/solution interface of the cavitation bubbles compared to naphthalene and phenanthrene. Once on the interface, pyrene reacts more efficiently with OH radicals compared to reactions in bulk solution, which is dependent on the diffusion of OH radicals from cavitation bubbles to bulk solution. Decreased formation of hydroxyterephthalate, a measure of bulk solution OH radical, during sonolysis in the presence of pyrene but not in the presence of naphthalene or phenanthrene was consistent with pyrene accumulation on cavitation bubble interfaces. In addition, increased bulk solution temperature and naphthalene solution concentration increased the degradation

rates of naphthalene. These two operating parameters increased the amount of naphthalene diffusing into cavitation bubbles available for pyrolysis. Finally, sonolytic degradation rate constants with 0.5  $\mu\text{M}$  each of these PAHs in a mixture were lower compared to sonolysis of aqueous solutions containing these compounds individually. Naphthalene and phenanthrene, which diffused faster than pyrene, inhibited the accumulation of pyrene at the interface. Conversely, pyrene on cavitation bubble interfaces reacted with interfacial  $\bullet\text{OH}$  decreasing  $[\bullet\text{OH}]$  in bulk solution available for reaction with naphthalene and phenanthrene.

## 2.2. Introduction

With sufficient ultrasonic intensity, during the rarefaction of ultrasound waves, bubbles are formed at the weak spots (i.e., dissolved gas, micelles) in solution<sup>25</sup>. These micron-sized bubbles undergo growth through compression and rarefaction phases, and eventually collapse at a critical size ( $R_{\text{max}}$ ), almost adiabatically producing hot spots in solution<sup>27</sup>. Average bubble temperatures of these hot spots can reach 4200 K with peak core temperatures of 17000 K and pressures of 500 atm<sup>31,68</sup>. These extreme conditions within and surrounding these bubbles give rise to three reaction sites; namely within the cavitation bubble, on gas- liquid interfaces of cavitation bubbles, and in bulk solution<sup>27</sup>. Within the cavitation bubble, high temperature and pressure combustion reactions (i.e., pyrolysis) occur. Under these conditions, the water vapor inside the bubbles undergoes dissociation to form  $\text{H}\bullet$  and  $\bullet\text{OH}$ . These radicals recombine, react with other species present in the bubbles, or diffuse outside the bubble. On bubble interfaces and in surrounding liquid, reactions occur via pyrolysis and radical



chemistry. In the bulk solution, reaction occurs via radical chemistry. These parallel pathways in ultrasonic systems are often described as<sup>31</sup>

$$-\frac{d[C]}{dt} = k_{obs} [C] = k_{\bullet OH} [\bullet OH][C] + k_{pyrolysis} [C] = k_{\bullet OH}' [C] + k_{pyrolysis} [C] \quad (2.1)$$

where  $k_{obs}$  is the observed overall first-order reaction rate constant,  $k_{pyrolysis}$  is the first-order reaction rate constant for pyrolysis within the cavitation bubble,  $k_{\bullet OH}$  is the second-order rate constant for OH radical reaction with C,  $[C]$  is the solution concentration of the compound C, and  $[\bullet OH]$  is the concentration of  $\bullet OH$ . In sonolysis reactions,  $[\bullet OH]$  is assumed to be unchanged since  $\bullet OH$  is constantly produced hence  $k_{\bullet OH} [\bullet OH]$  can be written as  $k_{\bullet OH}'$ , the pseudo first-order reaction rate constant for  $[\bullet OH]$  reactions with C.

Attempts have been made to relate the rate of degradation to various physical/chemical properties of the solute<sup>28,32,34,36,46,57,123,124</sup>. For volatile compounds such as trichloroethylene (TCE) and tetrachloromethane, studies have shown that they react primarily inside the collapsing cavitation bubbles<sup>25,34,35,39</sup> thus yielding primarily thermal decomposition or combustion byproducts<sup>28,41-44</sup>. In particular, Jiang et al. reported the formation of brown carbonaceous particles are present throughout the ultrasonic irradiation process, which are consistent with soot formation under pyrolytic conditions<sup>44</sup>. Because degradation occurs primarily inside the collapsing cavitation bubbles<sup>25,34,35,39</sup>, rate of degradation can be simplified to

$$-\frac{d[C]}{dt} \approx k_{pyrolysis} [C]_{bubble} \quad (2.2)$$

where  $[C]_{bubble}$  is the concentration of the solute in the bubble during collapse of the cavitation bubble. The concentration of the solute in the bubble ( $[C]_{bubble}$ ) was approximated by Ayyildiz et al.<sup>46</sup> from a mass balance between liquid and gas phases as

$$V_B \frac{d[C]_{bubble}}{dt_{lifetime}} = A_B K_L ([C] - [C]^*) \quad (2.3)$$

where  $V_B$  is the volume of individual bubble,  $A_B$  is the surface area of the bubble,  $K_L$  is the overall liquid phase mass transfer coefficient, and  $[C]^*$  is the hypothetical liquid phase solute concentration if the system was in equilibrium which is

$$[C]^* = \frac{[C]_{bubble}}{K_H} \quad (2.4)$$

where  $K_H$  is the Henry's law coefficient. Equation 2.3 assumes the volume of the cavitation bubble to be constant<sup>46</sup>. Ayyildiz et al.<sup>46</sup> reported that the Henry's law coefficient seemed to exert a greater influence on the sonochemical degradation rate of TCE and ethylene dibromide (EDB) compared to the diffusion coefficient and these parameters can be used to calculate partitioning of solute into the cavitation bubble (i.e.,  $[C]_{bubble}$ ) but they fall short when used for polar compounds because the dominant sonolytic degradation pathway of these compounds may include hydroxyl radical reactions<sup>46</sup>. The dependence of sonolytic degradation of volatile compounds on Henry's law coefficient was also reported by Colussi et al.<sup>32</sup> Alternatively, it was reported that for sonolysis of

volatile compounds, the degradation rate is mainly governed by the diffusion rate of the solute<sup>34,36</sup> and on vapor pressure<sup>45,125</sup>.

Sonochemical reaction for non-volatile and hydrophobic compounds occurs primarily with  $\bullet\text{OH}$ <sup>38</sup> in the bubbles and at the interfacial. Hydrophobicity<sup>28</sup>, log octanol-water partition coefficient<sup>59</sup>, surface excess<sup>60,61,126</sup>, and enrichment of the solute<sup>38,57</sup> have been used to explain the partitioning of the solute to the air-water interface. The importance of partitioning of the contaminants to the cavitation bubbles was illustrated by studies of sonolytic degradation rates of phenol and substituted phenol<sup>57,58</sup>. The sonolytic degradation rate constants of 4-nitrophenol (protonated species) appeared to be much faster than deprotonated species<sup>57</sup>. Tauber et al. suggested that the deprotonated species are unavailable for partitioning to the interface hence reaction is dominated by  $\bullet\text{OH}$  reaction in the bulk whereas the sonolytic degradation of 4-nitrophenol, the protonated species, is dominated by oxidative-pyrolytic reaction due to hydrophobic enrichment of 4-nitrophenol at the interface of the cavitation bubble<sup>57</sup>. These studies suggested that the greater the hydrophobicity of a solute, the more readily it can be expected to enter and be accumulated in the gas bubbles<sup>38</sup>.

PAHs is a group of hydrophobic and semi-volatile compounds. Therefore it is reasonable to assume that they partly degrade through thermal reactions occurring inside the bubble<sup>50</sup>. Although their sonolytic degradation potential and byproduct had been investigated in various studies<sup>48-51,127-129</sup>, the objectives of their studies were based primarily on examining the sonochemical degradation of

these compounds in different matrices (i.e., natural organic matter, purging gases)<sup>51,127</sup> and effects of instrumental parameters (i.e., pH, ultrasound intensity) on degradation rates<sup>48,129</sup>. For example, Psillakis et al. showed that the complete sonochemical degradation of naphthalene, acenaphthylene and phenanthrene was achieved in up to 120 min treatment<sup>50</sup>.

In this study, the sonolytic degradation rate constants of three PAHs (naphthalene - NAP, phenanthrene - PHEN and, pyrene – PYR) at different solution temperatures and concentrations were investigated. These compounds are the lower molecular weight members of PAHs. To our knowledge, no study has been conducted to attempt to understand how diffusion coefficient,  $K_H$ , octanol-water partition coefficient, and reactivity with  $\bullet OH$  may account for degradation kinetics of semi-volatile compounds. Understanding the degradation kinetics of PAHs is important because semi-volatile compounds may undergo sonochemical degradation within the bubble, at the interface, and in the bulk solution. We seek to relate these physical/chemical properties to trends observed for sonolytic degradation of semi-volatiles by investigating the sonolytic degradation of NAP, PHEN and, PYR in aqueous solution. NAP, PHEN and PYR were chosen because they have similar bond structures (2, 3 and 4 fused-benzene rings, respectively) and they are more soluble than other larger molecular weight PAHs and have structural similarities to many of the higher order PAHs currently recognized as being hazardous to health<sup>48</sup>. Because of their similar composition, these PAHs require similar amounts of energy to break C-C bonds during pyrolysis.

### 2.3. Experimental Methods

**Reagents.** Naphthalene (Sigma-Aldrich, > 99%), phenanthrene (Sigma-Aldrich, > 99.5%), pyrene (Sigma-Aldrich, > 99%), terephthalic acid (Fluka, > 99%), sodium phosphate (Fisher Scientific, 99.98%), sodium hydroxide (Fisher-Scientific, 98.5%) potassium phosphate (Sigma-Aldrich, > 99%) and methanol (Fisher-Scientific, HPLC grade) were used as received.

**Solution Preparation.** All glassware used was washed with water, rinsed 3 times with methanol and heated at 70°C for a minimum of 24 hours. Concentrated stock solutions of phenanthrene and pyrene, which have very low solubility in water, were prepared in methanol and stored in sealed 2 ml glass vials wrapped with Teflon tape and stored at 4°C. For the preparation of phenanthrene and pyrene working solutions, a small amount of the stock solution was transferred to a 1 L glass volumetric flask and the methanol evaporated under nitrogen at 50 psi for 4 minutes. Water, from a MilliQ water purification system ( $R = 18.2 \text{ M}\Omega \text{ cm}^{-1}$ ), was then added to the flask. For naphthalene, the stock solution was prepared by diluting 0.025 g naphthalene in MilliQ water. Working solutions of naphthalene were then diluted from this stock solution.

**Ultrasound equipment.** A 20-kHz ultrasonic direct immersion probe (model 550, Fisher Scientific), which emitted ultrasound from a  $1.20\text{-cm}^2$  area tip was used. Batch experiments for each time point were conducted with a sonicating volume of 85 mL. The total reactor volume of the glass rosette reactor was 100 mL with a neck that fitted tightly into a collar attached to the probe to provide a closed system for reaction. The reactor was equipped with a cooling jacket, allowing the

temperature to be controlled by flowing cooling water from a Fischer Scientific Isotemp 1016S cooling system through it. The reactor was wrapped in aluminum foil to prevent photo degradation. 1 mL samples were taken and filtered with 0.2  $\mu$ M Millipore filters to remove any titanium particles in solution as a result of cavitation pitting of the probe, prior to analysis. Experiments were performed in triplicate unless otherwise stated.

**Hydroxyterephthalate measurement.** Terephthalic acid (TA) was used as an  $\bullet$ OH scavenger. In the presence of  $\bullet$ OH, TA forms a compound known as Hydroxyterephthalate (HTA), a fluorescent molecule, which can be detected and measured using a Shimadzu Spectrofluorophotometer, RF 5301PC at 426 nm. Hydroxyterephthalate used for calibration was synthesized using the method outlined in Mason et al.<sup>130</sup>. This method is used frequently for measuring  $\bullet$ OH production in aqueous solution<sup>130-133</sup>. Briefly, the TA formulation involved the use of 2.2 mM terephthalic acid, 4.4 mM potassium phosphate, 6.9 mM sodium phosphate, and 5.1 mM sodium hydroxide as the  $\bullet$ OH scavenging solution. For HTA measurement in the absence of PAHs, the  $\bullet$ OH scavenging solution was used as is. For HTA measurement in the presence of phenanthrene or pyrene, the predetermined amount of phenanthrene or pyrene was placed in 1 L volumetric flask and methanol evaporated before adding the TA formulation. For HTA measurement in the presence of naphthalene, a predetermined amount of stock was placed in 1 L volumetric flask followed by TA formulation. These solutions were stirred for 24 hrs before use.

**Sonicated system.** 85 mL of working solution was placed in the 100 mL glass reactor. The reactor was sealed with a collar attached on the probe. The solution was sonicated for a specific time and stopped. A 1 mL sample was then taken for PAHs analysis. The remaining solution was discarded. The reactor was washed and rinsed with MilliQ water. For each data point, 85 mL fresh working solution was used.

**HPLC Analysis.** Samples were analyzed with a HP1100, High Performance Liquid Chromatography and a C18 Hypersil ODS column. Mobile phase used were 80% by volume acetonitrile with 20% water at a flow rate of 0.5 mL/min.

## 2.4. Results and Discussion

**Sonochemical Degradation.** Sonolytic degradation rates of 0.5  $\mu\text{M}$  initial concentrations of NAP, PHEN and PYR individually in aqueous solution was investigated at a bulk solution temperature of 34  $^{\circ}\text{C}$ . As shown in Figure 2.1 the degradation rate constant of PYR ( $k = 0.067 \pm 0.003 \text{ min}^{-1}$ ) was observed to be about 2 times faster than PHEN ( $k = 0.030 \pm 0.002 \text{ min}^{-1}$ ) and NAP ( $k = 0.032 \pm 0.004 \text{ min}^{-1}$ ). In order to explain these trends, it is important to examine some of the physical/chemical properties of these compounds.

Table 2.1 shows the Henry's law coefficient ( $K_{\text{H}}$ ), second-order reaction rate constant for reaction with  $\bullet\text{OH}$  ( $k_{\bullet\text{OH}}$ ), solubility, octanol-water partitioning coefficient ( $K_{\text{ow}}$ ), and diffusion coefficient of these three compounds. The  $K_{\text{H}}$  of NAP is 200 times larger than for PYR. Moreover, the diffusion coefficient of NAP is also larger than PYR. Given the larger  $K_{\text{H}}$  and diffusion coefficient of

NAP and PHEN, and following the studies on volatile compounds<sup>32,34,36,46</sup>, we would expect a faster degradation rate constant for NAP and PHEN compared to PYR. However, Figure 2.1 does not follow this trend. There are two possible explanations for the enhancement in the reactivity for PYR: (1) it has a much faster reaction rate via the •OH pathway and/or (2) PYR is accumulating at the interface to a greater degree than NAP and PHEN.

Reported second-order reaction rate constants<sup>134-136</sup> for these three compounds, listed in Table 2.1, are kinetically similar. This similarity in •OH reaction rates eliminates the first explanation (i.e., PYR has a faster reaction rate via the •OH pathway).

For some solutes (i.e., surfactants), surface accumulation is determined based on surface excess (i.e., reduction in surface tension)<sup>60,61,126</sup>. Attempts to measure the surface tension of pyrene at 0.5 µM showed no significant deviation from water at 20 °C (i.e.,  $71.5 \pm 0.1$  dyne/cm<sup>2</sup>) suggesting that PYR is not surface-active. However, this method may not be an accurate measure of accumulation on the interface for compounds with very low aqueous solubilities because surface tension may not be significantly impacted in the soluble region of the compound. The lack of surface tension reduction does not necessarily mean accumulation does not occur. For example, for PYR, Humphry-Baker et al. showed that pyrene molecules at saturation are indeed surface active<sup>137</sup>. In addition, the surface-bulk equilibrium partitioning constant,  $K_{sw}$ ,

$$K_{sw} = \frac{\text{surface concentration (mol m}^{-2}\text{)}}{\text{aqueous concentration (mol m}^{-3}\text{)}} \quad (2.5)$$



calculated using the equilibrium relation determined by Valsaraj<sup>138</sup> for PYR, PHEN and NAP are  $1.82 \times 10^{-4} \text{ m}^{-1}$ ,  $1.31 \times 10^{-4} \text{ m}^{-1}$  and  $4.68 \times 10^{-7} \text{ m}^{-1}$ , respectively. For the same aqueous concentration, these  $K_{sw}$  constants suggest that PYR partitions to the surface to a slightly greater extent compared to PHEN and by more than 2 orders of magnitude compared to NAP.

Although  $K_{sw}$  may be useful in explaining the faster sonolytic degradation rate constant of PYR compared to NAP, the slightly greater partitioning of PYR compared to PHEN cannot fully account for PYR having a first-order sonolytic degradation rate constant 2 times greater than PHEN. This partitioning constant ( $K_{sw}$ ) determines the equilibrium concentration on the interface. It does not provide information on the rate of accumulation on the interface.

In the case of surfactants in non-equilibrium systems, the accumulation of molecules on the interface involves the movement of molecules from the bulk solution to the subsurface layer (i.e., a layer immediately adjacent to the liquid interface, at a thickness of a few molecular diameters) followed by transfer of molecules from the subsurface to the surface<sup>139</sup>. When solutes adsorb on the interface, it will decrease the concentration on the subsurface, resulting in diffusion of solutes from the bulk solution to the subsurface<sup>139</sup>. The first step is a bulk mass transfer process dependent on the rate of diffusion of the molecules while the latter is an adsorption process<sup>139</sup>, dependent on the rate of adsorption<sup>139</sup>.

It has been suggested that aromatic hydrocarbons on the water surface are oriented parallel to the air-water interface thus implying that the greater the surface area of the molecule, the greater will be the interaction energy with the

water surface<sup>138</sup>, which affects the rate of adsorption and strength of PAH-water molecule on water interface. Following this, PYR may be forming a more stable interaction with water compared to PHEN. During bubble compression cycle, PYR adsorbed on the interface may experience greater resistance to desorb compared to PHEN due to greater interaction between PYR and water molecules on the surface. This finding is consistent with the study by Henglein and Kormann who found that the greater the hydrophobicity of the solute, the more readily it can be expected to enter and be accumulated in the gas bubbles to act as •OH scavenger<sup>38</sup>.

Hydrophobicity is characterized by the tendency of a substance to repel water or to be incapable of completely dissolving in water<sup>59</sup>. In some studies<sup>46,59</sup>, octanol-water partitioning coefficient ( $K_{ow}$ ) of the solute was used to predict hydrophobicity and the sonolytic degradation rate.  $K_{ow}$  is one of the parameters used to describe the polarity of an organic solute with the higher log  $K_{ow}$  representing more hydrophobicity<sup>46</sup>. Thus it was found that compounds with higher  $K_{ow}$  (PYR) tend to degrade faster than compounds with lower  $K_{ow}$  (PHEN)<sup>59</sup>. Following this, we expected the degradation rate of NAP to be the slowest. However, NAP exhibited statistically similar degradation rate as PHEN (Figure 2.1). This suggested that the larger  $K_H$  and diffusion coefficient for NAP maybe compensating for its lower  $K_{ow}$  compared to PHEN. This interrelated effects of  $K_{ow}$  and  $K_H$  on sonodegradation has been noted by Weavers<sup>123</sup>.

To test the validity of the hypothesis that PYR accumulated to a larger extent than PHEN and NAP on the interface, a scavenger of •OH in the bulk

solution, terephthalic acid (TA), was used. This was done with the intention of limiting the reaction of PAHs with bulk  $\bullet\text{OH}$  in order to investigate the sonolysis reaction in the bubble and on the interface.

Figure 2.2 shows the production of hydroxyterephthalate (HTA), from the reaction of TA in the bulk solution and  $\bullet\text{OH}$  produced from sonolysis at  $34^{\circ}\text{C}$  in the absence and presence of the three PAHs individually. The amount of TA (2.2mM) used in these experiments was approximately 4400 times the concentration of the PAHs ( $0.5\ \mu\text{M}$ ). Figure 2.2 shows that the production of HTA during sonolysis was unaffected by the presence of NAP and PHEN while the HTA formation in the presence of PYR during sonolysis was decreased by approximately 25%. This trend may be due to PYR reacting faster with  $\bullet\text{OH}$  compared to TA and/or PYR reacting more effectively with  $\bullet\text{OH}$  because of its accumulation on the interface. It is thus important to re-evaluate the reaction kinetics of the PAHs with  $\bullet\text{OH}$ .

From Table 2.1, the second-order rate constants of NAP, PHEN and PYR with  $\bullet\text{OH}$  are all of the same order of magnitude. If PYR reacted faster with  $\bullet\text{OH}$  in the bulk as compared to TA, NAP and PHEN would exhibit the same inhibitive effect for the production of HTA (i.e., faster reaction with  $\bullet\text{OH}$  in the bulk). However, from Figure 2.2, only the PYR solution affected HTA formation. This result suggests that the  $\bullet\text{OH}$  reactivity of PYR does not account for the reduction of HTA formation during sonolysis. Rather, PYR may be accumulating on the interface to a greater extent than NAP and PHEN, therefore enabling PYR to react

with more  $\bullet\text{OH}$  before  $\bullet\text{OH}$  diffused into the bulk solution for reaction with TA during sonolysis.

In addition, hydrophobic organic carbons (HOCs) tend to aggregate and limit their interaction with the aqueous phase<sup>140</sup>. PYR is the most hydrophobic of the three compounds and at 0.5  $\mu\text{M}$ , it is near the saturation concentration of 0.69  $\mu\text{M}$ . Therefore, it is also possible that PYR molecules forms aggregates in solution due to its higher hydrophobicity and lower solubility compared to PHEN. These aggregates are potential weak spots for the production of cavitation bubbles that can enhance degradation of PYR and production of HTA. However Figure 2.2 shows a decrease in HTA production in the presence of PYR, thus implying that PYR aggregates in solution may not be the appropriate explanation.

**Temperature Effect.** Simulated results by A.V. Prabhu et al. showed that as temperature increases (20 - 60  $^{\circ}\text{C}$ <sup>141</sup> and 1 - 50  $^{\circ}\text{C}$ <sup>142</sup>) the collapse temperature of the cavitation bubble would decrease (16483.3 – 9973.8 K<sup>141</sup>) while other studies have shown that with initial increase in solution temperature (5 - 10  $^{\circ}\text{C}$ <sup>143</sup> and 20 - 30  $^{\circ}\text{C}$ <sup>144</sup>), the rate of reaction increases (~15 % - 30% conversion of thymine<sup>144</sup>) due to a greater fraction of volatile compounds partitioning into the cavity and further increase in solution temperature (10 – 50  $^{\circ}\text{C}$ <sup>143</sup> and 30 - ~65  $^{\circ}\text{C}$ <sup>144</sup>) leads to a decrease in the rate of reaction (~13 - 5  $\mu\text{mol hr}^{-1}$  of Iodide formation @ 20 kHz and 42 W<sup>143</sup>, and ~30 % - 10 % conversion of thymine<sup>144</sup>). To provide some basis for applying sonolysis to degrade PAHs, it is beneficial to understand the effect of temperature on their rates of degradation.

Figure 2.3 shows a variation in degradation rate constant with temperature. The degradation rate constant of NAP decreased slightly with increasing temperature, the rate constant of PHEN did not change with increasing temperature while for PYR the rate constant increased and decreased. The slight decrease in degradation rate observed for NAP maybe due to additional volatilization to the overhead (20 mL) as solution temperature increased. For PYR, increasing solution temperature also implies less favorable adsorption on the air-water interface<sup>138</sup> and increased diffusivity. These two factors act to affect the accumulation of PYR on the interface differently. As the temperature increased, the increased diffusivity may contribute to more pyrene at the subsurface ready for adsorption. Thus a slight increase in degradation rate constant was observed from 19 °C to 31.5 °C. The decreased in degradation rate constant at 34 °C may be due to less favorable adsorption resulting in reduced accumulation on the interface.

Effects of increasing temperature on sonolytic degradation rate constants were also examined for PHEN and NAP at higher concentrations (~80% saturation) of 4.8 µM and 198 µM, respectively, as shown in Figure 2.4. From Figure 2.4, the rate constants for NAP and PHEN increased with increasing temperature as shown in Figure 2.4. For partitioning into the bubble, increased solution temperature allows NAP and PHEN molecules to move faster into the cavitation bubble (i.e., increase diffusivity). At higher solute concentration (~80 % saturation), more molecules will benefit from the temperature enhanced diffusivity compared to solute concentration of 0.5 µM and this may result in

increase in rate constant for NAP and PHEN with increasing solution temperature (34 °C - 19 °C). In addition, at higher solution temperature, the volatilization of NAP and PHEN may contribute to the apparent increased in degradation rate constant. Next, effect of NAP solution concentration will be investigated to determine the degradation capacity of this ultrasound system.

**Concentration effects of naphthalene.** Figure 2.5a and 2.5b show the degradation rate constants and initial degradation rates,  $kC_0$ , of NAP, respectively, with increasing NAP concentrations. Figure 2.5a shows that the degradation rate constants of NAP decreased with increasing NAP concentration while Figure 2.5b shows that the initial sonolytic degradation rate of NAP ( $k[C_0]$ ) (i.e., molecules degraded per time) increased with increasing NAP concentration.

This reduction in the degradation rate constant with increasing initial concentrations which is accompanied by an increase in degradation rates has been observed in previous studies<sup>31,50,60,145-147</sup>. The increase in initial sonolytic degradation rates can be explained by an increase in the amount of molecules migrating into the bubble for reaction as NAP concentration in solution increased (i.e., an increase in the aqueous concentration will increase the driving force of the molecules into the bubble). However, it is interesting to note that the first four points on Figure 2.5b seems to have a steeper slope than subsequent data points ( $[C_0] > 20 \mu\text{M}$ ) on the plot. This trend (Figure 2.5b) was observed by Petrier et al. (i.e., degradation rate increased linearly with phenol concentration from 0.05 mM to 0.5 mM but the degradation rate plateau slowly from 0.5 mM to 5 mM<sup>145</sup>). In addition, Serpone et al. found that the kinetics of 4-chlorophenol degradation

relation to 4-chlorophenol solution initial concentration ( $[CPOH]_i$ ) show two regimes: a low-concentration regime, and a second regime at higher concentrations where the rate displays saturation-type kinetics reminiscent of Langmuirian type behavior in solid/gas systems<sup>148</sup>.

Langmuir-Hinshelwood model is characterized by a concentration dependent regime followed by a concentration independent regime. Similarly, Figure 2.5c ( $1/k$  vs.  $[NAP]_i$ ) shows the 2 regimes with slopes of  $0.66 \mu M^{-1} \text{ min}$  and  $0.12 \mu M^{-1} \text{ min}$  indicating as  $[NAP]_i$  increases, the rate constant is less dependent on  $[NAP]_i$ . There are a number of possible explanations that can account for the saturation-type trend observed with increased  $[NAP]_i$ .

Firstly, as concentration increased, the  $\bullet OH$  pathway (i.e., from Figure 2.2, the formation of  $\bullet OH = 0.15 \mu M/\text{min}$  and from Figure 2.5b,  $k[NAP]_i = 0.46 \mu M/\text{min}$  @  $[NAP]_i = 20 \mu M$ ) may become exhausted if  $\bullet OH$  production remains constant with increasing NAP concentration. Any increase in degradation rate,  $k[NAP]_i$ , as  $[NAP]_i$  increased had to rely mainly on NAP movement into the bubble for thermolysis reaction. Without a proportional increase in degradation of NAP via  $\bullet OH$  pathway with increasing  $[NAP]_i$ , the overall degradation reaction rate cannot increase proportionally with NAP concentration in solution.

Secondly, the increased  $[NAP]_i$  translated to an increased in NAP concentration in the cavitation bubbles, thus potentially reducing the cavitation activity. For example, Drijvers et al. observed that increased vapor concentration in bubble resulted in the lowering of average specific heat ratio of the gas in the bubble<sup>25</sup> which will lower the cavitation collapse temperature. In addition,

Thompson et al. suggested that increasing vapor concentration acts to cushion bubble implosion and consequently resulted in reduced maximum temperature during bubble collapse<sup>26,50</sup>. These studies<sup>25,26,50</sup> implied that as the concentration of NAP in the bubble increased, this increased vapor concentration in the bubble and reduction of average specific heat ratio of the gas in the bubble may be sufficient to reduce the temperature of cavitation collapse. Thus increased in  $[NAP]_i$  did not result in proportional increase in rate of degradation.

**Mixtures.** In order to better understand the competitive effect of individual PAH during sonolysis, a mixture containing all three of these PAHs at 0.5  $\mu$ M initial concentrations for each individual solute was sonicated. The result is shown in figure 2.6. The order of degradation rates constant for sonolysis of this mixture is NAP, PYR and finally PHEN. From Figure 2.6, PHEN (79%) experiences the greatest reduction in the degradation rate constant compared to NAP (41%) and PYR (69%).

The reduction in sonolytic degradation of PYR may be a result of NAP and PHEN in the bubble that may compete for the  $\bullet OH$  produced in the cavitation bubble, which can migrate from the bubble to react with the PYR molecule on the interface. A reduction in this  $\bullet OH$  on the interface may substantially decrease the degradation rate constant of PYR. Moreover, NAP and PHEN migrated faster to the interface than PYR which may create resistance for PYR transfer to the interface. Conversely, for NAP and PHEN, the presence of PYR on the interface may act as a shield reducing the  $\bullet OH$  concentration in the aqueous phase hence



NAP also experienced some reduction in its degradation rates while PHEN was shown to be affected to a greater extent.

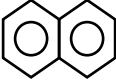
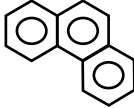

	NAP	PHEN	PYR
Structure			
Solubility ( $\mu\text{mol/L}$ ) @ 25 $^{\circ}\text{C}$ <sup>47</sup>	246.9	6.74	0.688
$K_H$ ( $\text{KPa}\cdot\text{m}^3/\text{mol}$ ) <sup>47</sup>	0.043	0.00324	0.00092
Second order $\bullet\text{OH}$ , k ( $\text{Lmol}^{-1}\text{ s}^{-1}$ ) <sup>134,136</sup>	$9.4 \times 10^9$	$2.3 \times 10^{10}$	$1.5 \times 10^{10}$
Log $K_{ow}$ <sup>47</sup>	3.34	4.25	5.08
Diffusion coefficient in water, $D_w$ ( $10^{-6}$ ) <sup>149</sup>	8.69	7.24	6.97

Table 2.1: Physical properties of NAP, PHEN and PYR.

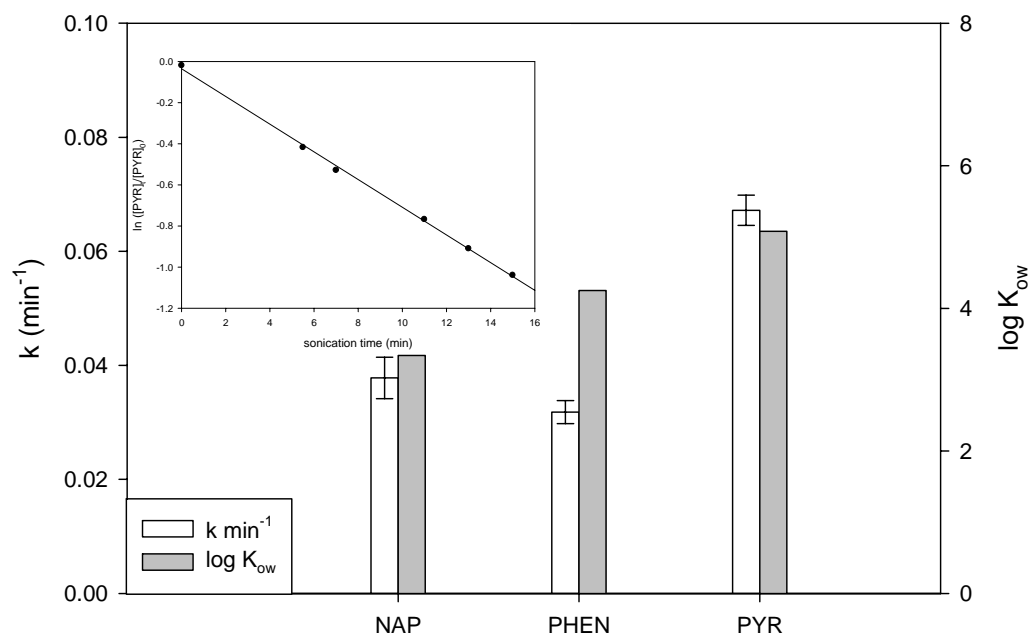


Figure 2. 1: The first-order sonolytic degradation rate constants of NAP, PHEN and PYR at 34 °C. (Sonication power = 430 W L<sup>-1</sup>, Sonicating volume = 85 mL, [C]<sub>0</sub> = 0.5 μM, error bar represents 95% confidence interval, n = 3). Inset is the 1<sup>st</sup> order plot for PYR at 34 °C.

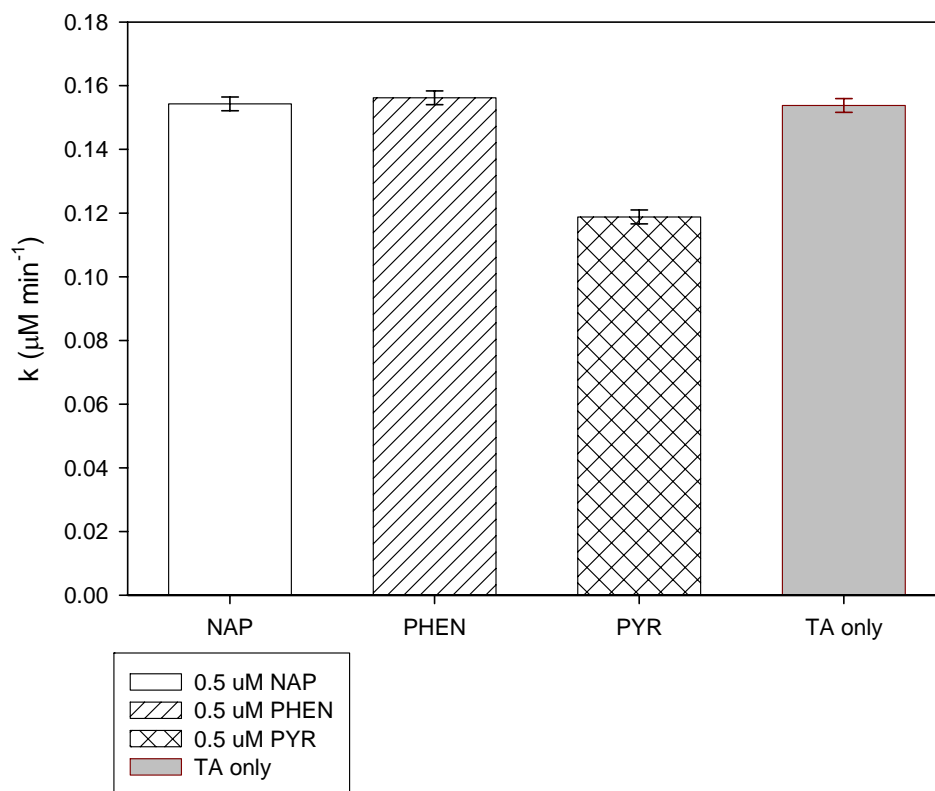


Figure 2. 2: HTA formation @ solution temperature of 34 °C with and without PAHs. (Sonication power = 430 W L<sup>-1</sup>, Sonicating volume = 85 ml, Reactor volume = 100 mL, [TA] = 2.2 mM, pH = 7.4, error bar represents 95% confidence interval, n = 3). The concentration of the HTA with time was quantified by Shimadzu Spectrofluorophotometer at 426 nm.

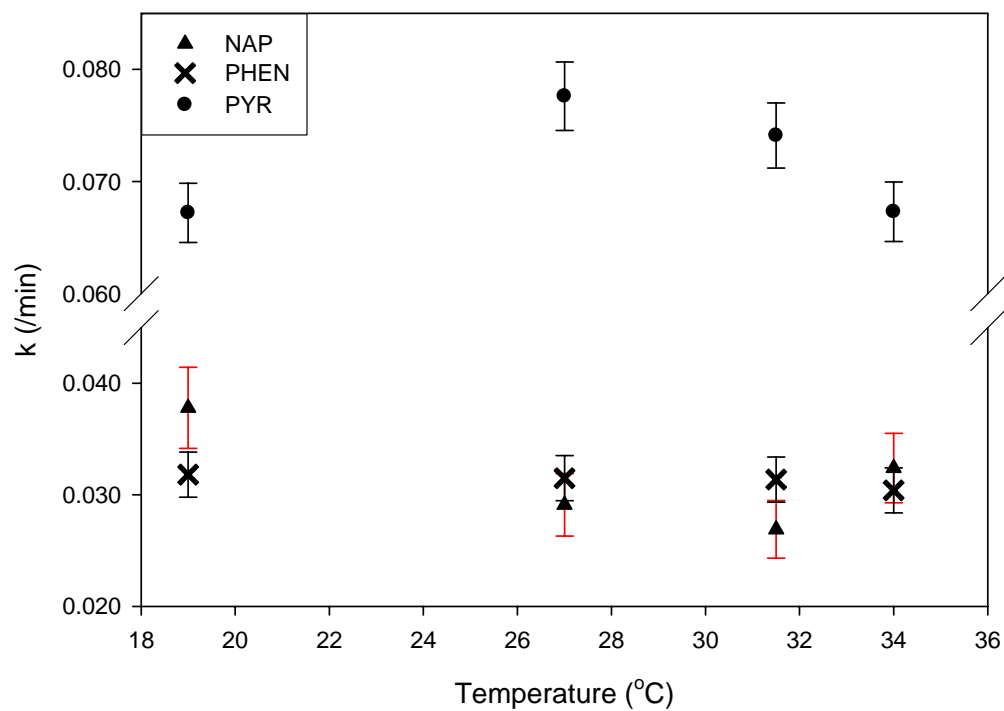


Figure 2. 3: Effect on degradation rate constants of 0.5  $\mu\text{M}$  of PAH with varying solution temperatures. (Sonication power = 430 W L<sup>-1</sup>, Sonicating volume = 85 ml, Reactor volume = 100 mL,  $[C]_0 = 0.5 \mu\text{M}$  error bar represents 95% confidence interval,  $n = 3$ ).

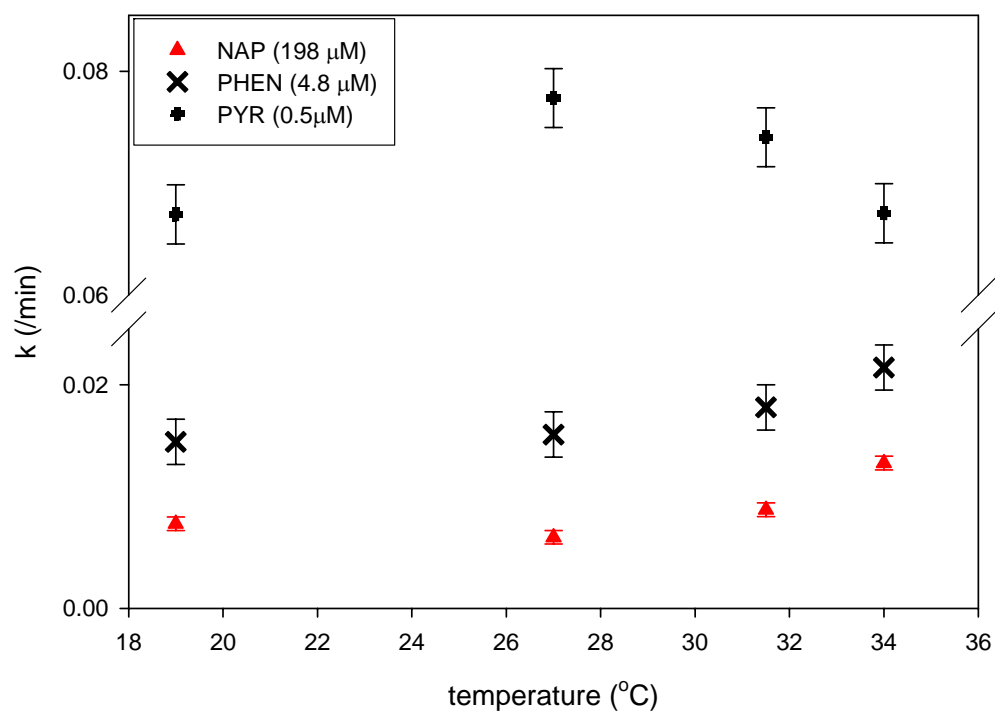
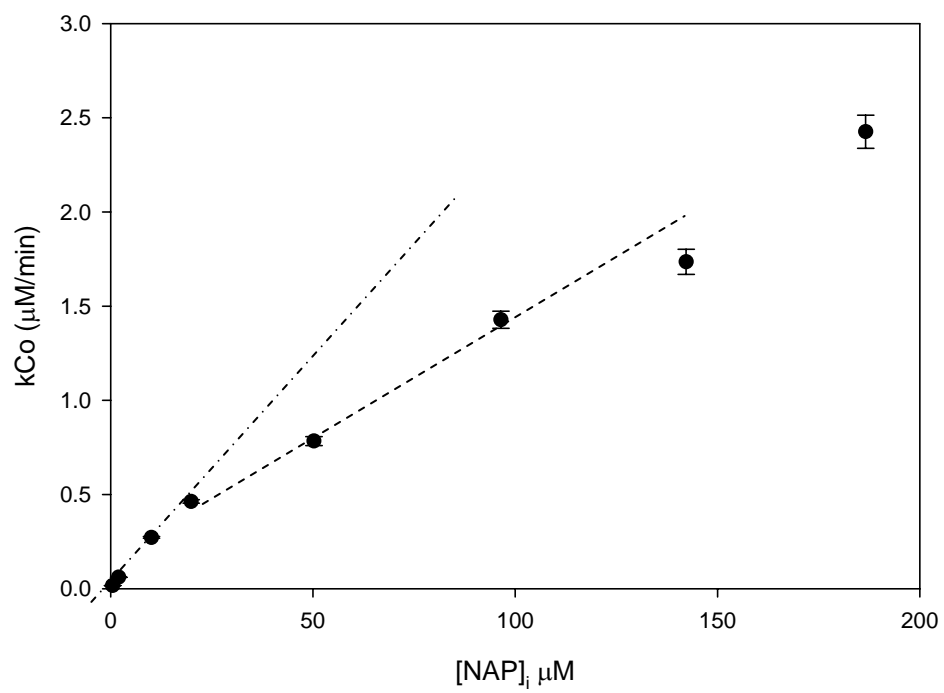
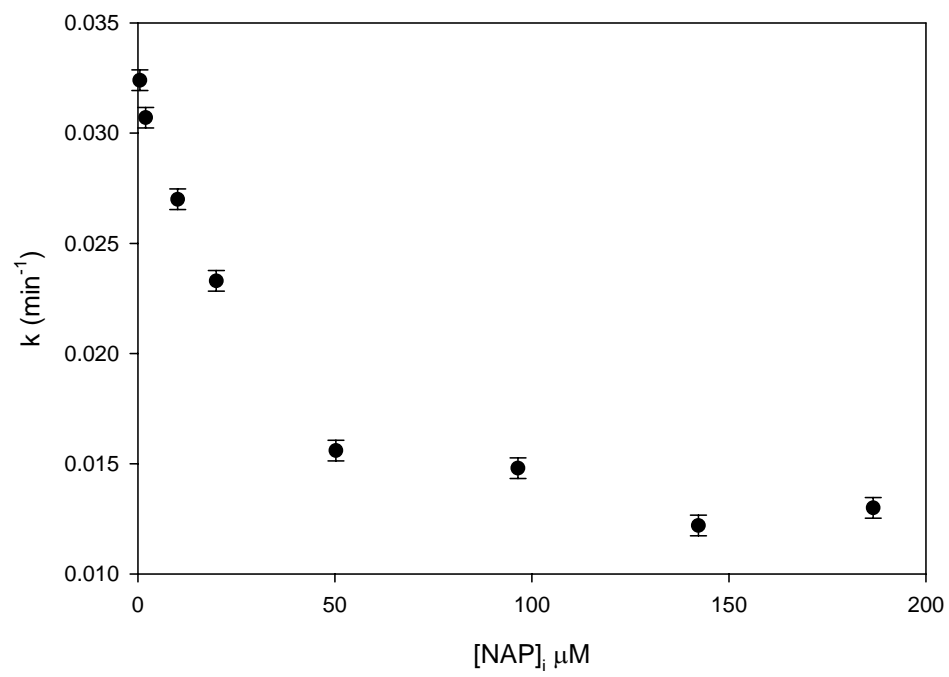
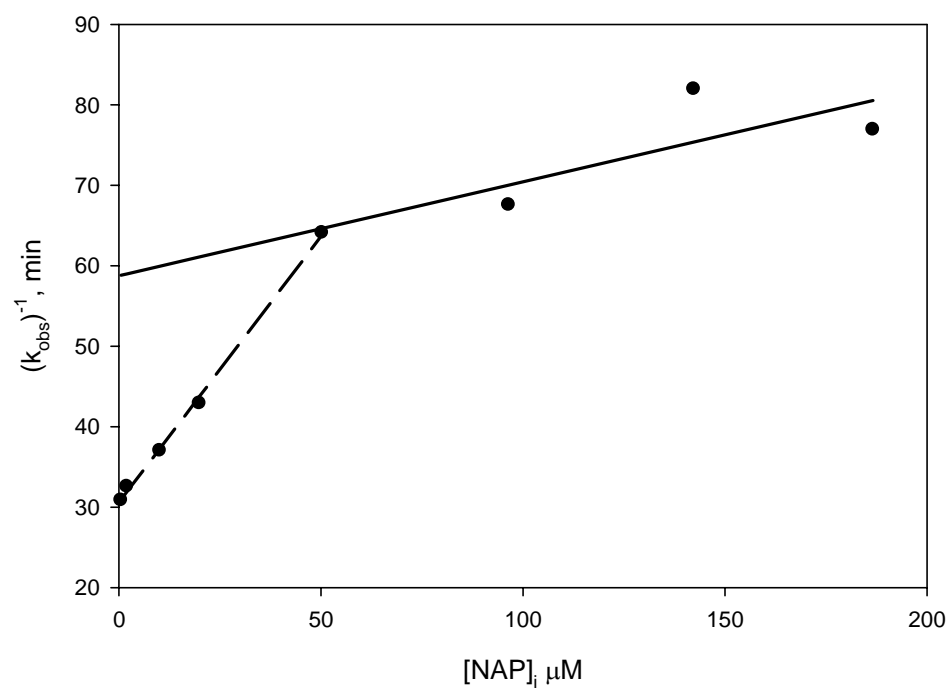


Figure 2. 4: Effect of degradation rate constants of PYR, PHEN and NAP at 80% solubility limit with varying solution temperature (Sonication power =  $430 \text{ W L}^{-1}$ , Sonicating volume = 85 ml, Reactor volume = 100 mL,  $[C]_0 = 0.80 [C]_{\text{solubility limit}}$ , error bar represents 95% confidence interval,  $n = 3$ ).

Figure 2. 5: Concentration Effect on degradation of NAP (Sonication power = 430 W L<sup>-1</sup>, Sonicating volume = 85 ml, Reactor volume = 100 mL, T = 34 °C, error bar represents 95% confidence interval, n = 3). (a) Degradation rate constants, (b) Rate of degradation with respect to concentration (c) Langmuir-Hinshelwood model.







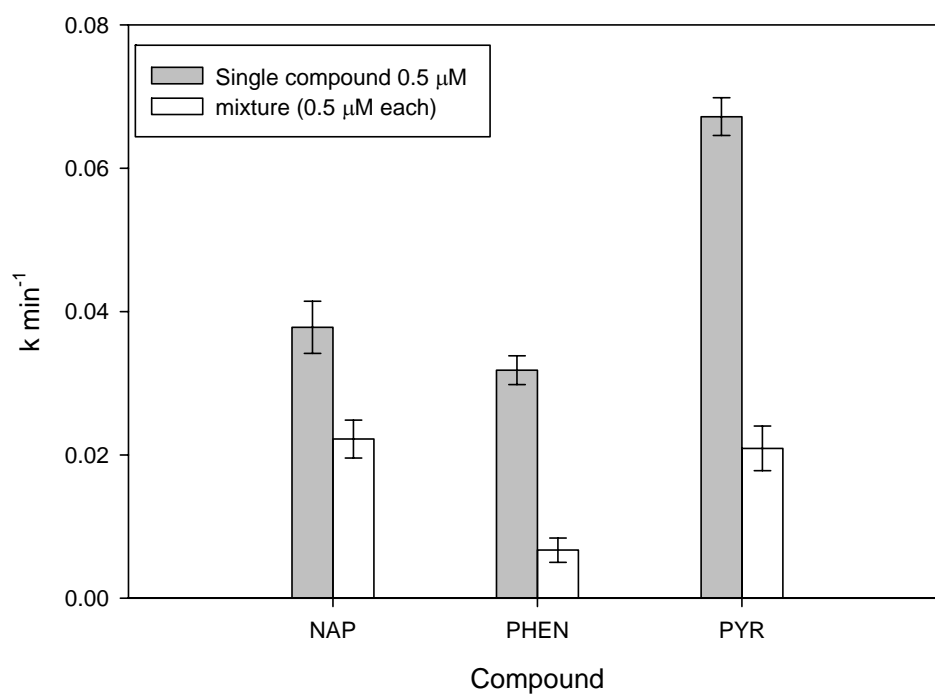


Figure 2. 6: Degradation rate constants for PAHs in a mixture and individually (Sonication power =  $430 \text{ W L}^{-1}$ , Sonicating volume = 85 ml, Reactor volume = 100 mL,  $[C]_{0,i} = 0.5 \mu\text{M}$ ,  $T = 34^\circ\text{C}$ , error bar represents 95% confidence interval,  $n = 3$ )

## CHAPTER 3

### SONOCHEMICAL TREATMENT OF POLYCYCLIC AROMATIC HYDROCARBON IN FRESHWATER SEDIMENTS

#### 3.1. Abstract

The application of ultrasound (20 kHz) for the remediation of polycyclic aromatic hydrocarbons (PAHs) in freshwater sediments was examined with the aim of exploiting ultrasound to both promote desorption of PAHs from the sediments and subsequently degrade PAHs sonolytically. After 60 min sonolysis of 12.5 g L<sup>-1</sup> of natural sediment suspended in MilliQ water, the combined solution and sediment concentrations of naphthalene, phenanthrene and pyrene extracted were reduced by 23 %, 15 %, and 23 %, respectively. A decrease in the solid-liquid ratio below 12.5 g L<sup>-1</sup> resulted in a reduction in the sonodegradation of the PAHs. This reduction was attributed to decreased particle-particle collisions and microjet formation which facilitated PAHs desorption from sediment to solution. An increase in the solid-liquid ratio above 12.5 g L<sup>-1</sup> resulted in a decrease in the sonodegradation of PAHs. This decrease was attributed to reduced ultrasonic intensity due to sound attenuation in the presence

of excess sediment particles, cavitation bubbles and/or limitations in the solubility of PAHs.

### **3.2. Introduction**

Soils and sediments contaminated by organic pollutants are of concern to the environment. Polycyclic aromatic hydrocarbons (PAHs) are among the most common contaminants in aquatic sediments<sup>1</sup>. The US EPA has classified 16 of the PAHs as priority pollutants based on toxicity, potential for human exposure and frequency of occurrence at hazardous waste sites<sup>4</sup>. Both in situ and ex situ sediment remediation technologies (e.g., bioremediation and chemical treatment) that reduce sediment contaminant concentrations require desorption of the contaminant for it to be accessible for treatment (i.e., by microbes or oxidizing agents) which typically interact with contaminants in the aqueous phase. This implies that remediation of these contaminated sediments involves a two-step process, namely mass transfer of the contaminants from the sediment into the aqueous phase, followed by degradation in the aqueous solution. However, hydrophobic organic contaminants such as PAHs become increasingly less available for desorption to the aqueous phase with residence time in soil<sup>87-90</sup>. Therefore to improve remediation effort, in this study, we propose the use of ultrasound as a technique for enhancing the rate of desorption of PAHs from two field-contaminated sediments.

Ultrasound has been shown to degrade a variety of contaminants in water<sup>23,33,150</sup>. In so-called homogeneous sonochemistry, three different reaction

sites exist: (i) High temperature and pressure (up to and above 5000 K and 1000 atmospheres, respectively) within the gaseous interiors of collapsing cavities creating localized “hot spots” for thermolysis of vaporized compounds such as water<sup>28</sup>; (ii) high temperature (ca 1000-2000 K), high temperature gradient, and high •OH concentration in the interfacial liquid surrounding the “hot spots”; and (iii) bulk solution at ambient temperature where secondary radicals and peroxide, formed during collapse, diffuse from the cavitation bubble<sup>26,27</sup>.

In addition to chemical effects, the collapse of cavitation bubbles results in a variety of physical and mechanical effects on the surface of solids which may promote desorption of PAHs from particle surfaces. In heterogeneous sonochemistry, where solid particles may exist in close vicinity to cavitation bubbles, the collapse of bubbles may occur asymmetrically depending on the size of the solids compared to the cavitation bubbles. When solids larger than 100-150  $\mu\text{m}$  are in contact with the bubbles, these asymmetric collapses will lead to the formation of microjets<sup>66,67</sup> in solution that pass through the collapsing bubbles with an estimated speed of 100m/s<sup>67</sup> and their impact on the surface of particles causes pitting and erosion<sup>26</sup>.

Symmetrical collapse of bubbles occurs away from the particles generating shockwaves that increase the momentum of solid particles in solution, causing the particles to collide with great force<sup>26</sup> (i.e. >500 km/hr<sup>66</sup>). These particles are fragmented during these collisions to produce smaller particles. Furthermore, the flow of liquid as a result of the oscillation of symmetrical bubbles gives rise to microstreaming, which creates shear stress on the particle

surface. Microstreaming and the after effect of shockwaves can enhance the rate of mass transfer near the surface of the particle<sup>26</sup>. The effects of microjets, shockwaves, and microstreaming promote particle-particle collisions, microscopic turbulence and/or thinning of the “solid-liquid film”(δ) to increase the mass-transfer coefficient ( $\tilde{k}_c$ )<sup>26</sup> (i.e., increase rate of mass transfer), produce interparticle melting<sup>67</sup>, enhance dissolution of solids<sup>26,71</sup>, change particle size and surface properties<sup>26,69</sup>, modify material structure<sup>26,72</sup>, improve the desorption kinetics of adsorbed compounds, and alter chemical equilibrium<sup>24</sup>.

The mechanical and thermal effects of cavitation described above alter the available active sites for adsorption and the number of adsorbate molecules in solution, giving rise to a new equilibrium condition<sup>151</sup>. For this reason, these mechanical effects of sonolysis have been exploited for the remediation of metal and organic contaminated sediments<sup>23,73-75,77,78,152,153</sup> and regeneration of polymeric resin<sup>154</sup> and granular activated carbon<sup>81</sup>. Ultrasound was shown to enhance the leaching<sup>152</sup> and extraction of metals<sup>153</sup> and decontaminate spiked organic contaminants on dredged sediment<sup>77</sup>, 4-chlorobiphenyl laden-synthetic alumina particles<sup>23</sup> and diesel contaminated sand<sup>78</sup>. All these studies involved spiking metal or organic contaminants onto natural sediment or synthetic particles; thus results reported may not represent realistic remediation scenarios containing contaminants aged on sediments that are increasingly less accessible with increasing residence time in soil<sup>87-90</sup>.

In this study, the sonochemical removal of naphthalene, phenanthrene and pyrene, through desorption and sonolytic degradation, from two natural

freshwater sediments was investigated. Our hypothesis was that ultrasound will improve mass transfer of PAHs aged on field-contaminated sediments into aqueous solution, hence enhancing the sonolytic degradation of these compounds following desorption. In an attempt to understand the effects of ultrasound on natural sediment properties; surface morphology, particle diameter, surface area, particle size distribution, and scanning electron microscope images were evaluated.

### **3.3. Materials and Methods**

**Reagents.** Naphthalene (Sigma-Aldrich, > 99%), phenanthrene (Sigma-Aldrich, > 99.5%), pyrene (Sigma-Aldrich, > 99%), hexane (Fisher-Scientific, HPLC grade), acetone (Fisher-Scientific, HPLC grade), dichloromethane (Fisher-Scientific, HPLC grade) and methanol (Fisher-Scientific, HPLC grade) were used as purchased. Deuterated solutions: naphthalene-d<sub>8</sub>, phenanthrene-d<sub>10</sub> and pyrene-d<sub>10</sub> were obtained through UltraScientific (North Kingstown, RI, USA). Water, from a MilliQ water purification system ( $R = 18.2 \text{ M}\Omega \text{ cm}$ ) was used in all experiments.

**Sample Preparation.** Two freshwater sediments were obtained from the Little Scioto River, Ohio (LS) and Gary, Indiana (GI). The LS site was undergoing cleanup and the GI site was an adjacent pond next to a superfund site. Both sediments were stored in a glass amber jar before air-drying on hexane-rinsed aluminum foil in the fume hood. After drying, the sediments were sieved (20 mesh screen, W.S. Tyler Company, Cleveland, Ohio). Both sediments were homogenized using an end-over-end tumbler for 1 week in the glass amber jar and

stored at 4 °C. The homogeneities of these two sediments were tested by taking random samples of the mixed sediments and analyzed using microwave extraction (method EPA 3546) for individual PAH concentrations, Malvern Mastersizer particle size analyzer for average particle size and Single point N<sub>2</sub> Brunauer-Emmett-Teller (BET) (Micromeritics® FlowSorb 2300) for particle surface area. Characteristics of these sediments are shown in Table 3.1.

**Ultrasonic System.** A 20-kHz ultrasonic direct immersion probe (model 550 manufactured by Fisher Scientific) emitting ultrasound from a tip ( $A=1.20\text{-cm}^2$ ) with power intensity measured by calorimetry to be  $430\text{ W L}^{-1}$  was used. Batch experiments were performed in a 60 mL conical shaped reactor with a neck that fitted tightly into a collar attached to the probe to provide a closed system for reaction. The aqueous volume used was 40 mL. The temperature of the 40 mL sample was kept constant (20°C) by means of an outer cooling jacket that surrounded the reactor vessel and was connected to a cooling system (model Isotemp 1016S; Fischer Scientific). The reactor was wrapped in aluminum foil as a precautionary measure to prevent photodegradation. Duplicate experiments were performed for each time point. Statistical analysis was performed using JMP® Statistical Discovery Software on these duplicate data points vs. time to obtain the range of maximum and minimum slope for degradation rates of varying solid-liquid ratios.

**Experimental procedure.** Batch experiments to investigate the effectiveness of sonolytic desorption and treatment of naphthalene, phenanthrene and pyrene from Little Scioto River, OH (LS) sediment were conducted. Initially,  $12.5\text{ gL}^{-1}$  of LS



sediment was sonicated in 40 mL of MilliQ water. At selected sonication time, the amount of each of the three PAHs in the solution ( $[PAH]_{sol,t}$ ) and on the sediment ( $[PAH]_{sed,t}$ ) were measured independently. The solid-liquid ratios were then varied ( $5.0 \text{ gL}^{-1}$ ,  $8.75 \text{ gL}^{-1}$ ,  $18.75 \text{ gL}^{-1}$  and  $25.0 \text{ gL}^{-1}$ ), sonicated and the amount of each of the PAHs in each phase quantified. The above experiment was repeated with  $12.5 \text{ gL}^{-1}$  of GI sediment.

### **Analytical Methods:**

**Calibration Standard.** Stock solutions for PAHs were prepared by dissolving the three PAHs in dichloromethane in three 10 mL volumetric flasks. These stock solutions were diluted to build the calibration curve. Deuterated naphthalene, deuterated phenanthrene, and deuterated pyrene were used as internal standards. These internal standards are assumed to behave similarly to the analogous PAH. The internal standard was prepared as follows: each ampule containing 1 mL of the deuterated PAHs were added to a 10 mL volumetric flask and diluted to 10 mL using hexane. This solution was then stored at  $4^\circ\text{C}$  to prevent volatilization of the deuterated PAHs and solvent. For all samples and calibration standard, 100  $\mu\text{L}$  of this internal standard solution was added, using a glass syringe (Hamilton, Reno, NV), for each mL of solution.

**Sample Processing.** After selected sonication times, samples (40 mL) were transferred to 50 mL Teflon centrifuge tubes and centrifuged for 10 min at 10000 rpm with a Sorvall Legend RT centrifuge (Thermo Scientific, Waltham, MA) to separate the supernatant and sediment particle fractions. 30 mL of the supernatant was removed for liquid-liquid extraction with hexane (5 mL) and the internal

standard solution (100  $\mu$ L) for 24 hrs. The hexane was then removed and concentrated to 1 mL for Gas Chromatography-Mass Spectrometry (GC-MS) analysis. Another 8 mL of the supernatant was used to measure the total organic carbon (TOC). Extraction of the sediments was performed with an Ethos EX closed microwave extraction system (Milestone, Shelton, CT, USA) equipped with 12 vessels that can withstand a pressure of 22 psi and maintain the temperature at  $\pm 1$   $^{\circ}$ C of the desired temperature. The sediment was transferred into the vessels with an equal amount of activated copper<sup>155</sup> (i.e., 0.5 g copper was added for 0.5 g sediment) to eliminate the possible interference of sulphur in the sediment. The internal standard solution (100  $\mu$ L) was added into the vessel to correct for possible losses in the extraction and concentration process. Extraction solvent (24 mL), 1:1 hexane:acetone mixture, was added to the vessel and the vessel was sealed. The extraction had a 5 min temperature ramp from room temperature to 120  $^{\circ}$ C followed by a 20 min hold at 120  $^{\circ}$ C. When completed, the vessels were removed from the microwave cavity and allowed to cool to room temperature before opening. The supernatant of the sample was removed and concentrated to 1 mL by nitrogen blow down and filtered using PTFE filters (25 mm, 45  $\mu$ m, Millipore) for analysis using GC-MS. This method was verified on Certified Reference Material (CRM) 122 (RTC, Laramie, Wyoming, USA) and Standard Reference Material (SRM) 1944 (NIST, Gaithersburg, Maryland, USA). Recoveries from Microwave extraction method (EPA 3546) were within the values reported for SRM 1944 and were above the values reported for CRM 122, which used soxhlet (EPA method 3540 C) and sonication (EPA method 3550).

**Gas Chromatography Mass Spectrometry.** Quantitative analysis of the three PAHs was performed with a gas chromatograph with ion trap mass spectrometer (Thermo-Finnigan Polaris GCQ) and a CP-5 fused silica capillary column (30 m x 250  $\mu$ m x 0.25  $\mu$ m, Varian). Helium was used as the carrier gas with a flow rate of 1.2 mL min<sup>-1</sup>. 1  $\mu$ L of the extract was injected using splitless mode. The injector temperature and ion source temperature was kept at 250 °C. The column temperature program was: 60 °C for 2 min, increased at 20 °C min<sup>-1</sup> to 250 °C, hold for 2 min, ramped at 10 °C/min to 300 °C, followed by 8 min at 300 °C. The temperature of the transfer line was kept constant at 300 °C. The mass spectrometer was operated in full scan mode (scan range 50 – 500 m/z, scan time is 0.49 s) for both calibration standards and samples from microwave extraction and liquid-liquid extraction.

**Sediment Properties.** Size distribution of the sediments was performed using a Malvern Mastersizer particle size analyzer. Single point N<sub>2</sub> Brunauer-Emmett-Teller (BET) (Micromeritics® FlowSorb 2300) was used for determining the surface area of the sediments, and scanning electron microscope (SEM) was used for surface characterization. These sets of experiments were performed independent of the experiments to examine PAH change due to treatment. During the course of ultrasonic exposure, 0.5 mL – 1.0 mL aliquots of the sediment/liquid mixture were removed from the reactor for particle size analysis following sonication. Sediments were oven dried for 2 weeks prior to BET and SEM measurements. For SEM measurement, samples were mounted on stainless steel stubs using double-stick carbon tape and sputter-coated with gold (Au).

**Control Experiments.** LS sediment at a solid-liquid ratio of 0.5 g L<sup>-1</sup> was placed in Teflon tubes on a benchtop shaker (New Brunswick Scientific, Edison, NJ), operating at 300 rpm, for 1, 2 and 6 hours. The amount of PAHs in the solution and on the solid were quantified by liquid-liquid extraction and microwave extraction followed by GC-MS. There was no significant loss in the combined amount in the solution and on the sediment for each of the three PAHs.

### 3.4. Results and Discussion

#### *Effects of sonication on amount of PAH in sediment.*

The extractable amount of each of the three PAHs remaining in the aqueous ( $n_{PAH,sol,t}$ ) and sediment phase ( $n_{PAH,sed,t}$ ) with increasing sonication time were measured and compared to the initial amount of PAH in the sediment,

$n_{PAH,i}$ . The fraction of pyrene in the aqueous phase ( $\frac{n_{PAH,sol,t}}{n_{PAH,i}}$ ), on the sediment

( $\frac{n_{PAH,sed,t}}{n_{PAH,i}}$ ) and the combined amount ( $\frac{n_{PAH,sol,t} + n_{PAH,sed,t}}{n_{PAH,i}}$ ) are shown in Figure

3.1. The pyrene fraction measured on the sediment decreased linearly with time and naphthalene and phenanthrene exhibited the same trend as shown for pyrene in Figure 3.1. The concentrations of naphthalene, phenanthrene and pyrene (i.e., 0.012  $\mu$ M, 0.010  $\mu$ M and 0.003  $\mu$ M, respectively) in solution following 10 - 60 min sonolysis were barely 1% of their combined molar amount in the aqueous solution and sediment but substantially higher than their concentrations in the aqueous phase following hydrodynamic mixing at 2 and 6 hrs ( $5 \times 10^{-4}$   $\mu$ M

naphthalene,  $3 \times 10^{-3}$   $\mu\text{M}$  phenanthrene,  $3 \times 10^{-4}$   $\mu\text{M}$  pyrene), suggesting that ultrasound was more effective at releasing PAHs compared to mechanical mixing. The combined amount ( $n_{PAH,sol,t} + n_{PAH,sed,t}$ ) of each of the three PAH in the solution and on sediment were found to decrease with sonication time. For example, at 60 min sonication, the combined mole fraction of naphthalene, phenanthrene or pyrene remaining in the aqueous phase and on the sediment was 0.76, 0.85 and 0.77 of the initial amount of PAHs on the sediment, respectively.

The higher concentrations of PAHs in solution after sonication compared to hydrodynamic mixing may result from the action of shockwaves and microjets generated during the collapse of cavitation bubbles on or in close vicinity to the sediment particles leading to enhanced bond breaking between the PAHs (adsorbate) and the sediment particles (adsorbent surface)<sup>81</sup>. He et al. showed that upon sonication, these mechanical effects released mercury very quickly from alumina particles<sup>24</sup> and Lu et al. showed that sonolysis of 4-chloro biphenyl (4-CB) laden synthetic sediment, rapidly released 4-CB into the aqueous phase<sup>23</sup>. Furthermore, Feng and Aldrich showed that sonolytic treatment of sand contaminated with diesel reduced the diesel content on the sand<sup>78</sup> and Koparal et al. showed that ultrasound is more effective than the simple mechanical stirring in Tar removal from Tar-contaminated sand<sup>79</sup>. On the basis of these studies, we expected that the equilibrium concentrations of PAHs would shift dramatically towards the aqueous phase due to improved mass transfer resulting from cavitation<sup>73</sup>.

However, the percentage of PAHs released upon sonication in this study (1%, Figure 3.1) was much less than observed for the sonolytic release of mercury (33%)<sup>24</sup> and 4-CB (i.e., 90% desorption and degradation at 20 min<sup>23</sup>) from synthetic particles. The low PAH percentage released into solution upon sonication is not attributed to the PAH reaching their solubility limits ([naphthalene] = 246.9  $\mu\text{M}$ , [phenanthrene] = 6.18  $\mu\text{M}$  and [pyrene] = 0.668  $\mu\text{M}$ <sup>47</sup>) because these three PAHs in solution after sonication were well below their solubility limits.

A possible explanation is that the PAHs desorbed and then re-adsorbed during the centrifugation step of our experiments. This hypothesis that the rate of adsorption of PAHs to natural sediment is so fast that the centrifugation time is sufficient to establish a new equilibrium in place of the sonolytic established partitioning of PAHs in solution and on sediment was tested by adding 40 mL solution containing [naphthalene] = 3.0  $\mu\text{M}$ , [phenanthrene] = 4.5  $\mu\text{M}$  and [pyrene] = 0.5  $\mu\text{M}$  to 0.50 g of Little Scioto sediment and immediately centrifuging for 10 min. We found that after centrifugation, the amount of naphthalene, phenanthrene or pyrene remaining in the aqueous phase was reduced to  $66.8 \pm 0.7 \%$ ,  $17 \pm 1 \%$ , and  $8.7 \pm 0.4 \%$  of their initial concentrations, respectively. This supports the hypothesis that the amount of PAHs measured in the aqueous phase after centrifugation does not represent the actual amount of PAHs desorbed to the aqueous phase upon sonolysis.

A second possibility that may account for the low solution concentrations of the PAHs after sonication was the ineffective release of PAHs from field-contaminated sediment compared to laboratory contaminated systems. For example, the PAHs may be sequestered by organic carbon in field-contaminated sediment. Sequestration can occur via absorption or partitioning in the organic matter (OM) and diffusion through intra-aggregate porosity<sup>89,94,156</sup> resulting in PAHs being trapped by glassy OM containing rigid cavities<sup>156</sup> and entrapped in voids created from constricted geometries<sup>157</sup>. These PAHs may be inaccessible to sonolytic activity thus low aqueous phase PAH concentrations were observed compared to the release of mercury and 4-CB from synthetic particles<sup>23,24</sup>. However, from Figure 3.1, the combined sorbed and aqueous concentrations of each PAH in aqueous phase were observed to decrease with sonolysis suggesting that some fraction of PAHs were released for sonolytic treatment in the aqueous phase.

In many previous studies, PAHs were shown to undergo sonolytic degradation in the aqueous phase<sup>48,50,51,127,129</sup>. A reduction in combined amount of the PAHs observed in Figure 3.1 may be a result of (1) ultrasonically induced occlusion as observed for mercury adsorbed on alumina particles<sup>24</sup>, rendering these PAHs unavailable for extraction, or (2) degradation of the PAHs upon sonolytic desorption. We assume that if PAHs are either degraded or occluded and non-extractable during a hexane:acetone microwave extraction at 120 °C, then this non-extractable fraction is nonlabile and “treated”. Hence in this study,

we used the term sonolytic degradation to represent the reduction in the amount of PAHs.

Next, we explored the role of the solid-liquid ratio on the rate of sonolytic degradation in the system. The sonolytic rates of degradation

$$\left( \left( \frac{d(n_{PAH, sed, t} + n_{PAH, sol, t})}{dt} \right)_{combined} \right)$$

for five different solid-liquid ratios are shown in Figure 3.2. At solid-liquid ratios below 12.5 g L<sup>-1</sup>, the sonolytic rates of degradation of naphthalene, phenanthrene and pyrene increased with increasing solid-liquid ratio (5.0 g L<sup>-1</sup>, 8.75 g L<sup>-1</sup> and 12.5 g L<sup>-1</sup>). At solid-liquid ratios above 12.5 g L<sup>-1</sup>, the sonolytic rates of degradation of phenanthrene and pyrene decrease slightly with a further increase in solid-liquid ratio (12.5 g L<sup>-1</sup>, 18.75 g L<sup>-1</sup> and 25 g L<sup>-1</sup>). A solid-liquid ratio of 12.5 g L<sup>-1</sup> appeared to be the optimum ratio for the sonolytic degradation rate. The rate of sonolytic degradation of pyrene from a second freshwater sediment, GI, at solid-liquid ratio of 12.5 g L<sup>-1</sup> is also shown in Figure 3.2. Sonolytic rate of degradation of pyrene for GI sediment is slightly lower, after taking into account statistical error, than for 12.5 g L<sup>-1</sup> LS sediment. For all solid-liquid ratios, there appeared to be sufficient turbulent mixing in the reactor.

There are a number of possible effects that can account for increasing sonolytic rates of degradation of PAHs with increasing solid-liquid ratio below 12.5 g L<sup>-1</sup>. First, the reaction is desorption limited at this solid-liquid ratio range. In other words, all PAHs that are desorbed react and if more PAHs are desorbed the treatment rate will increase. As the solid-liquid ratio is increased, the available



PAHs that may potentially be desorbed by the effect of sonication were increased. Additional PAHs that are released either undergo sonodegradation or are readsorbed onto the sediment during centrifugation. If the sonodegradation capacity of this ultrasonic system was reached, these additional PAHs that were released will completely readsorb onto the sediment. From Figure 3.2, at solid-liquid ratios below  $12.5 \text{ g L}^{-1}$ , it appeared that the sonolytic rates of degradation of pyrene increased with increasing solid-liquid ratios, suggesting that the sonodegradation capacity has not been reached.

Second, the presence of particles in solution has various effects on cavitation. It is known that particles with different acoustic impedances than the sound transmitting medium (e.g., water) act to attenuate (i.e., scatter and adsorb) sound waves<sup>68,69</sup>. Particles much larger than cavitation bubbles<sup>70</sup> (i.e., greater than  $100\text{-}150 \text{ }\mu\text{m}$ <sup>66,67</sup>) allow for the formation of microjets while particles smaller than the cavitation bubble have no effect on the bubble collapse. Particles in solution create solid-liquid interfaces with lower tensile strength than bulk solution thus allowing more bubbles to grow into active cavitation bubbles<sup>69</sup>. The opposing factors of sound attenuation and additional solid-liquid interface coexist in sonication systems in the presence of particles. Sound attenuation acts to dissipate sound waves resulting in decreased ultrasonic intensity while additional active cavitation bubbles may allow for more sonodegradation compared to a system in the absence of particles.

The Little Scioto sediment used in this study has a mean particle size of about  $75 \text{ }\mu\text{m}$  but a large portion ( $\sim 42 \%$ ) of the LS sediment has a particle

diameter greater than 100-150  $\mu\text{m}$ . The particles larger than the cavitation bubbles may be agglomerated or distinct particles that result in the formation of microjets<sup>66,67</sup>. For the concentrations in Figure 3.2, it appears that both additional nucleation sites and additional microjets occur as a result of increasing solid-liquid ratio. Further, these phenomena played a more significant role than increased sound attenuation due to the presence of more particles in suspension. This hypothesis is consistent with the observation that as the solid-liquid ratio increased from 5.0  $\text{g L}^{-1}$  to 12.5  $\text{g L}^{-1}$ , the degradation rates of the PAHs were increased.

In the presence of solid-liquid ratios above 12.5  $\text{g L}^{-1}$  (Figure 3.2), sound scattering (i.e., reduced sound intensity) by sediment particles increased such that it acted to hinder the cavitation process of the system limiting any possible benefit resulting from either increasing the amount of PAHs available to desorb or from increasing nucleation sites provided by the presence of more particles. Moreover, the solution concentration of the PAHs at any point in time during sonication may have already reached a maximum at a solid-liquid ratio of 12.5  $\text{g L}^{-1}$  and a further increase in the solid-liquid ratio cannot result in any further increase in PAH concentration in the aqueous phase. Hence the sonolytic rates of degradation of PAHs decreased for solid-liquid ratios of 12.5  $\text{g L}^{-1}$ , 18.75  $\text{g L}^{-1}$  and 25  $\text{g L}^{-1}$  because of decreased ultrasound intensity and solubility limitation of PAHs. In order to investigate the possibility that the solubility limit of the PAHs were reached for solid-liquid ratios above 12.5  $\text{g L}^{-1}$ , the total organic carbon (TOC) of the aqueous phase, which measures the amount of carbon released from the

sediment, at different solid-liquid ratios were measured and are shown in Figure 3.3.

The TOC at each solid-liquid ratio was found to increase very quickly initially and then reach a plateau. For example, for a solid-liquid ratio of  $12.5 \text{ g L}^{-1}$ , the TOC of the aqueous phase increased from  $16 \text{ mg L}^{-1}$  before sonication to  $45 \text{ mg L}^{-1}$  after 12 min sonication. After 32 min sonication, the TOC reached a plateau at  $65 \text{ mg L}^{-1}$ . This trend was observed for the other four solid –liquid ratios as well. For the five solid ratios ( $5.0 \text{ g L}^{-1}$ ,  $8.75 \text{ g L}^{-1}$ ,  $12.5 \text{ g L}^{-1}$ ,  $18.75 \text{ g L}^{-1}$  and  $25.0 \text{ g L}^{-1}$ ) investigated (Figure 3.3), the final TOC at 60 min reached 68 – 80 mg organic carbon  $\text{L}^{-1}$ , except for solid ratio of  $5.0 \text{ g L}^{-1}$  which reached a plateau at about  $40 \text{ mg organic carbon L}^{-1}$  (Figure 3.3). It was also observed from Figure 3.3 that the TOC reached a maximum faster for systems with higher solid-liquid ratios compared to systems with lower solid ratios (i.e., the time needed for TOC to reached a plateau follows the trend:  $5.0 \text{ g L}^{-1} > 8.75 \text{ g L}^{-1} > 12.5 \text{ g L}^{-1} > 18.75 \text{ g L}^{-1} > 25 \text{ g L}^{-1}$ ). This plateau in TOC may indicate saturation of dissolved organic matter (DOM), establishment of a sonolytically induced TOC equilibrium between the sediment and solution or the size of the DOM in solution was bigger than the capillary tubing equipped with our TOC analyzer, resulting in these DOM being excluded from the measured TOC values.

It is known that the sorption of hydrophobic organic contaminants (HOCs) is affected by OM<sup>92,93,158</sup> and DOM may enhance the apparent solubility of HOCs in water<sup>151</sup>. Sonication has been shown to desorb humic acid (HA) and mercury (Hg (II)) from Hg-HA laden aluminum oxide<sup>76</sup>. He et al. noted that higher

desorption of Hg (II) was associated with higher desorption of HA<sup>76</sup>. Similarly, we expect that the sonolytic desorption of PAHs from natural sediments may be correlated to the amount of OM desorbed during sonication. When TOC reaches a maximum, it may indicate that the amount of PAHs in the solution has also reached a maximum. For example, for the sonication of 12.5 g L<sup>-1</sup> LS sediment, the TOC increased from 16 mg L<sup>-1</sup> to 65 mg L<sup>-1</sup> from 0 min to 32 min sonication implying that the solution concentration of PAHs was also increasing during sonication. After 32 min sonication, the change in TOC was less significant (i.e., 60 min sonication, TOC = 68 mg L<sup>-1</sup>) suggesting that the concentration of PAHs in solution at 32 min and 60 min may be similar.

One of the important differences observed between the graphs for the different solid-liquid ratios is that after 20 min of sonication, the TOC of these systems (8.75 g L<sup>-1</sup>, 12.5 g L<sup>-1</sup>, 18.75 g L<sup>-1</sup> and 25 g L<sup>-1</sup>) did not vary greatly (~ 15 %). Assuming NOM and PAHs release similarly as was observed for HA and Hg (II) release from Hg-HA laden aluminum oxide<sup>76</sup>, the similarity in TOC for the different solid-liquid ratios may imply that PAH concentrations in the aqueous solution after 20 min sonication were similar for these four solid-liquid ratios thus this limitation and effects of sound attenuation resulted in decreased sonolytic rates of degradation for solid-liquid ratio greater than 12.5 g L<sup>-1</sup>.

Another important point to note from Figure 3.3 is that for a solid-liquid ratio of 5.0 g L<sup>-1</sup>, sonolysis appeared less effective in desorbing NOM. This may be attributed to less active nucleation sites and fewer particle-particle interactions as a result of less particles during sonolysis of 5.0 g L<sup>-1</sup> solution, therefore its

degradation rate (Figure 3.2) was also observed to be much smaller than the sonodegradation rates of 8.75 g L<sup>-1</sup>, 12.5 g L<sup>-1</sup>, 18.75 g L<sup>-1</sup> and 25 g L<sup>-1</sup> solutions.

Comparing the degradation rates of LS and GI sediments at a solid-liquid ratio of 12.5 g L<sup>-1</sup>, it was found that the degradation rate of pyrene was slightly lower for GI sediment than for LS sediment (Figure 3.2). The particle diameter of GI sediment (303 µm) was four times larger than LS sediment (75 µm) while the surface area of GI sediment (1.89 m<sup>2</sup>/g) is less than the surface area of LS sediment (4.49 m<sup>2</sup>/g) (Table 3.1). The effect that particle size has on ultrasound efficiency was investigated by Lu et al. on silica and alumina particles<sup>69</sup>. In their study, Lu et al. showed that the degradation of contaminants following desorption is expected to be highest with smaller particle sizes and particles with larger solid surface areas<sup>69</sup> as they provide the most cavitation nuclei to compensate for the detrimental effects of scattering and attenuation of sound waves by the particles. In relation to this study, LS sediment has a smaller mean particle diameter and larger surface area which may allow sonication of LS sediment solution to have more cavitation nuclei and less sound attenuation compared to GI sediment. Therefore this may account for the slightly lower sonodegradation rates with LS sediment compared to GI sediment. In addition to the particle size and surface area difference between the LS and GI sediments, the physical differences, such as organic carbon content, degree of aging of the PAHs and the nature of the NOM, in the LS and GI sediments may also affect the sonolytically induced desorption and subsequent sonochemical degradation rate of the sediments.

GI and LS sediments were found to contain  $4.0 \pm 0.2 \%$  and  $7.6 \pm 0.2 \%$  organic carbon. Higher organic content has been associated with greater sorption and formation of bound species<sup>159,160</sup> and reduction in biota-sediment accumulation factor (BSAF) model<sup>161</sup> suggesting slower rate of desorption of sorbed contaminants. Thus from the perspective of organic carbon content, the PAHs on LS sediment are expected to desorb slower than for GI sediment. From Figure 3.3, sonodegradation rate of LS sediment is higher than GI sediment, which is opposite to the trend expected for desorption based on % carbon content. In addition to organic carbon content, the sorption strength is also determined by the type of binding sites present in the sediment.

Sediment is composed of a continuum of pores ranging in size from micropores  $< 0.1 \mu\text{m}$  in diameter through to macropores  $>20 \mu\text{m}$ <sup>91</sup>, a continuum of compartments from rubbery (loose, flexible) to glassy (condensed, rigid) organic matter<sup>92,93</sup> ordered by their desorption rate constants<sup>94</sup> and degree of sorption<sup>95</sup>. The release of contaminants from these sites is often considered to occur in biphasic stages: a fast desorbing contaminant fraction in equilibrium with contaminant in solution and a slow desorbing contaminant fraction that is not in equilibrium with the contaminant in solution<sup>93,96-98</sup>.

This fast desorbing fraction consists of amorphous materials<sup>100,101</sup> and adsorption sites in the outer regions of the sediment aggregates which are in close contact with the aqueous phase<sup>97</sup> allowing for rapid and reversible desorption<sup>162</sup> and has been positively correlated to bioavailability of contaminants in sediment<sup>103,104</sup>. The relation between fast desorbing fraction and

bioavailability<sup>102,104,121,122</sup> was made because this fraction allow for fast desorption of contaminants to the aqueous phase, a step essential for uptake by biota<sup>103</sup>. The slow desorbing fraction is a result of slow diffusion of contaminants within the particles<sup>94,97,162</sup> and strongly bound sorption on carbonaceous particles which has been shown to be unavailable for biological treatment or for uptake in earthworms<sup>17,109,110</sup>. As contaminants move into the micropores or sorbed onto carbonaceous particles, it will limit the release of PAHs into the bulk liquid phase<sup>163</sup>. For example, the sorption of PAHs was observed to be 10-1000 times stronger on black carbon compared to other types of organic carbons<sup>164</sup>. There is also a third fraction of non-desorbable, (possibly) non-extractable covalently, electrostatically bound or physically entrapped contaminants<sup>99</sup>, which is considered “nonlabile”.

For PAHs with longer residence times with the sediment, a greater fraction of PAHs are sequestered by organic matter<sup>87-90</sup>. These sequestered sites may be less available for desorption by ultrasound because these pores are smaller than the size of a collapsing cavitation bubble (100  $\mu\text{m}$ <sup>66</sup>). Thus if the PAHs in GI sediment were sequestered to a greater extent, they will be less susceptible to the effect of cavitational events.

Furthermore, the nature of the NOM can also affect the binding of PAHs to the sediment and OH scavenging capacity. It was found that PAHs sorbed on carbonaceous particles (i.e., black carbon (BC), coal, and kerogen<sup>101</sup>) in sediments were strongly bound and unavailable for biological treatment or for uptake in earthworms<sup>17,109,110</sup>. Thus the effect of sonolysis to desorb PAHs may possibly be

less intense at these sites. However, as these sediments are actual field contaminated sediments, we do not have information on the time frame of PAH sequestration or the nature of the NOM in LS and GI sediments.

***Sonication effects on the size and morphology of sediment.***

As were observed in other studies for alumina particles<sup>24</sup> and metal powder<sup>66</sup>, changes in sediment size and morphology over time under the experimental conditions studied were investigated using particle size analysis and SEM to verify that ultrasound fragments and changes the surface structure of sediment. The particle size distribution of LS sediment is shown in Figure 3.4 and Figure 3.5 as a function of sonication time and solid-liquid ratio. From Figure 3.4, as the sonication time increased, the mean particle diameter decreased and conformed to a mean particle diameter of 5-8  $\mu\text{m}$ . The largest decrease in mean particle size was observed between 0 min and 6 min. As expected, the mechanical effects of ultrasound in breaking up particles seem most effective at the beginning of ultrasound application compared to longer sonication time (i.e., 6-80 min) because of the presence of a greater number of relatively large particles ( $> 100 \mu\text{m}$ ) that can induce microjets and allow for sufficient momentum during particle-particle collisions for particle fragmentation (i.e., effect of shockwaves). This reduction in mean particle diameter is further evidence that sonication exposed additional particle surfaces thus reducing the path length for the desorption of PAHs from LS sediment.



In addition to particle size distribution with sonication time, particle size distribution for solid-liquid ratios of 8.75 g L<sup>-1</sup>, 12.5 g L<sup>-1</sup>, 18.75 g L<sup>-1</sup> and 25.0 g L<sup>-1</sup> after 80 min sonication was also examined and is shown in Figure 3.5. The size distribution profiles show that solid-liquid ratios of 18.75 g L<sup>-1</sup> and 25.0 g L<sup>-1</sup> yielded more particles above 100 µm compared to a solid-liquid ratio of 12.5 g L<sup>-1</sup> after 80 min sonication. Given this trend, it appears that the degree of sound attenuation during sonication of solid-liquid ratios above 12.5 g L<sup>-1</sup> may have resulted in reduced ultrasound intensity. This reduction in ultrasound intensity at solid ratios above 12.5 g L<sup>-1</sup> may account for the reduction in degradation rates of PAHs for 18.5 g L<sup>-1</sup> and 25.0 g L<sup>-1</sup> (Figure 3.2).

The morphology of the particles was examined using SEM and is shown in Figure 3.6. Without sonication (Figure 3.6a), particles or agglomerations larger than 100 µm appear to be macroscopically smooth. With 80 min sonolysis (Figure 3.6b), the surfaces of these larger size particles or agglomeration appear rougher , which was also observed for sonication of alumina particles<sup>24</sup>.. For smaller particles (5-10 µm), the surface morphology before sonication (Figure 3.6c) and after sonication (Figure 3.6d) appear similar. These rougher surfaces observed in Figure 3.6b for sonicated particles larger than 100 µm may be a result of pitting, collision of particles, coagulation of smaller particles formed during sonication from microjets and particle-particle collisions (i.e., effect of shockwaves). For particles that are smaller (5-10 µm), the production of microjets and effective particle-particle collisions on the sediments were minimized.

The changes in morphology from smooth to rough (Figure 3.6a and 3.6b) suggested that pitting occurs on the surface of the particles allowing it to create a localized turbulent condition for desorption of PAHs from surfaces in close vicinity to the microjets. The mean particle diameter implied that there was an increased in surface area after sonication. The new surfaces created resulted in increased contact between the PAHs on the particles and the aqueous phase, thus enhancing the release of PAHs.

		LS	GI
% Dry Weight		93.0 ± 0.1	99.0 ± 0.2
BET (cm <sup>2</sup> /g)		4.49	1.89
pH		7.5	7.9
Organic carbon (%)		7.6 ± 0.2	4.0 ± 0.2
Inorganic carbon (%)		2.90 ± 0.07	1.57 ± 0.03
Particle Diameter (μm)		75	303
Concentration (nmol/g) <sup>+</sup>	Naphthalene	334 ± 22	-
	Phenanthrene	890 ± 20	-
	Pyrene	638 ± 8	606.0 ± 0.4

Table 3.1: Properties: % dry weight, surface area (BET), particle diameter and concentration of PAHs of Little Scioto (LS) and Gary, Indiana (GI).

<sup>+</sup>Concentrations are the average of triplicate values from EPA microwave extraction method 3546. % Organic carbon was calculated by taking the difference between % Total Organic and % Inorganic carbon. % Inorganic carbon was determined using EPA Methods 9060A<sup>165</sup> and % Total Organic carbon was determined using International Standard, ISO 10694:1995(E)<sup>166</sup>. PAH concentrations and carbon contents were calculated to 95% confidence interval with 6 samples and 3 samples, respectively.

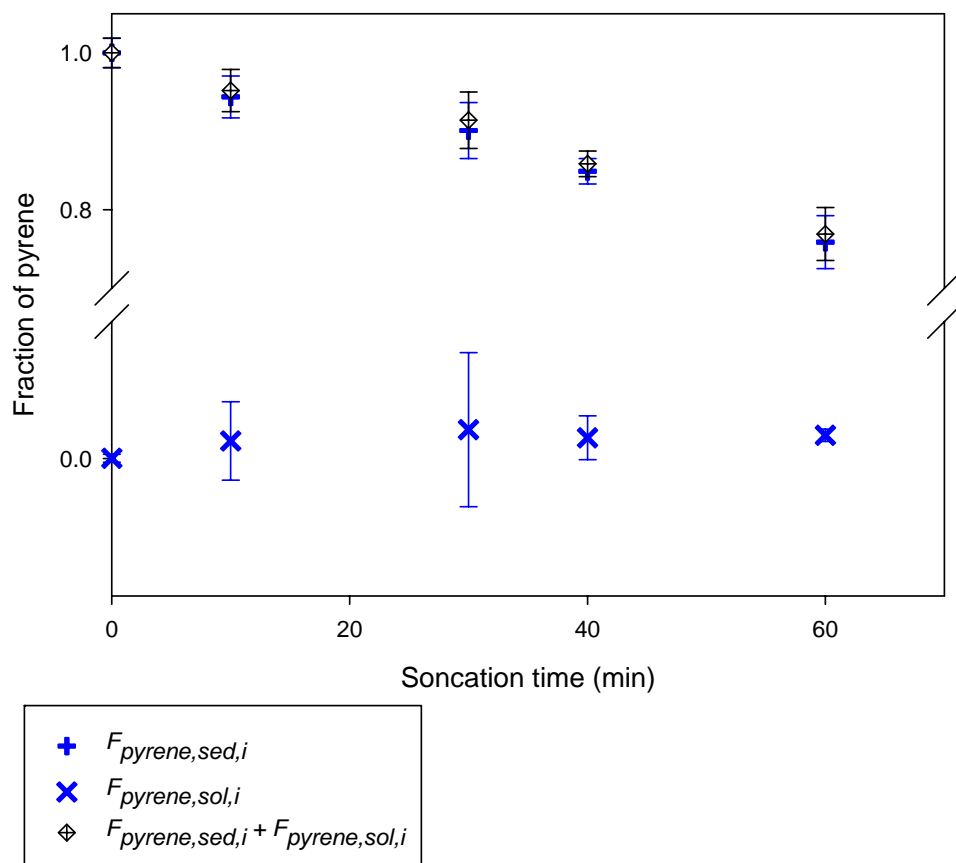


Figure 3. 1: Fraction of pyrene in aqueous phase and sediment as a function of sonication time, determined using liquid-liquid hexane extraction and microwave extraction, respectively (LS sediment,  $T = 20\text{ }^{\circ}\text{C}$ ,  $[\text{particle}] = 12.5\text{ g L}^{-1}$ ,  $[\text{Pyrene}]_{\text{initial on particle}} = 0.319\text{ }\mu\text{mol g}^{-1}$ ,  $D_0 = 75\text{ }\mu\text{m}$  ).

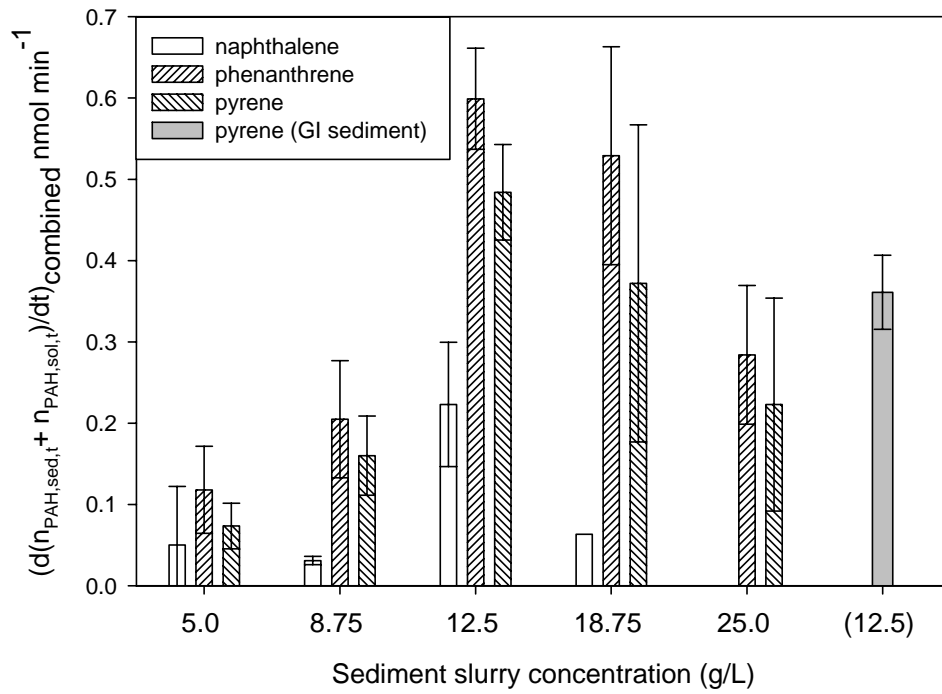


Figure 3. 2: Rate of sonodegradation of PAHs  $\left( \left( \frac{d(n_{PAH,sed,t} + n_{PAH,sol,t})}{dt} \right)_{combined} \right)$

for varying solid-liquid ratio for LS (Little Scioto, Marion, OH) and GI (Gary, Indiana) sediments. Solid-liquid ratios represent LS sediment particle concentrations unless otherwise noted. (T = 20 °C, sonication power 430 W L<sup>-1</sup>, Sonication time = 60 min, D<sub>0</sub> for LS = 75 μm, D<sub>0</sub> for GI = 303 μm).

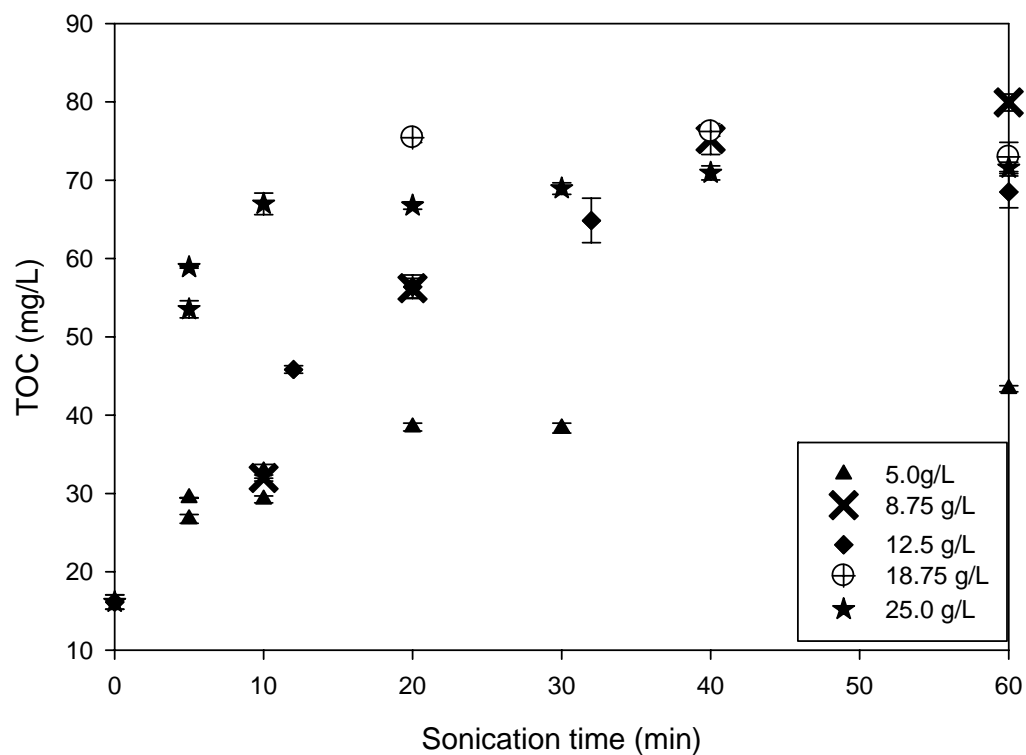


Figure 3. 3: TOC released into the aqueous phase during sonication of: (i) 5.0 g L<sup>-1</sup>, (ii) 8.75 g L<sup>-1</sup>, (iii) 12.5 g L<sup>-1</sup>, (iv) 18.75 g L<sup>-1</sup>, and (v) 25.0 g L<sup>-1</sup> solid-liquid ratio of LS sediment. The aqueous solution (8 ml) was removed from sonicated mixture after 10 min centrifugation.

Figure 3. 4: % volume of sediment with particle diameter, measured by Malvern Mastersizer, for sediment treated with different sonication time ( $T = 20\text{ }^{\circ}\text{C}$ ,  $[\text{particle}] = 12.5\text{ g L}^{-1}$ , sonication power  $430\text{ W L}^{-1}$ ,  $D_0 = 75\text{ }\mu\text{m}$ ).

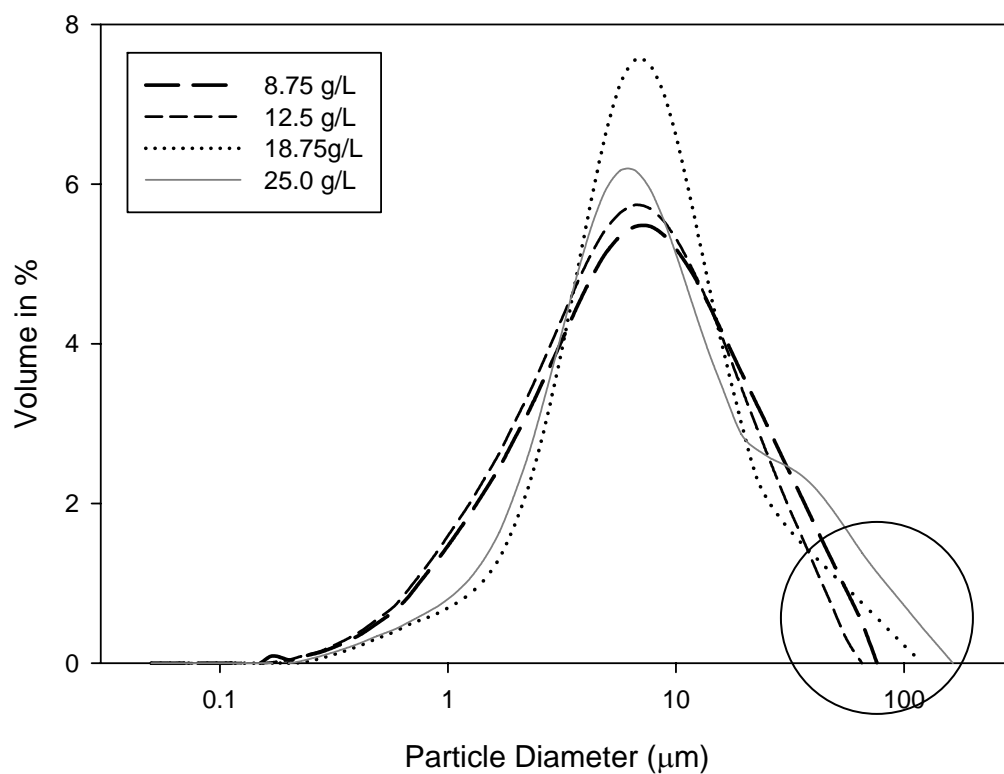
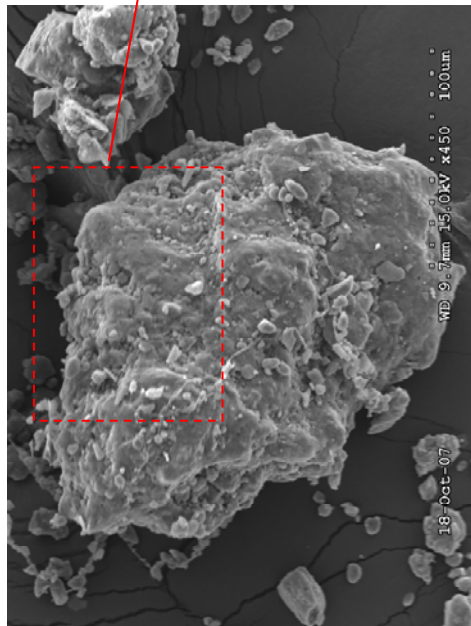
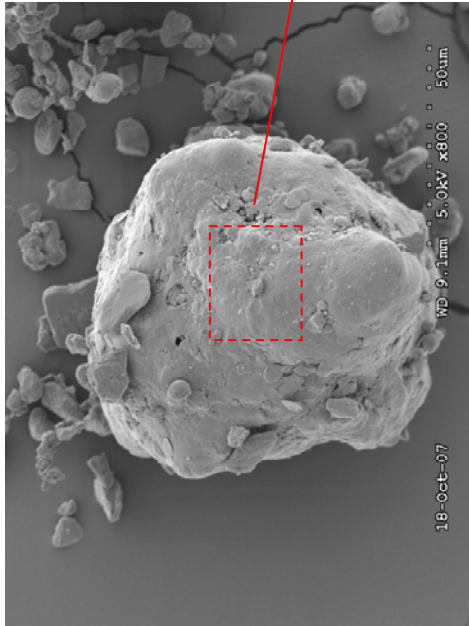
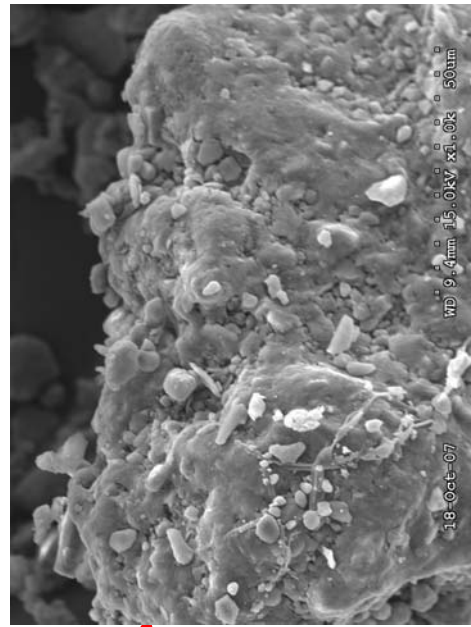
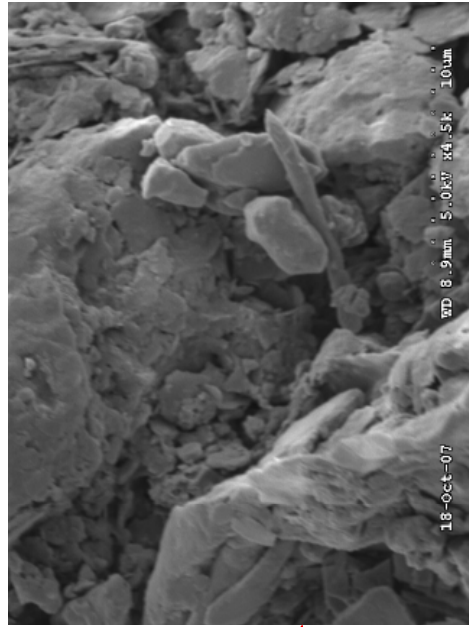


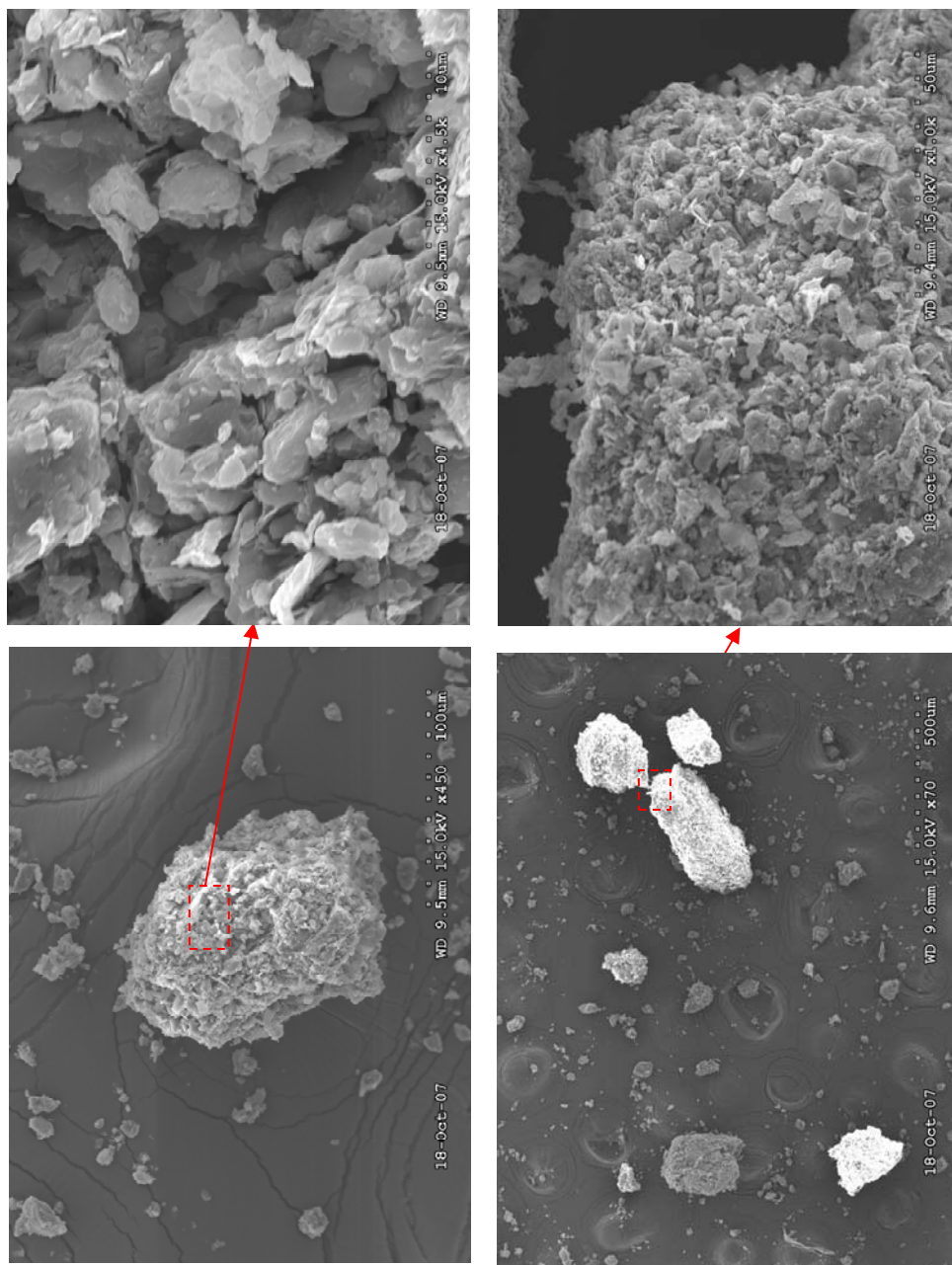
Figure 3. 5: % volume of sediment with particle diameter, measured by Malvern Mastersizer, after 80 mins sonication for various solid-liquid ratios ( $T = 20\text{ }^{\circ}\text{C}$ , sonication power  $430\text{ W L}^{-1}$ ,  $D_0 = 75\text{ }\mu\text{m}$ ).



Figure 3. 6: Particle morphology from SEM images (a) before sonication (size > 75 $\mu\text{m}$ ), (b) after 80 min sonication (size > 75 $\mu\text{m}$ ), (c) before sonication (size  $\sim 5 - 10 \mu\text{m}$ ), and (d) after 80 min sonication (size  $\sim 5 - 10 \mu\text{m}$ ). (T = 20  $^{\circ}\text{C}$ , t = 80 min, sonication power = 430 W L $^{-1}$ , D $_0$  = 75  $\mu\text{m}$ ).



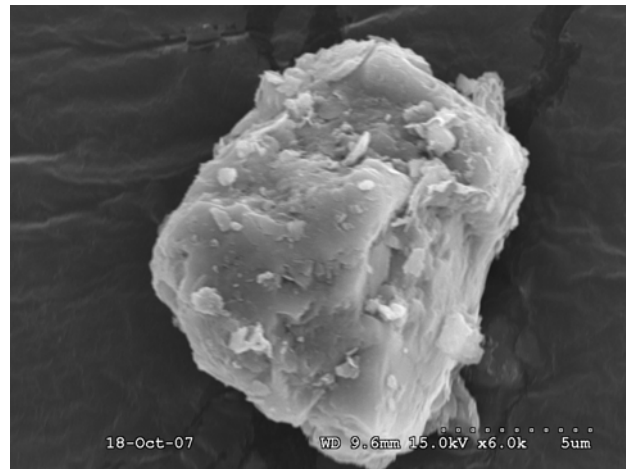
(a) Particles before sonication ( $D > 75 \mu\text{m}$ )



(b) Particles after 80 min sonication ( $D > 75 \mu\text{m}$ )



(c) Particles before sonication ( $D \sim 5 - 10 \mu\text{m}$ )



(d) Particles after 80 min sonication ( $D \sim 5 - 10 \mu\text{m}$ )

## **CHAPTER 4**

### **EFFECT OF ULTRASOUND ON THE BIOACCESSIBILITY OF PAHs ON SEDIMENT**

#### **4.1. Abstract**

The effect that ultrasound has on polycyclic aromatic hydrocarbons (PAHs), naphthalene, phenanthrene and pyrene, in fast and slow desorbing fractions on a river sediment from the Little Scioto River, Ohio was examined. After 60 min of ultrasonic treatment, the microwave extractable fraction of the PAHs in the sediment-water slurry mixture were reduced to 76%, 85% and 77% of the initial concentrations on the sediment for naphthalene, phenanthrene and pyrene, respectively. Conversely, the fast desorbing fraction of pyrene was found to increase after 20 min of sonication and then plateaus with a slight decrease at 120 min, while the increase in fast desorbing fraction of phenanthrene was less significant. Slow desorbing phenanthrene and pyrene fractions on the sediment decreased with sonication time. This result suggests that ultrasonic irradiation of sediment releases the PAHs from the slow desorbing sites. Although PAHs sorbed on the slow desorbing sites are considered the less accessible fraction, they are potential sources for PAH release and are difficult to treat using bioremediation due to limited desorption rates.

## 4.2. Introduction

Polycyclic aromatic hydrocarbons (PAHs) are among the most common contaminants in aquatic sediments<sup>1</sup>. The US EPA has classified 16 PAHs as priority pollutants based on toxicity, potential for human exposure, frequency of occurrence at hazardous waste sites, and the extent of information available<sup>4</sup>. Both in situ and ex situ sediment remediation technologies that reduce sediment contaminant concentrations require desorption of the contaminant to the aqueous phase for treatment (i.e., bioremediation)<sup>117</sup>. This implies that remediation of these contaminated sediments involves a two-step process, namely mass transfer of the contaminants from the sediment into the aqueous phase, followed by degradation in the aqueous solution. However, hydrophobic organic contaminants such as polycyclic hydrocarbons (PAHs) become increasingly less available with residence time in soil<sup>87-90</sup>.

Ultrasound has been used to enhance the leaching<sup>152</sup> and extraction of metals<sup>153</sup>, decontaminate organic contaminants spiked on dredged sediment<sup>77</sup>, release and degrade 4-chlorobiphenyl (4-CB) from humic acid laden alumina particles<sup>23</sup> and decontaminate diesel and tar contaminated<sup>78,79</sup> sand. This previous work demonstrated the ultrasonic degradation of a variety of contaminants in water<sup>23,33,150</sup>, increased mass transfer of contaminants from solids to solution<sup>26,71</sup> and removal of coatings off surfaces<sup>66</sup>.

In homogeneous sonochemistry three different reaction sites exist: (i) High temperature and pressure (up to and above 5000 K and 1000 atmospheres, respectively) within the gaseous interiors of collapsing cavities creating localized “hot spots” for thermolysis of vaporized compounds such as water<sup>28</sup>; (ii) The interfacial liquid

surrounding the “hot spot” has high temperatures (ca. 1000-2000 K), high •OH concentrations and large temperature gradients; and (iii) The bulk solution at ambient temperature where secondary radicals and peroxide, formed during collapse, diffuse from the cavitation bubble, and react with organic contaminants<sup>28</sup>.

In addition to chemical effects, the collapse of cavitation bubbles results in a variety of physical and mechanical effects on the surface of solids, which may promote desorption of PAHs from particle surfaces, an endothermic process. In heterogeneous sonochemistry, where solid particles may exist in close vicinity to cavitation bubbles, the collapse of bubbles may occur asymmetrically depending on the size of the solids compared to the cavitation bubbles. When solids are much larger than cavitation bubbles (typically 100-150 µm), asymmetric collapses will lead to the formation of microjets<sup>66,67</sup> in solution that pass through the collapsing bubbles with an estimated speed of 100m/s and their impact on the surface of particles causes pitting and erosion<sup>26,67</sup>.

The mechanical and thermal effects of cavitation described above alter the available active sites for adsorption and the number of adsorbate molecules in solution, giving rise to new equilibrium condition<sup>151</sup>. Previous studies conducted to investigate the application of ultrasound for contaminant remediation<sup>23,77,78</sup> have not considered the effect of ultrasound on altering the bioaccessibility of these contaminants.

Typically, the availability of the contaminants for biota, the bioaccumulation is measured in each sediment sample with bioassays<sup>104</sup>. However, this method is tedious and expensive<sup>104</sup>. For bioaccumulation and metabolism of the contaminants to occur, the contaminants must first desorb from sediment to the pore water<sup>104</sup>. Therefore chemically

measuring desorption rates and pore water concentrations to assess the potential for bioavailability, called bioaccessibility, has been used<sup>104,117</sup>. Techniques for measuring bioaccessibility include non-exhaustive organic solvent extraction (i.e., shaking), chemical oxidation, and aqueous based-extraction techniques<sup>117</sup>. It is accepted that it is primarily the fast (pore-water-interchangeable, water soluble, or loosely sorbed) and perhaps, slowly desorbing fractions that are available to biota<sup>117</sup>. Hence the objective of this study was to evaluate the effect of ultrasound on the bioaccessibility of PAHs using a Tenax extraction method<sup>104,122</sup>. This method is a non-exhaustive technique efficient at maintaining a maximum solid-liquid concentration gradient thus triggering further release of the slowly desorbing fraction<sup>117</sup>.

#### **4.3. Materials and Methods**

**Reagents.** Naphthalene (Sigma-Aldrich, > 99%), phenanthrene (Sigma-Aldrich, > 99.5%), pyrene (Sigma-Aldrich, > 99%), hexane (Fisher-Scientific, HPLC grade), acetone (Fisher-Scientific, HPLC grade), dichloromethane (Fisher-Scientific, HPLC grade) and methanol (Fisher-Scientific, HPLC grade) were used as purchased. Deuterated solutions: naphthalene-d<sub>8</sub>, phenanthrene-d<sub>10</sub> and pyrene-d<sub>10</sub> were obtained through UltraScientific (North Kingstown, RI, USA). Water, from a MilliQ water purification system ( $R = 18.2 \text{ M}\Omega \text{ cm}$ ) was used in all experiments.

**Sample Preparation.** Two freshwater sediment were obtained from the Little Scioto River, Ohio (LS). The LS site was undergoing cleanup. The LS sediment was stored in a glass amber jar before air-drying on hexane-rinsed aluminum foil in a fume hood. After drying, the sediments were sieved (20 mesh screen, W.S. Tyler Company, Cleveland,



Ohio). These two sediments were homogenized using an end-over-end tumbler for 1 week in a glass amber jar and stored at 4 °C. The homogeneities of these two sediments were tested by taking random samples of the mixed sediments and analyzing for individual PAH amounts, average particle size and particle surface area. The general characteristics of these sediments are shown in Table 1. The concentrations of the PAHs in the different samples were found to be within 5 % .

**Ultrasonic System.** A 20-kHz ultrasonic direct immersion probe (model 550 manufactured by Fisher Scientific) emitting ultrasound from a tip ( $A=1.20\text{-cm}^2$ ) with power intensity of  $430\text{ W L}^{-1}$  as measured by calorimetry was used. Batch experiments were performed in a 60 mL conical shaped reactor with a neck that fit tightly into a collar attached to the probe to provide a closed system for reaction. The aqueous volume used was 40 mL. The temperature of the 40 mL sample was kept constant (20°C) by means of an outer cooling jacket that surrounded the reaction vessel and was connected to a cooling system (model Isotemp 1016S; Fischer Scientific). The reactor was wrapped in aluminum foil as a precautionary measure to prevent photodegradation. Duplicate experiments were performed for each time point. Statistical analysis was performed using JMP® Statistical Discovery Software.

**Experimental procedure.** Batch experiments to investigate the effectiveness of sonolytic desorption and treatment of naphthalene, phenanthrene and pyrene from Little Scioto River, OH (LS) sediment were conducted.  $12.5\text{ gL}^{-1}$  of LS sediment was sonicated for selected times in 40 mL of MilliQ water. Following sonolysis, the amounts of each of the three PAHs in the solution ( $n_{PAH,sol,t}$ ) and on the sediment ( $n_{PAH,sed,t}$ ) were measured

independently. For bioaccessibility measurements, the sonicated samples were poured directly into 100 mL separation funnels.

**Bioaccessibility using Tenax beads.** Tenax beads have been used previously to evaluate the bioaccessibility of HOCs<sup>95,97,102,104,121,167</sup>. These studies indicated that the Tenax extracted HOC concentration is positively correlated to the bioavailability of sediment<sup>102</sup>. In particular, the bioaccessibility of PAHs on sediment was evaluated using the Tenax extraction method by Cornelissen et al., and Macrae and Hall<sup>103,168</sup>. Tenax extraction method was used as a measure of the bioaccessibility of PAHs in the sediments with and without treatment.

The steps used in our experiments were modified from the method used by Cornelissen et al. to investigate the desorption kinetics of PAHs<sup>97</sup>. After a selected sonication time, the resultant sediment/PAC-water mixture was transferred to a 100 mL separation funnel. 30 mL of MilliQ water was used to rinse the sediment from the reactor into the funnel (i.e., total aqueous volume = 70 mL). 1 g of Tenax beads was weighed and added into the funnel. The separation funnel was sealed and placed on a benchtop shaker (New Brunswick Scientific, Edison, NJ), at 300 rpm to ensure that the sediment and Tenax beads were well-dispersed. Tenax was removed for extraction after 6 hr. Separation of sediment from Tenax was achieved by allowing the sediment to sink to the bottom of the funnel and opening the tap for the sediment to flow out. Tenax beads remained in the funnel due to buoyancy and were washed with 5 mL of MilliQ water to remove any remaining sediment. Next, the water was drained. Finally, the beads were flushed from the funnel using 20 mL hexane and collected in a 25 mL Teflon centrifuge tube. 100  $\mu$ L of the deuterated internal standard was added and the resultant hexane-

Tenax mixture was shaken for 24 hr at 300 rpm to extract the PAHs. The hexane fraction was then removed using a disposable glass pipette. This hexane fraction was blown-down to 1 mL using nitrogen gas prior to quantitative analysis.

#### **Analytical Methods:**

**Calibration Standard.** Stock solutions for PAHs were prepared by dissolving the three PAHs in dichloromethane in three 10 mL volumetric flasks. These stock solutions were diluted to build the calibration curve. Deuterated naphthalene, deuterated phenanthrene, and deuterated pyrene were used as internal standards. These internal standards are assumed to behave similarly to the analogous PAH. The internal standard was prepared as follows: each ampule containing 1 mL of the deuterated PAHs were added to a 10 mL volumetric flask and diluted to 10 mL using hexane. This solution was then stored at 4 °C to prevent volatilization of the deuterated PAHs and solvent. For all samples and calibration standard, 100 µL of this internal standard solution was added, using a glass syringe (Hamilton, Reno, NV), for each mL of solution.

**Sample Processing.** After selected sonication times, the sample (40 mL) was transferred to a 50 mL Teflon centrifuge tube and centrifuged for 10 min at 10000 rpm with a Sorvall Legend RT centrifuge (Thermo Scientific, Waltham, MA) to separate the supernatant and sediment particle fractions. 30 mL of the supernatant was removed for liquid-liquid extraction with hexane (5 mL) and the internal standard solution (100 µL) for 24 hrs. The hexane was then removed and concentrated to 1 mL for Gas Chromatography-Mass Spectrometry (GC-MS) analysis. Another 8 mL of the supernatant was used for total organic carbon (TOC) measurement. Extraction of the sediments was performed with an Ethos EX closed microwave extraction system (Milestone, Shelton, CT, USA) equipped

with 12 vessels that can withstand a pressure of 22 psi and maintain the temperature at  $\pm 1$  °C of the desired temperature. The sediment was transferred into the vessels with equal amount of activated copper <sup>155</sup> to eliminate the possible interference of sulphur in the sediment. The internal standard solution (100  $\mu$ L) was added into the vessel to correct for possible losses in the extraction and concentration process. Extraction solvent (24 mL), 1:1 hexane:acetone mixture, was added to the vessel and the vessel was sealed. The extraction had a 5 min temperature ramp from room temperature to 120 °C followed by a 20 min hold at 120 °C. When completed, the vessels were removed from the microwave cavity and allowed to cool to room temperature before opening. The supernatant of the sample was removed and concentrated to 1 mL by nitrogen blow down and filtered using PTFE filters (25 mm, 45  $\mu$ m, Millipore) for analysis using GC-MS. This method was verified on Certified Reference Material (CRM) 122 (RTC, Laramie, Wyoming, USA) and Standard Reference Material (SRM) 1944 (NIST, Gaithersburg, Maryland, USA). Recoveries from Microwave extraction method (EPA 3546) was within the values reported for SRM 1944 and were above the values reported for CRM 122, which used soxhlet (EPA method 3540 C) and sonication (EPA method 3550).

**Gas Chromatography Mass Spectrometry.** Quantitative analysis of the three PAHs was performed with a gas chromatograph with ion trap mass spectrometer (Thermo-Finnigan Polaris GCQ) and a CP-5 fused silica capillary column (30 m x 250  $\mu$ m x 0.25  $\mu$ m, Varian). Helium was used as the carrier gas with a flow rate of 1.2 mL min<sup>-1</sup>. 1  $\mu$ L of the extract was injected using splitless mode. The injector temperature and ion source temperature was kept at 250 °C. The column temperature program was: 60 °C for 2 min, increased at 20 °C min<sup>-1</sup> to 250 °C, hold for 2 min, ramped at 10 °C min<sup>-1</sup> to 300 °C,

followed by 8 min at 300 °C. The temperature of the transfer line was kept constant at 300 °C. The mass spectrometer was operated in full scan mode (scan range 50 – 500 m/z, scan time is 0.49 s) for both calibration standards and samples from microwave extraction and liquid-liquid extraction.

**Sediment Properties.** Size distribution of the sediments was performed using a Malvern Mastersizer particle size analyzer. Single point N<sub>2</sub> Brunauer-Emmett-Teller (BET) (Micromeritics® FlowSorb 2300) surface area analyzer was used for determining the surface area of the sediments. These sets of experiments were performed independent of the experiments to examine PAH change due to treatment. Sediments were sonicated for the selected time and oven dried for 2 weeks prior to BET measurements.

**Control Experiments.** LS sediment at solid-liquid ratio of 0.5 g L<sup>-1</sup> was placed in Teflon tubes on a benchtop shaker (New Brunswick Scientific, Edison, NJ), operating at 300 rpm, for 1, 2 and 6 hours. The PAH amounts in the solution and on the solid were quantified by liquid-liquid extraction and microwave extraction followed by GC-MS. There was no significant loss in the combined amount in the solution and on the sediment for each of the three PAHs.

#### 4.4. Result and Discussion

##### *Sonochemical desorption and degradation of naphthalene, phenanthrene and pyrene.*

The extractable amounts (nmol) of each of the three PAHs remaining in the aqueous ( $n_{PAH,sol,i}$ ) or sediment phase ( $n_{PAH, sed,i}$ ) with increasing sonication time were measured and shown in Figure 4.1 (a), 4.2 (a) and 4.3 (a). The fraction of each of the PAHs in

aqueous phase ( $F_{aq} = \frac{n_{PAH,sol,t}}{n_{PAH,i}}$ ,  $n_{PAH,i}$  is the microwave extracted amount of PAH in

sediment before sonolysis), on the sediment ( $F_{sed} = \frac{n_{PAH,sed,t}}{n_{PAH,i}}$ ) and combined fraction

( $F_{comb} = \frac{n_{PAH,sol,t} + n_{PAH,sed,t}}{n_{PAH,i}}$ ) are shown in Figures 4.1 (b), 4.2 (b) and 4.3 (b). The  $F_{aq}$  for

the three PAHs were less than 1 % of  $F_{comb}$  for the sonication time investigated with the majority of the PAHs found on the sediment. After 60 min sonication, the  $F_{comb}$  of naphthalene, phenanthrene or pyrene remaining in the aqueous phase and on the sediment was 0.76, 0.85 and 0.77 of the initial amount of PAHs on 0.5 g of sediment, respectively.

It is well- known that sonication of compounds in aqueous solution results in degradation<sup>48,50,51,127-129</sup>. For example, Psillakis et al. showed that the complete sonochemical degradation of naphthalene, acenaphthylene and phenanthrene was achieved in up to 120 min treatment<sup>50</sup> and byproduct from sonolysis of phenanthrene was phenanthrene diol suggesting that the reaction pathway to involved hydrogen abstraction reactions from the hydrocarbon skeleton<sup>28,51</sup>. However, in the presence of other organic compounds (i.e., benzoic acid, humic acid, fulvic acid, pentane, pentanol), the degradation of phenanthrene, anthracene, and pyrene were reduced<sup>127,128</sup>.

In addition to the sonodegradation of organic compounds in aqueous solution, the degradation of 4-chlorobiphenyl (4-CB) sorbed on humic acid laden alumina particles<sup>23</sup> and occlusion of mercury by alumina<sup>24</sup> has also been observed after sonolysis. When particles are added to the solution, the collapse of bubbles may occur symmetrically or asymmetrically depending on the proximity and size of the particles compared to the

cavitation bubbles. Collapse of cavitation bubble produces shockwaves, microstreaming and microjets.

Shockwaves generated during cavitation collapse in close vicinity to sediment particles cause nearby particles to move away from the cavitational event in a radial direction with great speed<sup>65</sup> resulting in particle-particle collisions ( $> 500 \text{ kmhr}^{-1}$  <sup>66</sup>). These collisions between the particles have been shown to produce interparticle melting<sup>67</sup> and agglomeration of zinc particles<sup>66</sup>. Acoustic microstreaming has been shown to enhance the mass and heat transfer at interfacial films surrounding nearby adsorbent particles and within the pores<sup>62</sup>. Microjets occur on the surfaces of solid particles that are several orders of magnitude larger than the bubble<sup>65</sup> result in pitting and surface cleaning. Thus the reduction in combined fraction of the PAHs may be due to (1) ultrasonically induced occlusion resulting from the physical effects of sonication (observed for mercury adsorbed on alumina particles<sup>24</sup>), rendering these PAHs unavailable for extraction, or (2) degradation of the PAHs upon sonolytic desorption.

**Bioaccessibility.** The contact time between sediment-PAH (i.e., aging) is one of the most critical bioavailability factors governing the fate and transport of PAHs in sediment<sup>87</sup>. Sediment is composed of a continuum of pores ranging in size from micropores  $< 0.1 \text{ }\mu\text{m}$  in diameter through to macropores  $> 20 \text{ }\mu\text{m}$ <sup>91</sup>, a continuum of compartments (i.e., rubbery (loose, flexible) to glassy (condensed, rigid) organic matter<sup>92,93</sup>) ordered by their desorption rate constants<sup>94</sup> and degree of sorption<sup>95</sup>. The release of contaminants from these sites is often considered to occur in biphasic stages: a fast desorbing contaminant fraction in equilibrium with contaminant in solution and a slow desorbing contaminant fraction that is not in equilibrium with the contaminant in solution<sup>93,96-98</sup>.

This fast desorbing fraction consists of amorphous materials<sup>100,101</sup> and adsorption sites in the outer regions of the sediment aggregates which are in close contact with the aqueous phase<sup>97</sup> allowing for rapid and reversible desorption<sup>162</sup> and has been positively correlated to bioavailability of contaminants in sediment<sup>103,104</sup>. The relation between fast desorbing fraction and bioavailability<sup>102,104,121,122</sup> was made because this fraction allows for fast desorption of contaminants to the aqueous phase which is essential for uptake by biota<sup>103</sup>. The slow desorbing fraction is a result of slow diffusion of contaminants within the particles<sup>94,97,162</sup> and strongly bound sorption on carbonaceous particles which has been shown to be unavailable for biological treatment or for uptake in earthworms<sup>17,109,110</sup>. As contaminants move into the micropores or sorbed onto carbonaceous particles, it will limit the release of PAHs into the bulk liquid phase<sup>163</sup>. For example, the sorption of PAHs was observed to be 10-1000 times stronger on black carbon compared to other types of organic carbons<sup>164</sup>. There is also a third fraction of non-desorbable, (possibly) non-extractable covalently, electrostatically bound or physically entrapped contaminants<sup>99</sup>, which is considered “nonlabile”.

Although the combined amount (in the sediment-water system) for each of the PAHs decreased with sonication time, mechanical and thermal effects of cavitation will alter the available active sites for adsorption and the number of adsorbate molecules in solution, giving rise to new equilibrium conditions<sup>151</sup> of PAHs between the sediment and aqueous phase. This sonolytically induced equilibrium condition was observed in enhanced release of 4-chlorobiphenyl from humic acid laden-alumina particles<sup>23</sup>, reduction in the diesel and tar content on the sand contaminated with diesel<sup>78</sup> and tar<sup>79</sup>, increase rate of desorption of p-chlorophenol from granular activated carbon<sup>81</sup> and more



effective removed p-terphenyl from synthetic dredged sediments<sup>77</sup> after sonication. In particular, ultrasound was found to enhance the release of mercury from humic acid laden-alumina particles compared to both that from hydrodynamic mixing and that expected on the basis of the mercury sorption isotherm<sup>24</sup>. However, these studies did not evaluate the bioaccessibility of these new equilibrium condition, thus next, we will evaluate the bioaccessibility (i.e., the amount of contaminant released from soil making it available for adsorption) of PAHs after sonolysis.

In this study, the distribution of PAHs in the sediment was represented by

$$n_{Total} = n_{fast} + n_{slow} + n_{nonlabile} \quad (4.1)$$

where  $n_{Total}$  is the total amount ( $\mu\text{mol}$ ) of PAH on sediment,  $n_{fast}$  is the amount of PAH in the fast desorbing fraction ( $\mu\text{mol}$ ) that was measured using Tenax extraction,  $n_{slow}$  is the slow desorbing fraction that represents the PAHs that is more strongly bound to the sediment ( $\mu\text{mol}$ ) but can be release to the aqueous phase slowly, and  $n_{nonlabile}$  is the amount of PAHs that is non-desorbable, (possibly) non-extractable fraction comprising of covalently and electrostatically bound PAHs, as well as physically entrapped PAHs<sup>99,117</sup>.

Microwave extraction used in this study is likely going to underestimate  $n_{Total}$  because it cannot extract PAHs that are covalently, electrostatically bound and entrapped. Thus we rewrote the above equation as

$$n_{extracted} = n_{fast} + n_{slow} \quad (4.2)$$

where  $n_{extracted}$  is the moles of PAH measured through microwave extraction.

**Effect of Ultrasound on Bioaccessibility.** Ultrasonic irradiation was performed on sediment at selected times and the rapidly desorbing fraction ( $n_{fast}$ ) of the PAHs was

measured using 1.0 g Tenax beads mixed for 6 hrs<sup>102,104</sup> with the sonicated sediment.

Figure 4.4 shows the bioaccessible fraction extracted by 6 hr Tenax

$$(F_{fast} = \left( \frac{[PAH \text{ on Tenax}]_t}{n_{extracted}} \right)) \text{ where } [PAH \text{ on Tenax}]_t \text{ is the amount of PAH extracted by}$$

Tenax after sonolysis time  $t$ . From Figure 4.4, pyrene has a highest  $F_{fast}$  of the three PAHs examined. The  $F_{fast}$  follows the trend of the octanol-water partitioning coefficient ( $\log K_{ow}$ ). The  $\log K_{ow}$  of pyrene is 5.08<sup>47</sup>, phenanthrene is 4.25<sup>47</sup> and naphthalene is 3.34<sup>47</sup>.  $K_{ow}$  is characterized by partitioning between aqueous and organic, lipid-like phases and it provides a significant indication of the amount an organic compound will be taken up by aquatic organisms<sup>169</sup>. Organic compounds with high values of  $K_{ow}$  tend to be hydrophobic and hence partition to organic matter, lipids (fat) and soil<sup>169</sup> and  $K_{ow}$  has been correlated to bioaccumulation<sup>170</sup>.

Tenax beads are a hydrophobic substrate that can be used for determining the bioaccumulation potential of organic compounds<sup>102,104,122</sup>. Therefore contaminants found to have higher bioaccumulation in organic matter, lipids and soil will also have higher partitioning to the Tenax beads. Accordingly pyrene was observed to have the highest accumulation on Tenax (i.e.,  $F_{fast}$ ) followed by phenanthrene and naphthalene. This higher bioaccessibility of pyrene compared to phenanthrene was also observed by Cornelissen et al.<sup>103</sup> in the three sediments they studied.

Next a mass balance was performed to examine changes in  $F_{fast}$  and  $F_{slow}$  fractions with sonication time. We assumed the decrease in the microwave extractable fraction was a result of sonodegradation (Figures 4.1, 4.2 and 4.3). This assumption is valid because if the PAHs were not extractable using microwave extraction at 120 °C with

hexane/acetone, it is reasonable to assume these PAHs to be nonlabile and treated. To incorporate the effect of sonolytic degradation, the mass balance for the system can be rewritten as

$$(n_{\text{extracted}} - n_{\text{degraded}}) = n_{\text{fast}} + n_{\text{slow}} \quad (4.3)$$

where  $n_{\text{degraded}}$  is the amount ( $\mu\text{mol}$ ) of phenanthrene or pyrene degraded which was determined through

$$n_{\text{degraded}} = kt \quad (4.4)$$

where  $k$  is the degradation rate of naphthalene, phenanthrene and pyrene calculated using JMP® statistical model to be  $0.22 \pm 0.08$  nmol/min,  $0.60 \pm 0.06$  nmol/min and  $0.48 \pm 0.06$  nmol/min, respectively, from Figures 4.1, 4.2 and 4.3. The  $n_{\text{slow}}$  is then calculated using

$$n_{\text{slow}} = (n_{\text{extracted}} - n_{\text{degraded}}) - n_{\text{fast}} \quad (4.5)$$

Figures 4.5a and 4.6a show the amount:  $n_{\text{degraded}}$ ,  $n_{\text{fast}}$ ,  $n_{\text{slow}}$ , and  $(n_{\text{fast}} + n_{\text{slow}})$  and

Figures 4.5b and 4.6b show their corresponding fractions:  $F_{\text{degraded}} \left( \frac{n_{\text{degraded}}}{n_{\text{extracted}}} \right)$ ,  $F_{\text{fast}}$

$\left( \frac{n_{\text{fast}}}{n_{\text{extracted}}} \right)$  and  $F_{\text{slow}} \left( \frac{n_{\text{slow}}}{n_{\text{extracted}}} \right)$  of phenanthrene and pyrene at 0 min, 20 min, 40 min, 60

min and 120 min. The graph for naphthalene is not shown because the error associated with calculated  $F_{\text{slow}}$  was too large (i.e., ~40% mostly contributed by error in  $k$ ) to observe any trend in  $F_{\text{slow}}$ . The  $F_{\text{fast}}$  of phenanthrene and pyrene increased at 20 min then plateaus with a slight at 120 min sonication time while the  $F_{\text{slow}}$  decreased with time. The changed in  $F_{\text{fast}}$  and  $F_{\text{slow}}$  of phenanthrene was less significant than pyrene. For example,

for pyrene, the  $F_{fast}$  increased from  $0.43 \pm 0.01$  at 0 min to  $0.62 \pm 0.01$  after 20 min sonication and  $F_{slow}$  decreased from  $0.57 \pm 0.07$  to  $0.31 \pm 0.04$ . At long sonication times (e.g., 120 min), the  $F_{fast}$  of pyrene plateau with a slight decrease ( $0.64 \pm 0.02$  at 60 min to  $0.59 \pm 0.02$  at 120 min sonication) and  $F_{slow}$  decreased from  $0.18 \pm 0.02$  at 60 min to  $0.049 \pm 0.006$ .

The plateau in  $F_{fast}$  and decrease in  $F_{slow}$  are attributed to sonolytic degradation of PAHs. The increase in the  $F_{fast}$  of pyrene in sediment during 20 min sonolysis may be a result of sonolytic desorption of PAHs from slow sites of the sediment (i.e., not extracted by 6 hr Tenax mixing time) as a result of increased localized turbulence in the solid-liquid film<sup>65</sup> and increased solubility in supercritical fluid at cavitation site<sup>26</sup>. Phenanthrene and pyrene that were released, if not degraded by sonolytic reaction, can be re-adsorbed on the surface of the particle, which is the shortest path length for re-adsorption. In addition, ultrasound irradiation of particles has been shown to increase interfacial area through interparticle collisions and pitting as a result of microjets<sup>26,65</sup>. The average particle diameter of the sediment was found to decrease from 75  $\mu\text{m}$  to approximately 9  $\mu\text{m}$  within 6 min sonication time indicating exposure of new surfaces. These newly exposed areas may be the slow desorption sites covered by agglomeration of particles. By allowing these sites to be in direct contact with the aqueous phase, the path length for desorption is greatly reduced. Both of these effects can contribute to increase in  $F_{fast}$ .

At 120 min,  $36.1 \pm 0.5$  % reduction in pyrene amount from initial microwave extraction value was observed. If total amount of pyrene released from the slow sites after 120 min sonolysis was less than this  $36.1 \pm 0.5$  %, an apparent decrease in the  $F_{fast}$

of the sediment will be observed. This indicated that the amount of PAHs that can be sonolytically desorbed or exposed from slow desorbing sites can be exhausted. Some sequestered sites may be unavailable for desorption by physical effects of cavitation collapse because their pores are smaller than the size of a collapsing cavitation bubble ( $100\text{ }\mu\text{m}^{66}$ ). When PAHs can no longer be desorb from sites cavitation bubble can access, a reduction in  $F_{fast}$  may be observed. In fact, we observed a slight decrease in  $F_{fast}$  at 120 min sonication for pyrene. This  $F_{fast}$  decrease occurred when  $F_{slow}$  was a small proportion of the total pyrene remaining, approximately 0.42.  $F_{slow}$  remained a high proportion of the phenanthrene fraction after 120 min sonication (0.59). Correspondingly,  $F_{fast}$  was not observed to decrease even after 120 min sonication for phenanthrene

Although  $F_{fast}$  after sonication was not less than  $F_{fast}$  before sonication, the slow desorbing fractions ( $F_{slow}$ ) of phenanthrene and pyrene decreased with sonication time (Figure 4.5 and 4.6) because sonolysis can desorb or expose PAHs from the less accessible sites for sonodegradation and re-adsorption on more accessible sites. These results suggest that  $F_{slow}$  is either preferentially degraded over  $F_{fast}$  or  $F_{slow}$  is transformed into  $F_{fast}$  over sonication, thus increasing  $F_{fast}$  and  $F_{fast}$  is fraction undergoing sonolytic degradation. These PAHs on the slow phase can make complete remediation difficult<sup>98</sup>, are unavailable for biological treatment or for uptake in earthworms<sup>17,109,110</sup> and may have a significant impact on the long-term fate and exposure of soil/sediment bound organic contaminants<sup>101</sup>. Therefore, the potential of decreasing this desorbing fraction using sonolysis is important for more complete remediation of contaminated sediment.

		LS
% Dry Weight		93.0 ± 0.1
BET (cm <sup>2</sup> /g)		4.49
pH		7.5
Organic carbon (%)		7.6 ± 0.2
Inorganic carbon (%)		2.90 ± 0.07
Particle Diameter (μm)		75
Concentration (nmol/g) <sup>+</sup>	Naphthalene	334 ± 22
	Phenanthrene	890 ± 20
	Pyrene	638 ± 8

Table 4. 1: Properties: % dry weight, surface area (BET), particle diameter and concentration of PAHs of Little Scioto.

<sup>+</sup> Concentrations are the average of triplicate values from EPA microwave extraction method 3546. % Organic carbon was calculated by taking the difference between % Total Organic and % Inorganic carbon. % Inorganic carbon was determined using EPA Methods 9060A<sup>165</sup> and % Total Organic carbon was determined using International Standard, ISO 10694:1995(E)<sup>166</sup>. Concentration and carbon contents were calculated to 95% confidence interval with triplicate samples.

Figure 4. 1: (a) Naphthalene (nmol) in aqueous solution and on sediment after selected ultrasonic exposure time; (b) the fraction of naphthalene in aqueous phase and sediment as a function of US time, determined using liquid-liquid hexane extraction and microwave extraction, respectively ( $T = 20\text{ }^{\circ}\text{C}$ ,  $[\text{particle}] = 12.5\text{ g L}^{-1}$ ,  $[\text{Naphthalene}]_{\text{initial on particle}} = 167\text{ nmol g}^{-1}$ ,  $D_0 = 75\text{ }\mu\text{m}$  ). The fraction of naphthalene is calculated through dividing total nmol of naphthalene in aqueous or sediment after sonolysis by total nmol of naphthalene in 0.50 g LS sediment before sonication.

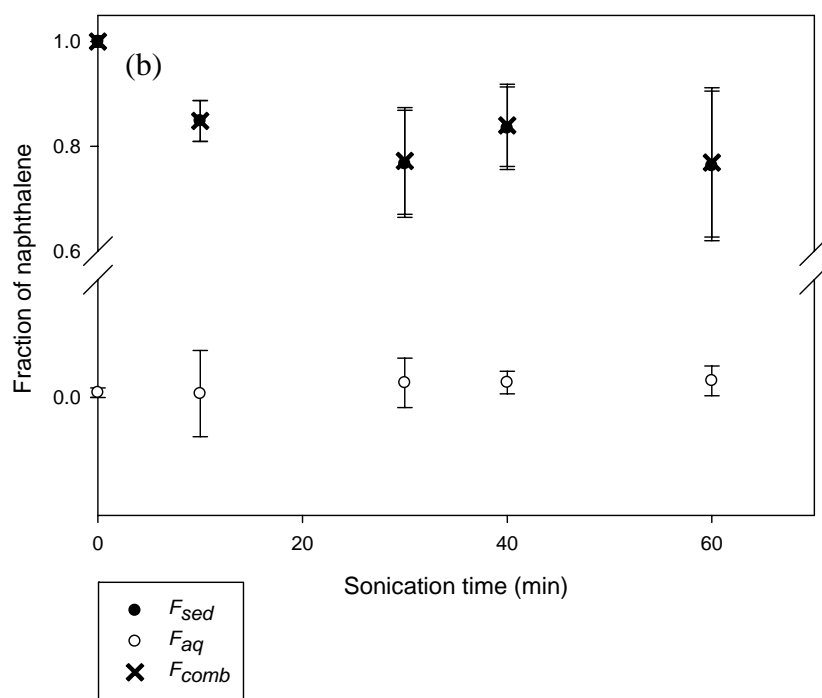
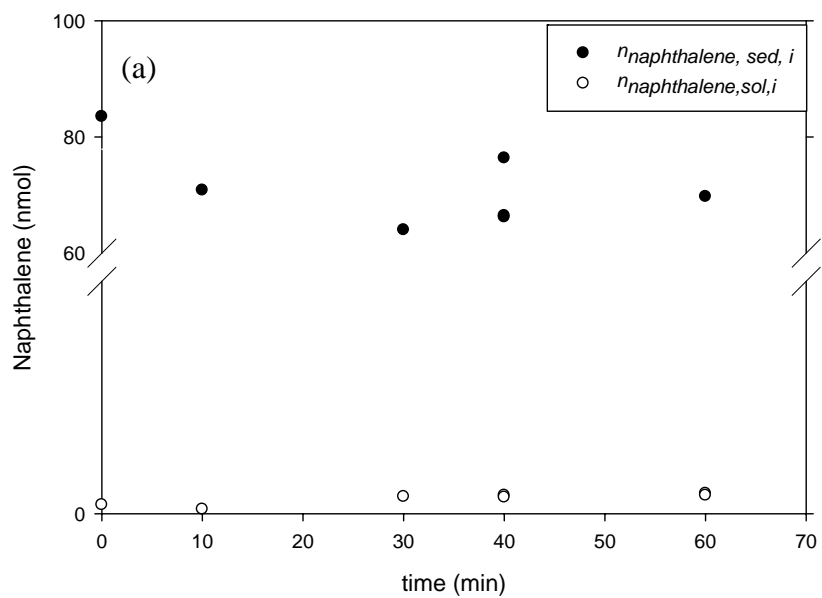




Figure 4. 2: Phenanthrene (nmol) in aqueous solution and on sediment after selected ultrasonic exposure time; (b) the fraction of phenanthrene in aqueous phase and sediment as a function of US time ( $T = 20\text{ }^{\circ}\text{C}$ ,  $[\text{particle}] = 12.5\text{ g L}^{-1}$ ,  $[\text{Phenanthrene}]_{\text{initial on particle}} = 446\text{ nmol g}^{-1}$ ,  $D_0 = 75\text{ }\mu\text{m}$  ).

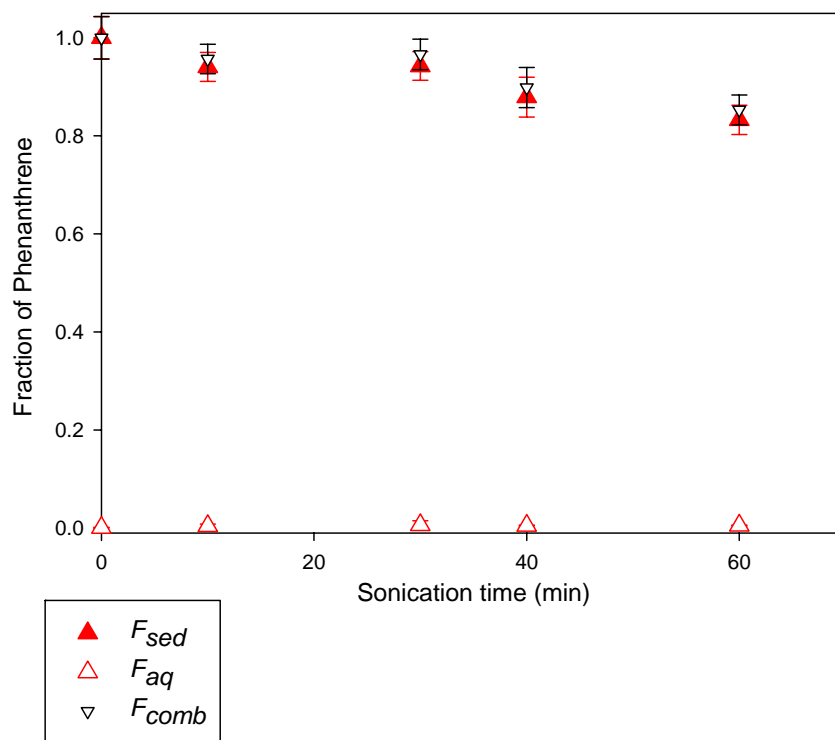
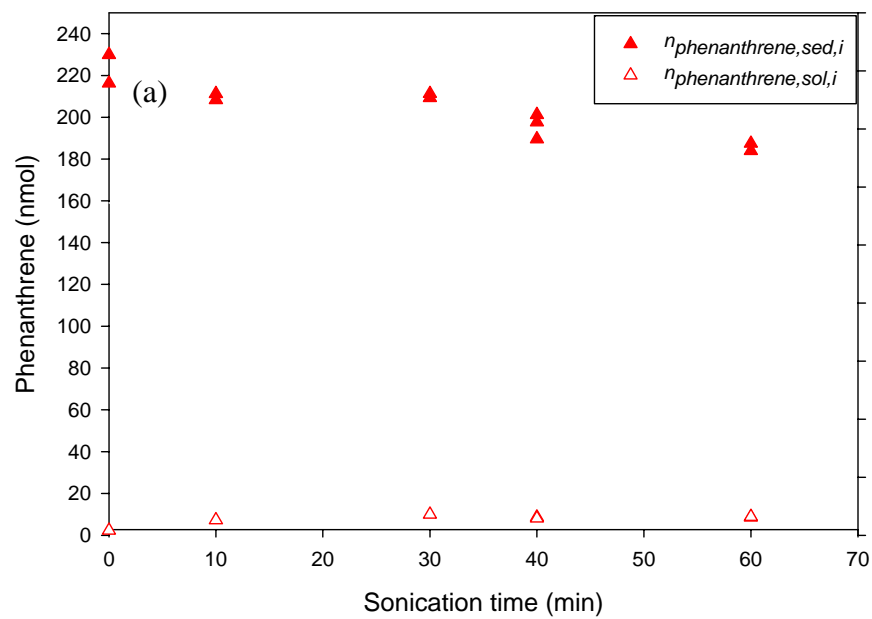
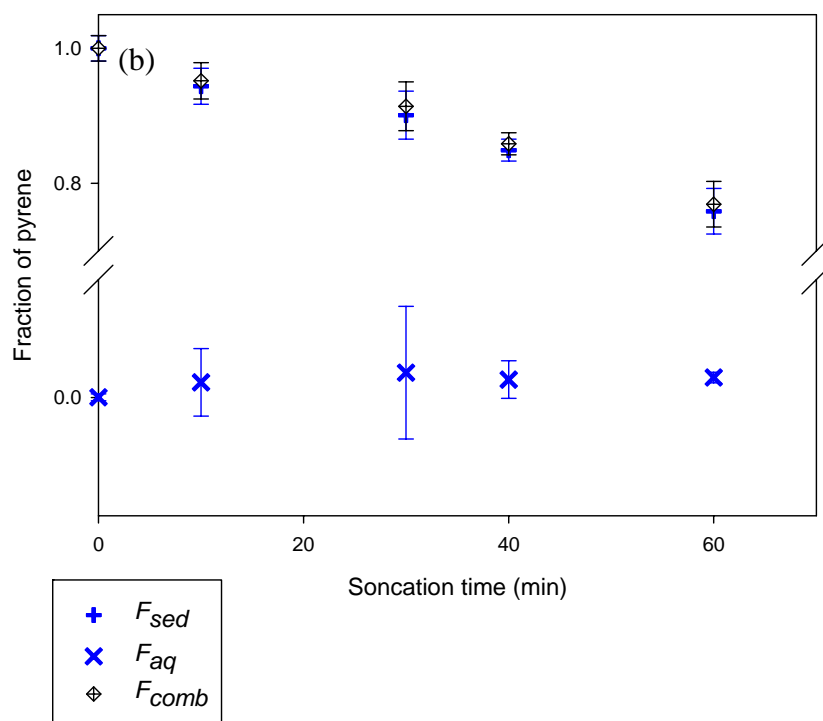
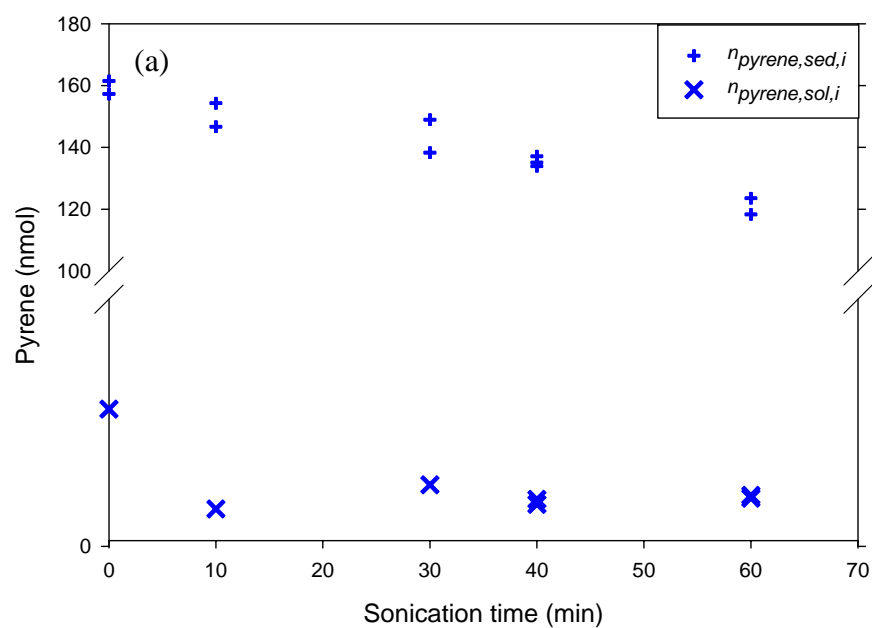


Figure 4. 3: (a) Pyrene (nmol) in aqueous solution and on sediment after selected ultrasonic exposure time (b) the fraction of pyrene in aqueous phase and sediment as a function of US time (T = 20 °C, [particle] = 12.5 g L<sup>-1</sup>, [Pyrene]<sub>initial on particle</sub> = 0.319 nmol g<sup>-1</sup>, D<sub>0</sub> = 75 μm ).



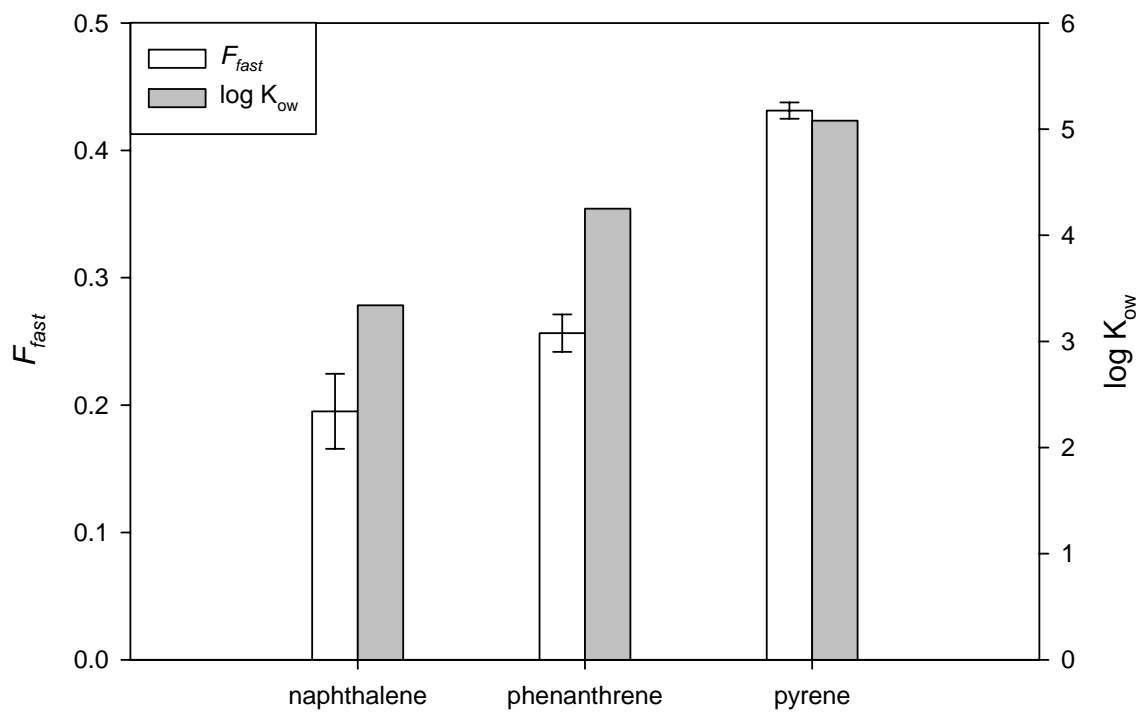


Figure 4. 4:  $F_{fast}$  of naphthalene, phenanthrene and pyrene in the absence of sonication and respective  $\log K_{ow}$ .

Figure 4. 5: (a) Amount of phenanthrene (nmol) in fast and slow desorbing LS sediment sites in the presence and absence of sonication and sonolytically degraded; (b) the fraction of phenanthrene on fast desorbing sites ( $F_{fast}$ ), slow desorbing sites ( $F_{slow}$ ), and sonolytically degraded ( $F_{degraded}$ ), after sonolysis. The sum of these fractions is equal to 1 (Sonication power = 430 W L<sup>-1</sup>, Sonicating volume = 40 mL, Sonicating mass = 0.50 g sediment, Tenax mass = 1.0 g, T = 20 °C, Tenax adsorption time = 6 hr).

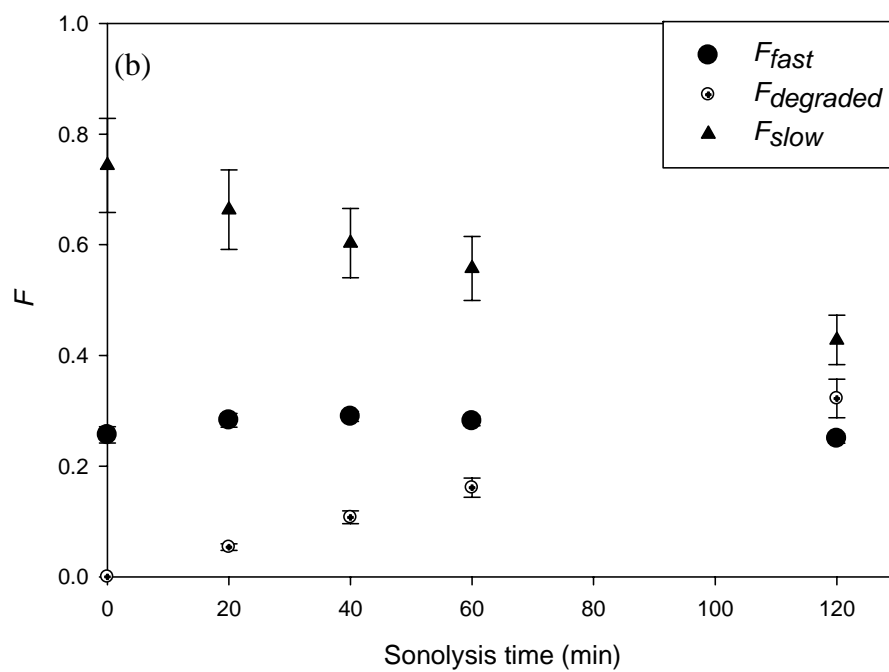
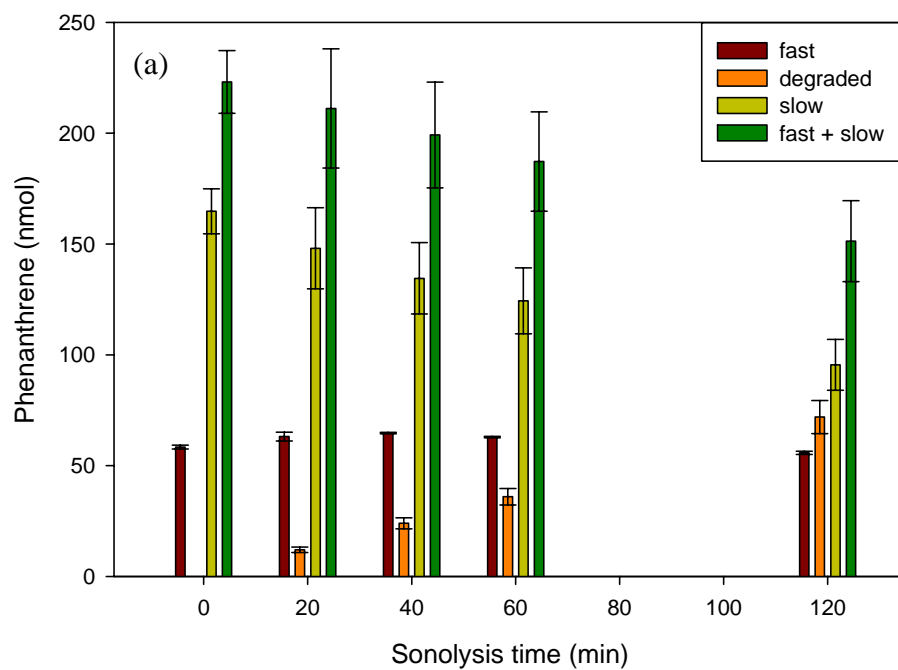
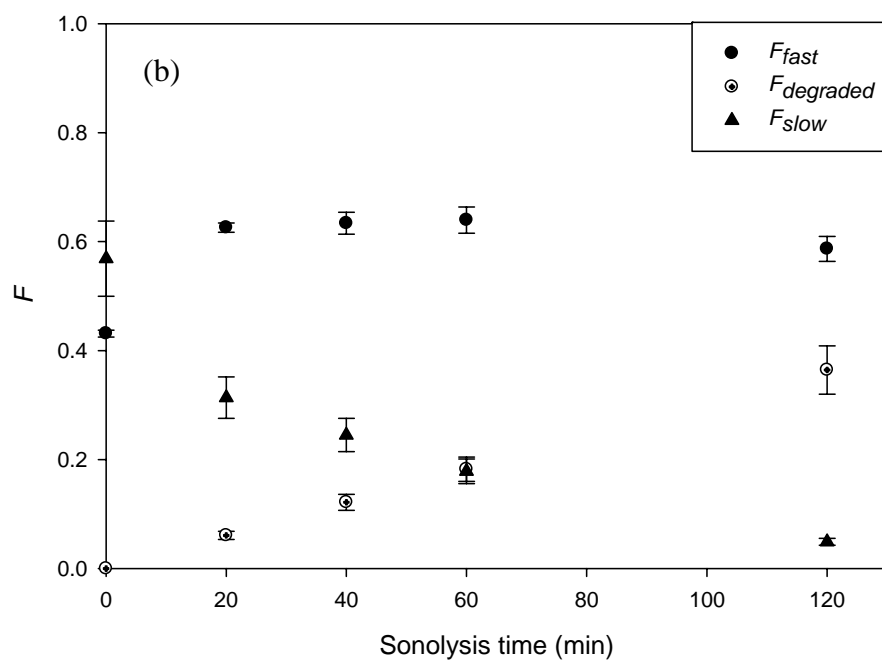
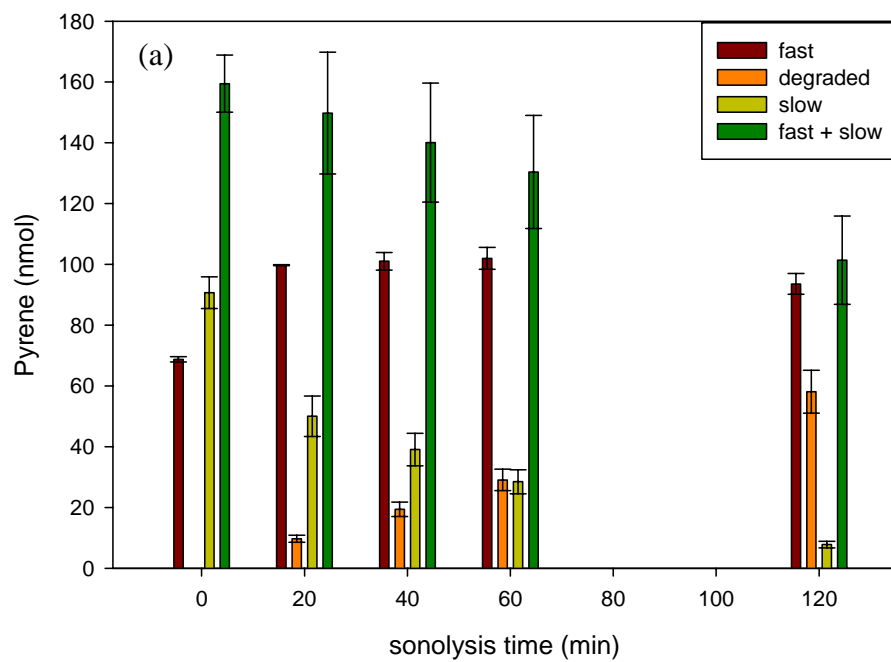


Figure 4. 6: (a) Amount of pyrene (nmol) in fast and slow desorbing LS sediment sites in the presence and absence of sonication and sonolytically degraded; (b) the fraction of pyrene on fast desorbing sites ( $F_{fast}$ ), slow desorbing sites ( $F_{slow}$ ), and sonolytically degraded ( $F_{degraded}$ ), after sonolysis. (Sonication power =  $430 \text{ W L}^{-1}$ , Sonicating volume = 40 mL, Sonicating mass = 0.50 g sediment, Tenax mass = 1.0 g, T = 20 °C, Tenax adsorption time = 6 hr).





## CHAPTER 5

### REMEDICATION OF POLYCYCLIC AROMATIC HYDROCARBON CONTAMINATED FRESHWATER SEDIMENTS USING AN ACTIVATED CARBON AMENDMENT ENHANCED BY ULTRASOUND

#### 5.1. Abstract

In this study, the use of a powdered activated carbon (PAC) amendment and sonication was employed to reduce the bioaccessibility of polycyclic aromatic hydrocarbons (PAHs) in three creosote contaminated sediments (Little Scioto, Ohio (LS); Gary, Indiana (GI) and Eagle Harbor, Washington (EH)). For these three sediments, sonochemically induced switching of phenanthrene and pyrene from sediment to PAC was more effective than mechanical mixing in decreasing the fast desorbing fraction ( $F_{Fast}$ ) (i.e., % reduction in  $F_{Fast}$ ; ultrasound: EH=  $91 \pm 3$  %, GI =  $67 \pm 3$  %, and LS =  $67 \pm 3$  %, mixing: EH=  $81 \pm 3$  %, GI =  $42 \pm 3$  %, and LS =  $53 \pm 3$  %). The enhancement effect observed for sediment treated with sonication was attributed to the facilitation of desorption of PAHs through localized turbulent liquid movement, microjets formation and particles fragmentation, exposing new surfaces to the aqueous phase.

## 5.2. Introduction

Sediment remediation technologies, such as bioremediation, are often slow due to limitations in the ability of contaminants to desorb from the sediment to the aqueous phase where the majority of remediation technologies are effective [ref]. As organic contaminants exist longer in natural sediment, the contaminants are slowly entrapped in small pores of the sediment particles, making them less accessible for remediation<sup>87-90</sup>.

The bioavailability of HOCs is a measure of the three phase equilibrium relationship between sediment, pore water and organism lipids<sup>82</sup>. The contact time between Soil-PAH (i.e., aging) is one of the most critical bioavailability factors governing the fate and transport of PAHs in soil<sup>87</sup>. Organic contaminants are found to sorbed at different strength on various adsorption sites present in soil. For example, the sorption of PAHs was observed to be 10-1000 times stronger on black carbon compared to other organic carbons<sup>164</sup>. Desorption of organic contaminants are considered to occur in two steps, the rapid release fraction followed by slow release fraction<sup>94,97</sup>.

Recent studies by McLeod et al.<sup>84</sup>, Werner et al.<sup>85</sup>, Zimmerman et al.<sup>86</sup> and Millward et al.<sup>18</sup> have proposed the use of activated carbon amendments to lower the bioavailability of hydrophobic organic carbons (HOCs) to biota exposed to the sediments. The addition of carbon to the sediment provides strong sorption sites for these HOCs and reduces the freely dissolved HOC concentrations and consequently, the amount available for organism uptake. In results presented by Millward et al.<sup>18</sup> for sediment in contact with activated carbon for 1 month, the bioavailability of polychlorinated biphenyl (PCB) was reduced by 70 and 82% for *Neanthes arenaceodentata* (worm) and *Leptocheirus plumulosus* (amphipod), respectively. With a contact time of 6 months, the bioavailability

reduction of the system improved marginally from 70% to 75% and from 82% to 87%, respectively. The initial release of PAHs for switching to PAC was more effective and became slower because of slow release of PCB from slow desorbing fraction.

Ultrasonic waves generate bubbles in solution during the rarefaction period of the sound waves. These bubbles grow over several wave cycles until they reach a critical size ( $R_{\max}$ ) and collapse almost adiabatically<sup>27</sup>. The collapse of the bubble produces high average temperatures of 4200 K, peak core temperatures of 17000 K, and pressures of 500 atm<sup>31,68</sup>. These local conditions result in the formation of three reactive zones (i.e., gaseous interiors, bubble interfaces and bulk solution) at which sonochemical reactions occur<sup>26,28</sup>.

Besides chemical effects, the collapse of cavitation bubbles results in a variety of physical and mechanical effects on the solid surfaces. These mechanical effects have been found to facilitate mass-transfer through reduction in solid-liquid films<sup>73</sup>, increase mass-transfer coefficients<sup>26</sup>, enhance dissolution of solids<sup>26,71</sup>, change particle size and surface properties<sup>26,69</sup>, produce interparticle melting<sup>67</sup>, and modify material structure<sup>26,72</sup>.

When cavitation bubbles are in the vicinity of solid particles, collapse occurs symmetrically or asymmetrically depending on the proximity and size of the solids, this result in three phenomena. Symmetric collapses generate shock waves, that result in particle-particle collisions causing particle fragmentation<sup>26</sup>. Shockwaves and liquid movement around cavitating bubbles lead to microstreaming, which increases liquid flow around particles. When solids that are much larger than cavitation bubbles are in close proximity to the cavitation bubbles, asymmetric collapse occurs, thus leading to the

formation of high velocity microjets of solvent that bombard the solid surface resulting in pitting and erosion<sup>26</sup>.

When sonication is applied to HOCs contaminated sediments, the exposure of new surfaces through particle fragmentation, pitting and erosion resulted in direct contact between the contaminants that was buried with aqueous solution. As a result of these new surfaces, increase dissolution of cinnabar, enhance the leaching<sup>152</sup> and extraction of metals<sup>153</sup>, decontaminate spiked organic on dredged sediment<sup>77</sup>, and rapidly desorb 4-chlorobiphenyl (4-CB) from model contaminated sediments<sup>23</sup> and diesel from contaminated sand<sup>78</sup> was observed. In particular, Lu and Weavers demonstrated enhanced desorption of 4-CB by ultrasound. Further kinetic modeling indicated that the presence of ultrasound eliminated mass transfer limitations present in mechanically mixed systems.

Our objective was to increase the rate of desorption of phenanthrene and pyrene from three natural freshwater sediments. Furthermore, powdered activated carbon (PAC) was mixed with the sediments to sorb the released phenanthrene and pyrene and reduce the bioaccessibility of the resultant carbon amended sediment. Hence in this study, ultrasound was evaluated as a possible technology for enhancing desorption of PAHs from sediments to the aqueous phase thereby improving subsequent sorption onto activated carbon. Changes in the bioaccessibility of phenanthrene and pyrene as measured by Tenax extraction experiments was monitored under a variety of conditions (i.e., sonication time and PAC concentration) to evaluate the effectiveness of ultrasound and PAC to reduce the bioaccessibility of PAHs in the sediment.

### 5.3. Experimental Methods

**Materials.** Phenanthrene (Sigma-Aldrich, > 99.5%), pyrene (Sigma-Aldrich, > 99%), hexane (Fisher-Scientific, HPLC grade), acetone (Fisher-Scientific, HPLC grade), dichloromethane (Fisher-Scientific, HPLC grade), methanol (Fisher-Scientific, HPLC grade) and powdered activated carbon (PAC) (Fisher-Scientific) were used as purchased. Deuterated solutions of phenanthrene-d<sub>10</sub> and pyrene-d<sub>10</sub> were obtained through UltraScientific (North Kingstown, RI, USA). Tenax TA 60/80 was purchased from Sigma-Aldrich. Water from a MilliQ water purification system ( $R = 18.2 \text{ M}\Omega \text{ cm}$ ) was used in all experiments.

**Sample Preparation.** Three freshwater sediments were obtained from Little Scioto River, Ohio (LS); a pond in Gary, Indiana (GI); and Eagle Harbor, Washington (EH). The LS site was undergoing cleanup. The GI sediment was from a pond beside an EPA superfund site. The EH sediment was from a former wood treatment plant that was contaminated as a result of creosote release. LS and GI sediments were stored in glass amber jars before air-drying on hexane-rinsed aluminum foil in a fume hood. EH sediment was stored in an air-tight 20 gallon bucket before drying. After drying, the sediments were sieved through a 20 mesh screen (The W.S. Tyler Company, Cleveland, Ohio), corresponding to an 840  $\mu\text{m}$  opening. Each sediment was homogenized using an end-over-end tumbler for 1 week in glass amber jars and stored at 4 °C. The homogeneities of these sediments were tested by taking random samples of the mixed sediments, performing microwave extraction (EPA method 3546) and analyzing for individual PAH compounds. For each sediment the concentrations of the PAHs, in the random samples were found to be within 5 %. A stock PAC solution was made by

weighing 3.0 g of PAC into a 100 mL volumetric flask and triple washed with MilliQ water and oven dried at 105 °C for 24 hrs before adding MilliQ water to make a 30 g L<sup>-1</sup> PAC stock solution. For 0.5 g of sediment, 0.5 mL of stock PAC solution was added (i.e. ~ 3% by weight PAC to sediment).

**Ultrasound Set-up.** A direct immersion probe model 550, manufactured by Fisher Scientific and operating at 20-kHz was used in all ultrasound experiments. Ultrasound was emitted from a 1.20-cm<sup>2</sup> tip with power intensity measured by calorimetry to be 430 W L<sup>-1</sup>. All experiments were operated in batch mode with a sonication volume of 40 mL and total conical reactor volume of 60 mL. The neck of the reactor was fitted into a Teflon collar attached to the probe to provide a closed system for sonolysis. Temperature was controlled using a Fischer Scientific Isotemp 1016S cooling system at 20°C via a cooling jacket on the reactor. The reactor was wrapped in aluminum foil to prevent photochemical reaction.

**Calibration Standard.** Stock solutions for PAHs were prepared by dissolving the three PAHs in dichloromethane in three 10 mL volumetric flasks. These stock solutions were diluted to build the calibration curve. Deuterated naphthalene, deuterated phenanthrene and deuterated pyrene were used as internal standards. The internal standard was prepared as follows: each ampule containing 1 mL of the deuterated PAHs was added to a 10 mL volumetric flask and diluted to a 10 mL mixture with hexane. This solution was then stored at 4 °C to prevent volatilization of the deuterated PAHs and solvent. 100 µL of this internal standard solution was added using a glass syringe (Hamilton, Reno, NV) per mL of calibration and sample solution.

**Sample Preparation.** At selected sonication times, the sample (40 mL) was transferred to a 50 mL Teflon centrifuge tube and centrifuged for 10 min at 10000 rpm with a Sorvall Legend RT centrifuge (Thermo Scientific, Waltham, MA) to separate the supernatant and particle fractions. 100 µL of internal standards were added to 30 mL of the supernatant prior to extraction with 5 mL hexane for 24 hrs. The hexane solution was then removed and concentrated to 1 mL prior to analysis by Gas Chromatography-Mass Spectrometry (GC-MS) analysis. Another 8 mL of the supernatant was used for total organic carbon (TOC) analysis. Extraction of the sediments was performed with an Ethos EX closed microwave extraction system (Milestone, Shelton, CT, USA) equipped with 12 vessels capable of withstanding 22 psi and with temperature feedback/control to maintain desired temperature at  $\pm 1$  °C following EPA method 3546. The sediment was transferred into the vessels with an equal amount of activated copper <sup>155</sup> to eliminate interferences due to sulphur in the sediment. 100 µL of the internal standard was added to each vessel to monitor and correct for possible losses during the extraction and concentration process. Finally, 24 mL of a 1:1 hexane:acetone mixture, was added to the vessel and the vessel was sealed. Samples were extracted under a 5 min temperature ramp from room temperature to 120 °C followed by a 20 min hold at 120 °C. When completed, the vessels were removed from the microwave cavity and allowed to cool to room temperature before opening. The supernatant of the sample was removed and concentrated to 1 mL by nitrogen evaporation and filtered using PTFE filters (25 mm, 45 µm, Millipore) prior to analysis with GC-MS. This method was verified on Certified Reference Material (CRM) 122 (RTC, Laramie, Wyoming) and Standard Reference Material (SRM) 1944 (NIST, Gaithersburg, Maryland, USA). Recoveries were within the values reported for SRM



1944 and were above the values reported for CRM 122, which used Soxhlet extraction (EPA method 3540 C) and sonication (EPA method 3550).

**Bioaccessibility using Tenax beads.** A Tenax extraction method was used as a measure of the bioaccessibility of PAHs in the sediments with and without treatment. Tenax beads were used for evaluating bioaccessibility of HOCs and was related to bioavailability<sup>95,97,102,104,121,167</sup>, and it was found that Tenax extracted concentration of hydrophobic organic carbons can be positively correlated to the bioavailability of sediment<sup>102</sup>. In particular, bioaccessibility of PAHs on sediments were evaluated using this technique by Cornelissen et al., and Macrae and Hall<sup>103,168</sup>. Cornelissen et al. noted that for PAHs, the rapidly desorbing fraction was depleted after more than 20 hr Tenax extraction time<sup>103,121</sup>. For our experiment, we chose 24 hr Tenax extraction time to represent bioaccessible fraction of our sediments. The steps used in our experiments were modified from the method used by Cornelissen et al. to investigate the desorption kinetics of organics<sup>97</sup>. After a selected sonication time, the resultant sediment/PAC-water mixture was transferred to a 100 mL separation funnel. 30 mL of MilliQ water was used to rinse the sediment from the reactor into the funnel (i.e. total aqueous volume = 70 mL). 1 g of Tenax beads was weighed and added into the funnel. The separation funnel was sealed and placed on a benchtop shaker (New Brunswick Scientific, Edison, NJ), at 300 rpm to ensure that the sediment and Tenax beads were well dispersed. Separation of sediment from Tenax was achieved by allowing the sediment to sink to the bottom of the funnel and opening the tap for the sediment to flow out. Tenax beads remained in the funnel due to buoyancy and were washed with 5 mL of MilliQ water to remove sediment and PAC that may be on the Tenax. Next, the water was drained. Finally, the beads were flushed

from the funnel using 20 mL hexane and collected in a 25 mL Teflon centrifuge tube. 100  $\mu$ L of the deuterated internal standard was added and the resultant hexane-Tenax mixture was shaken for 24 hr at 300 rpm to extract the PAHs. The hexane fraction was then removed using a disposable glass pipette. This hexane fraction was blown-down to 1 mL using nitrogen gas prior to quantitative analysis.

**Control experiments.** 0.5 g of the sediment and 40 mL of MilliQ water was placed in the separation funnel and mixed at 300 rpm on a benchtop shaker for selected times to determine PAH release from sediment with mixing but in the absence of ultrasound. After shaking, 30 mL of MilliQ water and 1g of 60/80 mesh Tenax beads were added. This mixture was placed again on a benchtop shaker for selected times to measure bioaccessibility by Tenax adsorption as described above.

**Quantitative analysis.** The 1 mL extract from the hexane extraction was analyzed with a gas chromatograph equipped with an ion trap mass spectrometer (Thermo-Finnigan Polaris GCQ) and a CP-5 fused silica capillary column (30 m x 250  $\mu$ m x 0.25  $\mu$ m, Varian). Helium was used as the carrier gas at a flow rate of 1.2 mL min<sup>-1</sup>. 1  $\mu$ L of the extract was injected using splitless mode. The injector temperature and ion source temperature was kept at 250 °C. The column temperature program was: 60 °C for 2 min, increased at 20 °C min<sup>-1</sup> to 250 °C, held for 2 min, ramped again at 10 °C/min to 300 °C, followed by 8 min at 300 °C. The temperature of the transfer line was constant at 300 °C. The mass spectrometer was operated in full scan mode (scan range 50 – 500 m/z, scan time 0.49 s) for both standards and extracts.

**Sediment Characterization.** Particle size distribution, particle surface area and particle surface morphology of the sediments were investigated using a Malvern Mastersizer

particle size analyzer, a Brunauer-Emmett-Teller (BET) surface area analyzer (Micromeritics® FlowSorb 2300) and scanning electron microscope (SEM). For SEM measurements, samples were mounted on stainless steel stubs using double-stick carbon tape and sputter-coated with gold.

## 5.4. Results and Discussion

**Reduction in Bioaccessibility using PAC and Ultrasound for LS.** 0.5 g LS sediment was sonicated in 40 mL MilliQ water and 3% PAC for selected times. The rapidly desorbing amount ( $n_{fast}$ ) of the slurry (i.e., sediment and water) was measured using Tenax beads. As control experiments, mechanical mixing at 300 rpm was conducted for the same selected time and the  $n_{fast}$  was measured. The rates of change in the amounts of phenanthrene and pyrene on the LS sediment in the absence of PAC were determined through sonolysis of 0.5 mL of LS sediment with 40 mL MilliQ water for selected time and quantifying the extractable amount ( $n_{extracted}$ ) of the PAHs using microwave extraction. The decrease in extractable amounts of phenanthrene and pyrene can be resulted from sonodegradation and occlusion as was observed during sonication of 4-chlorobiphenyl and mercury sorbed on alumina particles<sup>23,24</sup>. For the purpose of our discussion, we will consider this decreased in amount of extractable PAHs to be due to sonodegradation. This assumption is valid because if PAHs were occluded and not extractable by chemical method (i.e., microwave extraction at 120 °C with acetone/hexane mixture), these PAHs will not desorb into aqueous phase, thus can be assumed unavailable. The rate of degradation of phenanthrene and pyrene were  $0.60 \pm$

0.06 nmol/min and  $0.48 \pm 0.06$  nmol/min, respectively. The fast desorbing ( $F_{fast}$ ) and slow desorbing fractions ( $F_{slow}$ ) were calculated with the following mass balance:

$$F_{fast} = \frac{n_{fast}}{n_{extracted}} \quad (5.1)$$

$$F_{slow} = \frac{(n_{extracted} - n_{degraded}) - n_{fast}}{n_{extracted}} \quad (5.2)$$

where  $n_{degraded}$  is the amount of PAHs that are degraded during sonolysis ( $\mu\text{mol}$ ). In this equation, we assumed that the fraction that cannot be extracted by microwave extraction is “nonlabile” and will not be transferred from these “inaccessible” sites, thus  $n_{extracted}$  was considered total amount of PAH.

The  $F_{fast}$ ,  $F_{degraded}$  and  $F_{slow}$  after sonolysis and mixing of sediment with 3% weight PAC are shown in Figure 5.1 and Figure 5.2 for phenanthrene and pyrene. The  $F_{fast}$  of sonicated system, at all the selected sonolysis times, were less than the corresponding mixing control. For example, after 1 hr sonolysis, the  $F_{fast}$  ( $F_{fast, sonolysis} = 0.28 \pm 0.01$ ) was less than  $F_{fast}$  ( $F_{fast, mixing} = 0.354 \pm 0.003$ ) after 1 hr mixing. At longer mixing or sonolysis time, a further decrease in  $F_{fast}$  was observed. However, after 1 hr, the reduction in  $F_{fast}$  of pyrene and phenanthrene was less intense compared to the reduction observed from 0 to 1 hr sonication (i.e. for pyrene,  $F_{t=0} - F_{sonolysis, 1 \text{ hr}} = 0.67 - 0.28 = 0.39$ ,  $F_{sonolysis, 1 \text{ hr}} - F_{sonolysis, t=2 \text{ hr}} = 0.28 - 0.22 = 0.06$ ,  $F_{sonolysis, 2 \text{ hr}} - F_{sonolysis, t=2. \text{hr}} = 0.22 - 0.19 = 0.03$ ). For mixing system, a decrease in  $F_{fast}$  corresponded to an increase in  $F_{slow}$ . For sonolytic system, a decrease in  $F_{fast}$  and  $F_{slow}$  were observed with sonolysis time.

The larger decrease in  $F_{fast}$  after sonolysis compared to mixing can be attributed to enhanced sonolytic desorption from sediment, thus allowing more PAHs to be sorbed on PAC, which has been shown to be strong sorption sites with lower contaminant bioavailability<sup>84</sup>. Sonolysis has been shown to enhanced bond breaking between the adsorbate and the adsorbate surface from the action of shockwaves and microjets generated during the collapse of cavitation bubbles on or in close vicinity to the sediment<sup>81</sup> and these mechanical effects resulted in released of mercury<sup>24</sup> and 4-chloro biphenyl (4-CB)<sup>23</sup> very quickly from alumina particles. This can shift the equilibrium concentrations of PAHs dramatically towards the aqueous phase for PAC sequestration.

The less intense decreased in  $F_{fast}$  for sonolysis time longer than 1 hr may be explained using the following rationale: first, sonolysis can result in faster release of PAHs from the surface of the particles from increased localized turbulence in the solid-liquid film, and increased interfacial area through interparticle collisions and pitting<sup>26,65</sup>. However, cavitation bubble is not effective in accessing PAHs sorbed in the micro-pores of the particles. Sediment is composed of a continuum of pores ranging in size from micro-pores < 0.1  $\mu\text{m}$  in diameter through to macropores >20  $\mu\text{m}$ <sup>91</sup>, continuum of compartments (i.e., rubbery (loose, flexible) to glassy (condensed, rigid) organic matter<sup>92,93</sup>) ordered by their desorption rate constants<sup>94</sup> and degree of sorption<sup>95</sup>. Doktycz and Suslick estimated the diameter of collapsing bubble to be  $\sim 150 \mu\text{m}$ <sup>67</sup>. This suggested that cavitation bubble cannot collapse inside small macropores (<150  $\mu\text{m}$ ), micropores and nanometer-size voids found in glassy organic matter<sup>108</sup>. In the event that the PAHs in sites accessible by cavitation bubbles were desorbed and switched to the PAC, the remaining PAHs can only be desorbed through diffusion from the pores.

Second, the production of microjets and effective particle-particle collisions were greatly reduced after 1 hr sonication. Our study of mean particle size of LS upon sonication showed that at 6 min sonication, the mean particles size was decreased to 9  $\mu\text{m}$  from 75  $\mu\text{m}$ , and with longer sonication (6 min to 80 min), the particle diameter was confirm increasingly towards 9  $\mu\text{m}$  with the disappearance of larger particles (Figure 5.3) with no significant change in mean particle size. The limitation of particle size to 5 – 15  $\mu\text{m}$  during sonication of nickel powder was also observed by Suslick and Casadonte<sup>26,171</sup>.

It was noted by Doktycz and Suslick that for a 20 kHz ultrasound system microjets are produced in the presence of particles larger than 150  $\mu\text{m}$ <sup>67</sup>. Microjets can bring about localized surface cleaning<sup>26</sup>. In addition, there is a minimum particle mass at which the momentum of the particle becomes too small to create the impact required to cause particle fragmentation<sup>26</sup> rendering shockwaves ineffective. These new surfaces, turbulent condition and localized cleaning generated by microjets and particle-particle collision events are critical in facilitating the release of PAHs adsorbed on sediments. The decrease in particle size after the onset of ultrasound decreased the production of microjets and effective particle-particle collision thus decreases the overall mechanical effects of sonolysis.

From Figures 5.1 and 5.2, the benefit of ultrasound was also seen in the ability to decrease both  $F_{slow}$  and  $F_{fast}$ . For biodegradation, it is currently unclear if this slow desorbing fraction cannot be degraded at all once the easily available contaminants are exhausted which may drop the porewater concentrations below threshold required by microbes, or are degraded over long time spans (>years)<sup>101</sup> and may still be available to biota<sup>117</sup>. Therefore the ability of ultrasound to treat this fraction is significant.

**Reduction in Bioaccessibility using PAC and Ultrasound for EH and GI.** Next, we explored the effect of ultrasound and PAC amendments with two other sediments (EH and GI) to understand if the mechanism proposed with LS sediment could be generalized to sediments from other sites. Figure 5.4 shows  $F_{fast}$  for EH sediment under selected conditions. Similar to LS sediment, a PAC amendment coupled with 30 min sonolysis provided a greater reduction in  $F_{fast}$  compared to 30 min and 3 hrs of mechanical mixing. At sonication times greater than 30 min, the change in  $F_{fast}$  between sediment samples sonicated for 30 min ( $F_{fast, sonolysis}$  of pyrene =  $0.046 \pm 0.003$ ) and 3 hr ( $F_{fast, sonolysis}$  of pyrene =  $0.026 \pm 0.002$ ) was not as significant as was observed between 0 min ( $F_{fast} = 0.082 \pm 0.004$ ) and 30 min ( $F_{fast} = 0.046 \pm 0.003$ ).

As was the case for LS sediment, this can be attributed to the limitations of cavitation bubble to reach macro-pores, micro-pores, nanometer-size voids, reduced microjets and particle fragmentation resulting in reduced efficiency of ultrasound after 30 min. In addition, the PAC sites available to act as a sink for PAHs switching after 10 min sonication may be saturated. Besides releasing PAHs, sonolysis can also release other organics that can take up adsorption sites on PAC. To test this hypothesis that PACs adsorption sites were saturated sonolysis experiment with 6 % PAC by weight was conducted and the result is shown in Figure 5.5. The change between  $F_{fast}$  of pyrene for system with 3 % and 6 % PAC were statistically insignificant (i.e.,  $0.039 \pm 0.007$  and  $0.033 \pm 0.002$ ). Although the difference in  $F_{fast}$  of phenanthrene for 6% and 3% PAC were significant (i.e.,  $0.06 \pm 0.02$  and  $0.028 \pm 0.002$ ), 6% PAC did not decrease the  $F_{fast}$  of phenanthrene by half. Moreover, reduction in  $F_{fast}$  was still observed after 10 min sonolysis (i.e. there were still available sites on PAC). This suggested that the adsorption

sites of PAC maybe a contributing factor but not the predominant limiting factor to account for the inefficiency of sonolysis in reducing  $F_{fast}$  after 10 min for EH sediment.

PAC amendment coupled with US was also examined for a third sediment (GI). The trend in  $F_{fast}$  before and after sonication or mixing is shown in Figure 5.5. The  $F_{fast}$  trends observed for GI sediment was similar to EH and LS sediment (i.e., more significant decrease in  $F_{fast}$  after sonolysis compared to mixing). Although the  $F_{fast}$  of these three freshwater sediments (LS, GI and EH) has been shown to decrease faster using sonolysis coupled with PAC amendment compared to mechanical mixing coupled with PAC amendment, the effect of sonolysis was different for the 3 sediments.

To compare the effect of PAC amendment for these three sediments, the % decrease in  $F_{fast}$  (i.e., % decrease in  $F_{fast} = \frac{F_{fast,0\% PAC,0 min} - F_{fast,sonolysis / mixing}}{F_{fast,0\% PAC,0 min}} \times 100\%$ ) after treatment with US, mixing and % organic carbon for the three sediments were shown in Figure 5.7. The plot for LS is at 1 hr and the plots for EH and GI is at 30 min US/mixing time. From Figure 5.4, the  $F_{fast}$  of pyrene at 30 min did not change significantly from 1 hr sonolysis for EH sediment. Hence for GI sediment,  $F_{fast}$  at 30 min was assumed to be similar to its  $F_{fast}$  at 1 hr sonolysis and mixing and was used for comparison with LS and EH at 1 hr. The % organic carbon was the lowest for EH, followed by GI and LS sediment. The % decrease in  $F_{fast}$  was highest for EH followed by LS and GI sediments after mixing with 3 % PAC. For sediment sonicated with 3 % PAC, the % decrease in  $F_{fast}$  was again highest for EH, and GI shows statistically similar % decrease in  $F_{fast}$  to LS sediment.



The enhancement of PAC amendment coupled with mixing or US maybe affected by the carbon content in the sediments. It was discovered that organic matter in soils and sediments was the principal factor controlling sorption of organic compounds<sup>101</sup> suggesting that sediment with the least amount of organic carbon can release its contaminants more readily. From the % organic carbon measured in our three sediments, the release and subsequent PAC sequestration of PAHs which resulted in decreased in  $F_{fast}$  should be greatest for EH followed by GI and LS since % organic carbon followed the trend: EH < GI < LS. However from Figure 5.7, the desorption of PAHs for PAC sequestration did not follow the % organic carbon content for mixing or US treatment.

Besides % organic carbon, the desorption of PAHs from the sediments may be dependent on the types of organic carbon. The % organic carbon measured consist of amorphous carbon (i.e., partly degraded and/or reconstituted biopolymers (e.g., polysaccharides, lignins), lipoproteins, amino acids, lipids, and humic/fulvic substances) and carbonaceous geosorbents (i.e., black carbon, coal, and kerogen)<sup>101</sup>. Carbonaceous geosorbents are characterized by condensed, rigid, aromatic structures and narrow nanopores inside the sorbent<sup>100,101,172</sup>. It was hypothesized by Pignatello and Xing that slow diffusion in, or extensive sorption to, rigid parts of the organic matter matrix could be responsible for slow desorption<sup>94</sup>. In addition, PAHs associated with natural organic matter and mineral particles in sediments were found to be readily bioavailable while PAHs sorbed on carbonaceous particles in sediments were strongly bound and unavailable for biological treatment or for uptake in earthworms<sup>17,109,110</sup>. Thus, it is possible that the organic carbon in GI sediment may be comprised of a larger percentage

of rigid and carbonaceous sites than LS sediment that may hindered the release of PAHs for PAC sequestration.

In addition, from Figure 5.7, the effect of sonolysis appeared to enhance the % decrease in  $F_{fast}$  of GI (i.e., from  $42 \pm 3$  % for mixing to  $67 \pm 3$  % for sonolysis) to a greater extent than LS sediment (i.e., from  $53 \pm 3$  % for mixing to  $67 \pm 3$  % for sonolysis). Given that the production of microjets and particle fragmentation is dependent on particles that are larger than  $150 \mu\text{m}$ <sup>67</sup>, the larger mean particle size for GI sediment compared to LS may contribute to more microjets formation and greater momentum of the particles-particle collisions. Greater production of microjets and particle fragmentation results in exposure of more surfaces for direct contact of PAHs with aqueous solution. These additional surfaces allowed for decreased path length for the desorption and subsequent switching of PAHs to PAC. Therefore we observed a more significant percent of ultrasonic enhancement in reducing  $F_{fast}$  of PAHs in GI sediment compared to LS sediments.

		LS	EH	GI
% Dry Weight		93.0 ± 0.1	99.2 ± 0.02	99.0 ± 0.2
BET (cm <sup>2</sup> /g)		4.49	2.56	1.89
pH		7.5	7.9	7.9
% Organic carbon		7.6 ± 0.2	0.256 ± 0.007	4.0 ± 0.2
% Inorganic carbon		2.90 ± 0.07	0.006 ± 0.003	1.57 ± 0.03
Particle Diameter (μm)		75	561	303
Concentration (nmol/g) <sup>+</sup>	Phenanthrene	890 ± 20	138.2 ± 0.8	-
	Pyrene	638 ± 8	1100 ± 40	606.0 ± 0.4

Table 5. 1: Properties of Little Scioto (LS), Eagle Harbor (EH), and Gary (GI) Sediments.

<sup>+</sup> Concentrations are the average of triplicate values from EPA microwave extraction method 3546. % Organic carbon was calculated by taking the difference between % Total Organic and % Inorganic carbon. % Inorganic carbon was determined using EPA Methods 9060A<sup>165</sup> and % Total Organic carbon was determined using International Standard, ISO 10694:1995(E)<sup>166</sup>. Concentration and carbon contents were calculated to 95% confidence interval with triplicate samples.

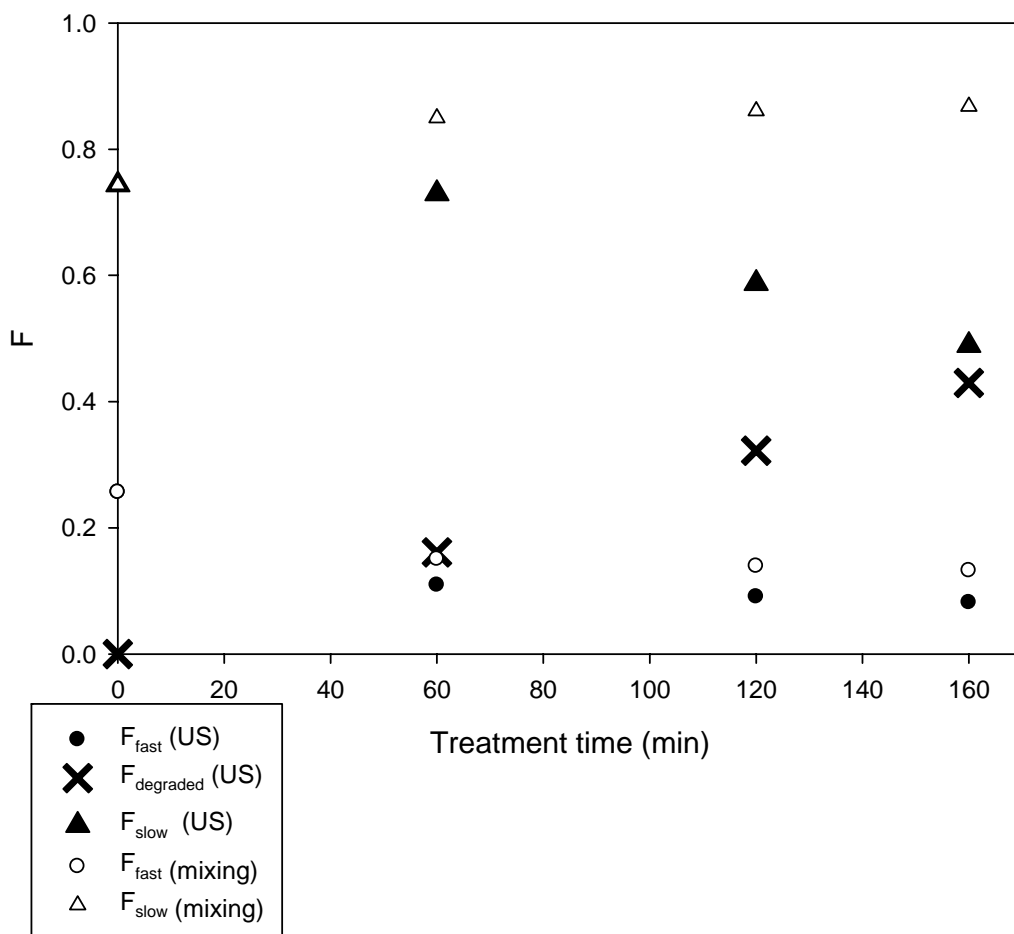


Figure 5. 1: Effect of addition of 3% PAC by mass to LS sediment on  $F_{fast}$ ,  $F_{degraded}$ , and  $F_{slow}$  for phenanthrene as a function of treatment time on LS sediment (Sonication power =  $430 \text{ W L}^{-1}$ , Sonicating volume = 40 mL, Sonicating mass = 0.50 g sediment, [PAC] = 3% by weight, Tenax mass = 1.0g,  $T = 20^\circ \text{C}$ , mechanical mixing = 300 rpm, duplicate were performed for selected points).

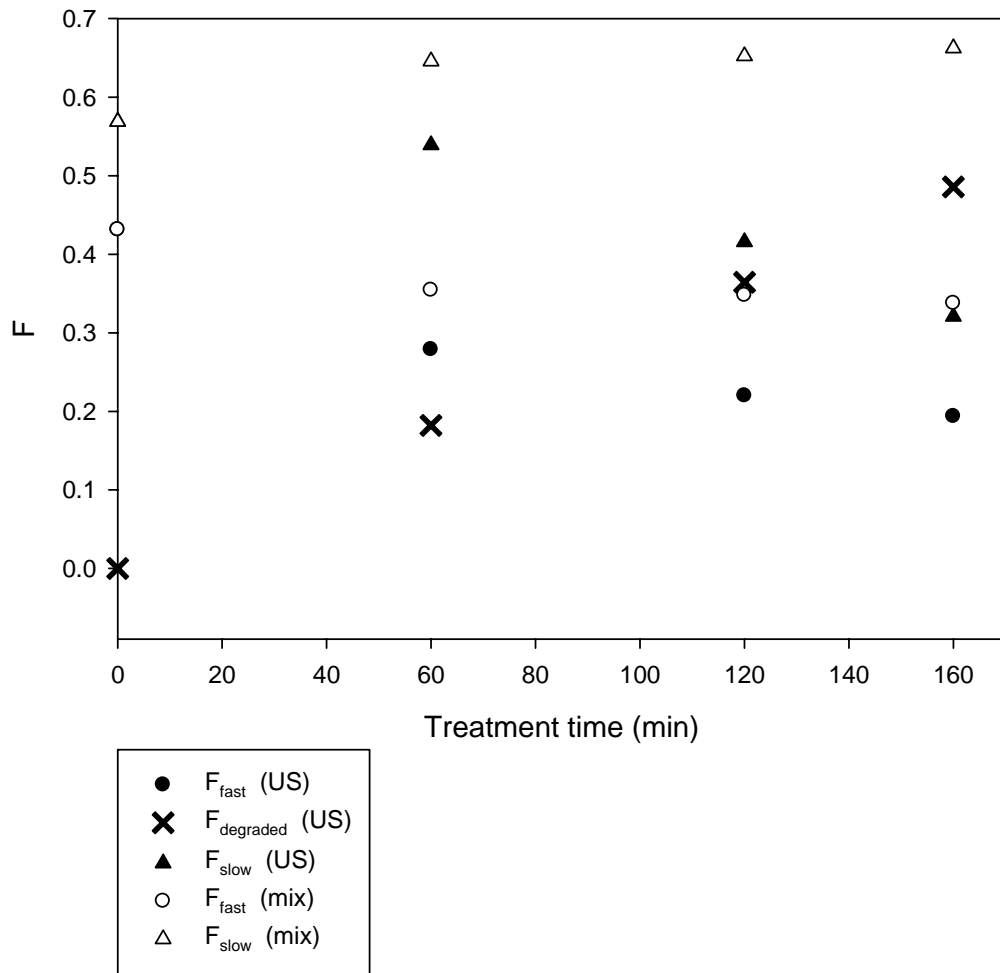


Figure 5. 2: Effect of addition of 3% PAC by mass to LS sediment on  $F_{fast}$ ,  $F_{degraded}$ , and  $F_{slow}$  for pyrene as a function of treatment time (Sonication power = 430 W L<sup>-1</sup>, Sonicating volume = 40 mL, Sonicating mass = 0.50 g sediment, [PAC] = 3% by weight, Tenax mass = 1.0g, T = 20 °C, mechanical mixing = 300 rpm, duplicate were performed for selected points).

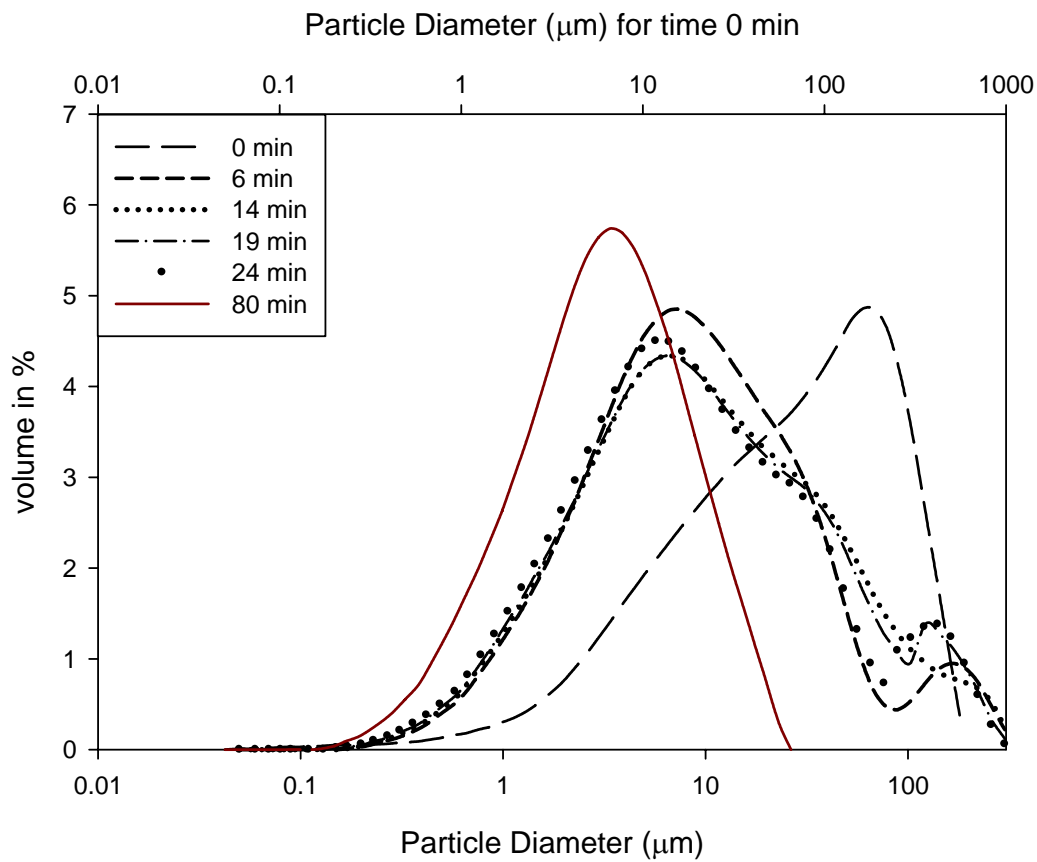


Figure 5. 3: % volume of LS sediment with particle diameter for selected sonication time ( $T = 20^{\circ}\text{C}$ , Sonication power =  $430 \text{ W L}^{-1}$ ,  $[\text{particle}] = 12.5 \text{ g L}^{-1}$ , Sonicating time = 80 min,  $D_0 = 75.411 \mu\text{m}$ ).

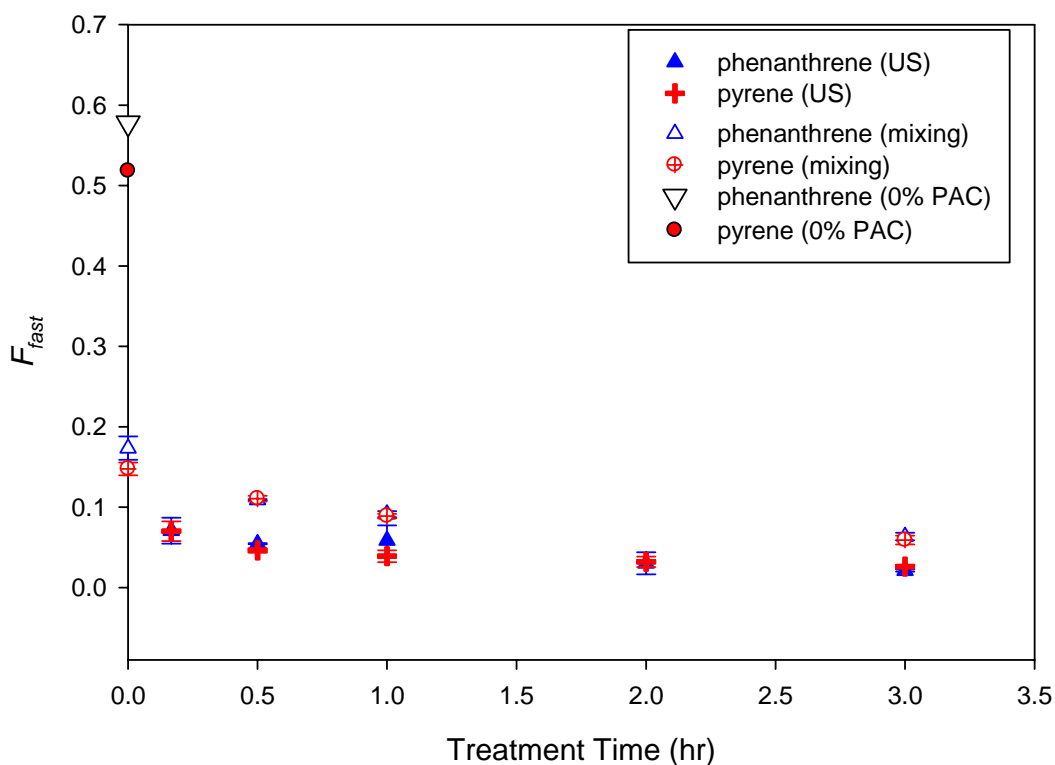


Figure 5. 4: The effect of adding 3% PAC on  $F_{fast}$  for phenanthrene and pyrene as a function of treatment time on Eagle Harbor (EH) sediment (Sonication power = 430 W L<sup>-1</sup>, Sonicating volume = 40 mL, Sonicating mass = 0.50 g sediment, [PAC] = 3% by weight, Tenax mass = 1.0g, T = 20 °C, Tenax adsorption time = 24 hr, error bar represents 95% confidence interval, n = 2).

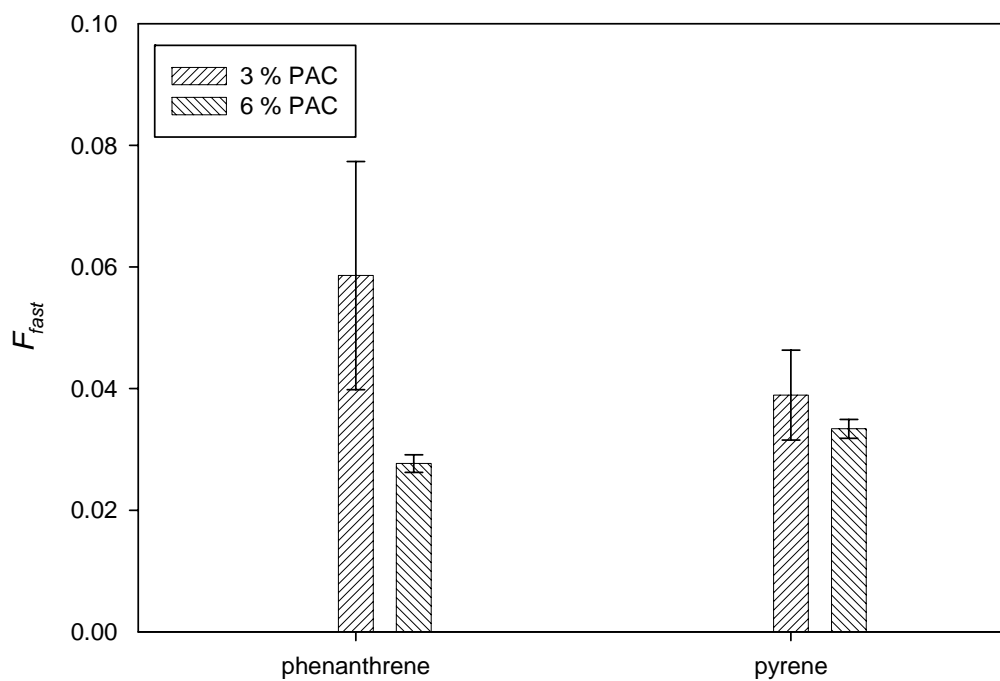


Figure 5. 5: The effect of adding 6% PAC and 3% PAC on  $F_{fast}$  of phenanthrene and pyrene on EH sediment (Sonication power = 430 W L<sup>-1</sup>, Sonicating volume = 40 mL, Sonicating mass = 0.50 g sediment, [PAC] = 3% by weight, Tenax mass = 1.0g, T = 20 °C, Tenax adsorption time = 24 hr, error bar represents 95% confidence interval, n = 2).



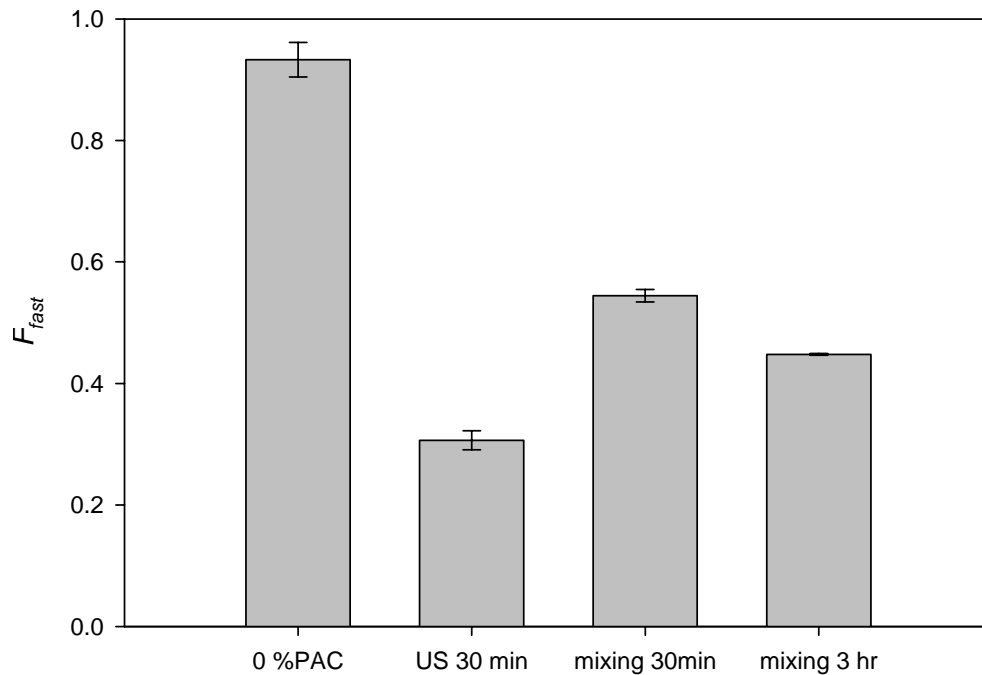


Figure 5. 6: The effect of adding 3% PAC and treating with ultrasound or mixing on  $F_{fast}$  of pyrene on Gary, Indiana (GI) sediment. Unless otherwise stated, 3 % PAC by sediment weight was added to sediment slurry. (Sonication power = 430 W L<sup>-1</sup>, Sonicating volume = 40 mL, Sonicating mass = 0.50 g sediment, Tenax mass = 1.0g, T = 20 °C, Tenax adsorption time = 24 hr, error bar represents 95% confidence interval, n = 2).

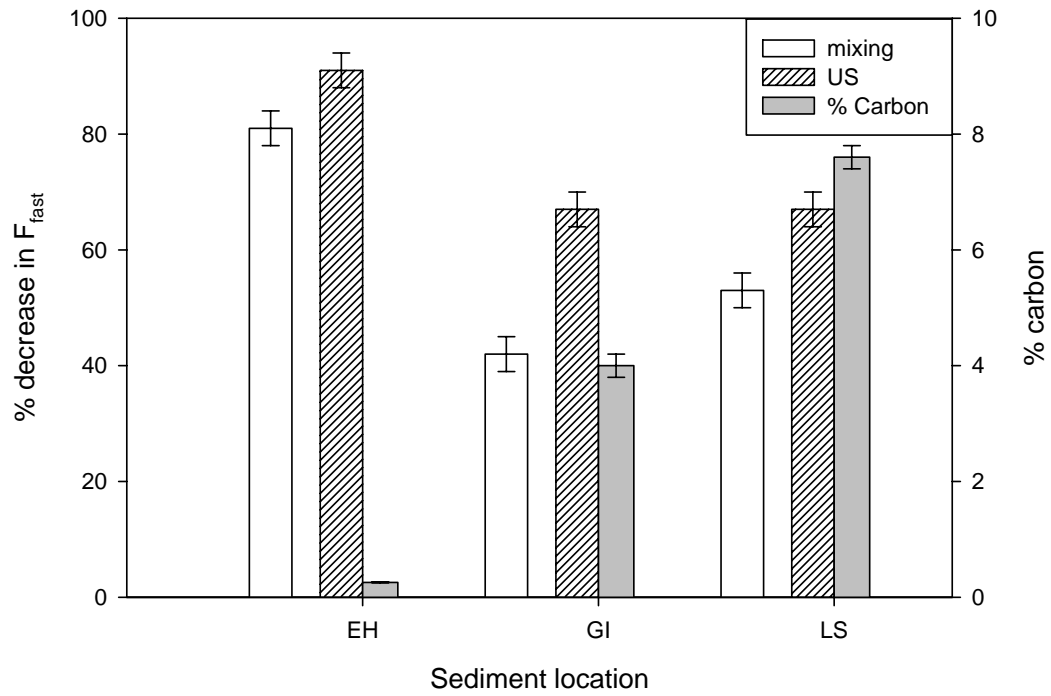


Figure 5. 7: Comparison of organic carbon content to % decrease in  $F_{fast}$  for EH, GI, and LS sediment.

## CHAPTER 6

### CONCLUSION AND FUTURE WORK

#### 6.1. Conclusion

Sonolysis has been shown in this study to firstly degrade polycyclic aromatic hydrocarbons (PAHs) in solution. The sonolytic degradation of pyrene in aqueous solution was faster compared to naphthalene and phenanthrene. Pyrene appeared to have faster accumulation on the interface due to higher surface-bulk equilibrium partitioning constant and greater interaction energy with the water surface than naphthalene and phenanthrene.

Secondly sonolysis was shown to degrade PAHs adsorbed on natural sediments obtained from Little Scioto River, OH (LS) and Gary, Indiana (GI). The combined concentrations of naphthalene, phenanthrene and pyrene in solution and on sediment were reduced by 23 %, 15 %, and 23 %, respectively after 60 min sonolysis of 12.5 g L<sup>-1</sup> of natural sediment (LS) in MilliQ water. The sonolytic rate of degradation was found to increase with increasing solid-liquid ratio at particle concentration below 12.5 g L<sup>-1</sup> (i.e. the degradation rates for pyrene were 7.35 x 10<sup>-5</sup>, 1.60 x 10<sup>-4</sup> and 4.84 x 10<sup>-4</sup> for solid-liquid ratios of 5 g L<sup>-1</sup>, 8.75 g L<sup>-1</sup>, and 12.5 g L<sup>-1</sup>, respectively). However, further increase in the solid-liquid ratio (>12.5 g L<sup>-1</sup>) resulted in a decrease in the degradation rate of

PAHs. This suggested that increasing particle concentration from  $12.5 \text{ g L}^{-1}$  to  $25.0 \text{ g L}^{-1}$  increased the PAHs concentration in solution for reaction and the additional particles provided more nucleation sites for the formation of cavitation bubble. At solid-liquid ratios above  $12.5 \text{ g L}^{-1}$ , the solubility limits of the PAHs were reached and/or the effect of sound attenuation was reducing the reaction capacity of the system. Although the amount of the PAHs in the sediment-water slurry decreased with sonolysis, the bioaccessible fractions of the PAHs were found to increase.

Thirdly, 3 % powdered activated carbon (PAC) was added to provide strong binding sites for the increased bioaccessible fractions of the PAHs to adsorb on. For these three sediments, our sonochemically induced switching of phenanthrene and pyrene from sediment to PAC was more effective than mechanical mixing at 300 rpm in decreasing the fast desorbing fraction ( $F_{fast}$ ) (i.e., % reduction in  $F_{Fast}$ ; ultrasound: EH=  $91 \pm 3 \%$ , GI =  $67 \pm 3 \%$ , and LS =  $67 \pm 3 \%$ , mixing: EH=  $81 \pm 3 \%$ , GI =  $42 \pm 3 \%$ , and LS =  $53 \pm 3 \%$ ). The slow desorbing fraction was also observed to decrease through sonodegradation which was not observed with system treated with mixing. The effect of ultrasound decreased as particle size decreased with increase in treatment time. Decrease in particle size resulted in reduced production of microjets and particle fragmentation which are important in the facilitation of mass transfer of PAHs from the surface of the particles to the aqueous solution.

These results show that sonolysis of PAHs can degrade and desorbed PAHs from three natural sediments that were obtained from different places. The sonolytic desorption of sediments appeared to decrease when particle sizes decreased during sonolysis. Hence

for application on natural sediment, it is important to evaluate the effect of particle size on sonolysis.

## **6.2. Future work**

Sonolysis of particles had been shown to be effective in decreasing the average diameter of particles and Lu et al. showed that the degradation of contaminants following desorption is expected to be highest with smaller particle sizes and particles with larger solid surface areas<sup>23,69</sup> as they provide the most cavitation nuclei to compensate for the detrimental effects of scattering and attenuation of sound waves. It is important to understand the effect of sonolysis on different size fractions of natural sediment for the application of ultrasound.

Eagle Harbor sediment (EH) will be packed through a series of sieves (The W.S. Tyler Company, Cleveland, Ohio) to separate the sediment into five fractions ranging from < 5 mm to >150 mm. These fractions will be sonicated. Changes in mean particle diameters, surface area and surface morphology will be determined by Malvern Mastersizer particle size analyzer, Single point N<sub>2</sub> Brunauer-Emmett-Teller (BET) (Micromeritics® FlowSorb 2300) and Scanning Electron Microscope (SEM), respectively.

Following this, it may be possible to determine the sonolytic degradation rates of these PAHs in the five fractions of natural sediment. The PAHs amounts at selected sonication time can be quantified using an Ethos EX closed microwave extraction system (Milestone, Shelton, CT, USA). We expect the smaller particle size fraction to have the

highest percentage of carbon hence the desorption of PAHs from this fraction for sonolytic degradation would be the slowest compared to the other size fractions.

The effect of sonication on bioaccessibility of PAHs on GI and EH sediments will also be examined and compared to LS sediment. This will provide additional information on the effect of initial particle size has on the release and re-adsorption of PAHs.

## BIBLIOGRAPHY

- (1) Hughes, J. B.; Becklers, D. M.; Chandra, S. D.; Ward, C. H. Utilization of bioremediation processes for the treatment of PAH-contaminated sediments. *Journal of Industrial Microbiology and Biotechnology* **1997**, *18*, 152-160.
- (2) ATSDR "CERCLA Priority List of Hazardous Substances," Center for Disease and Control, 2005.
- (3) Yang, M. H.; Kim, S. Y.; Lee, E.; Cheong, H. K.; Chang, S. S.; Kang, D. H.; Choi, Y. H.; Lee, S. M.; Jang, J. Y. Sources of polycyclic aromatic hydrocarbon exposure in non-occupationally exposed Koreans. *Environmental and Molecular Mutagenesis* **2003**, *42*, 250-257.
- (4) ATSDR "Toxicology profile for polyaromatic hydrocarbons. ATSDR's Toxicological Profiles on CD-ROM," 2005.
- (5) Wang, J. Z.; Guan, Y. F.; Ni, H. G.; Luo, X. L.; Zeng, E. Y. Polycyclic aromatic hydrocarbons in riverine runoff of the pearl river delta (China): Concentrations, fluxes, and fate. *Environmental Science & Technology* **2007**, *41*, 5614-5619.
- (6) Davis, J. A.; Abu-Saba, K.; Gunther, A. J. "Technical Report of the Sources, Pathways, and Loadings Workgroup," San Francisco Estuary Institute, 2001.
- (7) Canada, E. Priority substances list assessment report: polycyclic aromatic hydrocarbons. *Environment Canada* **1994**, *61*.
- (8) Su, M. C.; Christensen, E. R.; Karls, J. F. Determination of PAH sources in dated sediments from Green Bay, Wisconsin, by a chemical mass balance model. *Environmental Pollution* **1998**, *99*, 411-419.

- (9) McVeety, B. D.; Hites, R. A. Atmospheric Deposition of Polycyclic Aromatic-Hydrocarbons to Water Surfaces - a Mass Balance Approach. *Atmospheric Environment* **1988**, 22, 511-536.
- (10) Huntley, S. L.; Bonnevie, N. L.; Wenning, R. J. Polycyclic Aromatic Hydrocarbon and Petroleum Hydrocarbon Contamination in Sediment from the Newark Bay Estuary, New-Jersey. *Archives of Environmental Contamination and Toxicology* **1995**, 28, 93-107.
- (11) Gevao, B.; Jones, K. C. Kinetics and potential significance of polycyclic aromatic hydrocarbon desorption from creosote-treated wood. *Environmental Science & Technology* **1998**, 32, 640-646.
- (12) Bojes, H. K.; Pope, P. G. Characterization of EPA's 16 priority pollutant polycyclic aromatic hydrocarbons (PAHs) in tank bottom solids and associated contaminated soils at oil exploration and production sites in Texas. *Regulatory Toxicology and Pharmacology* **2007**, 47, 288-295.
- (13) Yu, K. S. H.; Wong, A. H. Y.; Yau, K. W. Y.; Wong, Y. S.; Tam, N. F. Y. Natural attenuation, biostimulation and bioaugmentation on biodegradation of polycyclic aromatic hydrocarbons (PAHs) in mangrove sediments. *Marine Pollution Bulletin* **2005**, 51, 1071-1077.
- (14) Urum, K.; Grigson, S.; Pekdemir, T.; McMenamy, S. A comparison of the efficiency of different surfactants for removal of crude oil from contaminated soils. *Chemosphere* **2006**, 62, 1403-1410.
- (15) USEPA "Contaminated Sediment Remediation Guidance for Hazardous Waste Sites," U.S. Environmental Protection Agency, 2005.
- (16) FRTR "Remediation Technologies Screening Matrix and Reference Guide," Federal Remediation technologies Roundtable.
- (17) Ghosh, U.; Gillette, J. S.; Luthy, R. G.; Zare, R. N. Microscale location, characterization, and association of polycyclic aromatic hydrocarbons on harbor sediment particles. *Environmental Science & Technology* **2000**, 34, 1729-1736.



- (18) Millward, R. N.; Bridges, T. S.; Ghosh, U.; Zimmerman, J. R.; Luthy, R. G. Addition of activated carbon to sediments to reduce PCB bioaccumulation by a polychaete (*Neanthes arenaceodentata*) and an amphipod (*Leptocheirus plumulosus*). *Environmental Science & Technology* **2005**, 39, 2880-2887.
- (19) Boopathy, R. Factors limiting bioremediation technologies. *Bioresource Technology* **2000**, 74, 63-67.
- (20) Heitkamp, M. A.; Cerniglia, C. E. Effects of Chemical Structure and exposure on the microbial/degradation of polycyclic aromatic hydrocarbons in fresh water and estuarine ecosystems. *Environmental Toxicology and Chemistry* **1987**, 6, 35.
- (21) Sims, R. C.; Doucette, W. J.; McLean, J. E.; Grenney, W. J.; Dupont, R. R. "Treatment potential for 56 EPA-listed hazardous chemicals in soil," USEPA, 1988.
- (22) Reynaud, S.; Deschaux, P. The effects of polycyclic aromatic hydrocarbons on the immune system of fish: A review. *Aquatic Toxicology* **2006**, 77, 229.
- (23) Lu, Y. F.; Weavers, L. K. Sonochemical desorption and destruction of 4-chlorobiphenyl from synthetic sediments. *Environmental Science & Technology* **2002**, 36, 232-237.
- (24) He, Z. Q.; Traina, S. J.; Bigham, J. M.; Weavers, L. K. Sonolytic desorption of mercury from aluminum oxide. *Environmental Science & Technology* **2005**, 39, 1037-1044.
- (25) Drijvers, D.; van Langenhove, H.; Kim, L. N. T.; Bray, L. Sonolysis of an aqueous mixture of trichloroethylene and chlorobenzene. *Ultrasonics Sonochemistry* **1999**, 6, 115-121.
- (26) Thompson, L. H.; Doraiswamy, L. K. Sonochemistry: Science and engineering. *Industrial & Engineering Chemistry Research* **1999**, 38, 1215-1249.
- (27) Suslick, K. S.; Hammerton, D. A.; Cline, R. E. The Sonochemical Hot-Spot. *Journal of the American Chemical Society* **1986**, 108, 5641-5642.

- (28) Adewuyi, Y. G. Sonochemistry: Environmental science and engineering applications. *Industrial & Engineering Chemistry Research* **2001**, *40*, 4681-4715.
- (29) Iida, Y.; Yasui, K.; Tuziuti, T.; Sivakumar, M. Sonochemistry and its dosimetry. *Microchemical Journal* **2005**, *80*, 159-164.
- (30) Hua, I.; Hoffmann, M. R. Optimization of ultrasonic irradiation as an advanced oxidation technology. *Environmental Science & Technology* **1997**, *31*, 2237-2243.
- (31) Weavers, L. K.; Malmstadt, N.; Hoffmann, M. R. Kinetics and mechanism of pentachlorophenol degradation by sonication, ozonation, and sonolytic ozonation. *Environmental Science & Technology* **2000**, *34*, 1280-1285.
- (32) Colussi, A. J.; Hung, H. M.; Hoffmann, M. R. Sonochemical degradation rates of volatile solutes. *Journal of Physical Chemistry A* **1999**, *103*, 2696-2699.
- (33) Cyr, P. J.; Paraskewich, M. R.; Suri, R. P. S. Sonochemical destruction of trichloroethylene in water. *Water Science and Technology* **1999**, *40*, 131-136.
- (34) DeVisscher, A.; VanEenoo, P.; Drijvers, D.; VanLangenhove, H. Kinetic model for the sonochemical degradation of monocyclic aromatic compounds in aqueous solution. *Journal of Physical Chemistry* **1996**, *100*, 11636-11642.
- (35) Drijvers, D.; DeBaets, R.; DeVisscher, A.; VanLangenhove, H. Sonolysis of trichloroethylene in aqueous solution: Volatile organic intermediates. *Ultrasonics Sonochemistry* **1996**, *3*, S83-S90.
- (36) Drijvers, D.; Van Langenhove, H.; Herrygers, V. Sonolysis of fluoro-, chloro-, bromo- and iodobenzene: a comparative study. *Ultrasonics Sonochemistry* **2000**, *7*, 87-95.
- (37) Goel, M.; Hu, H. Q.; Mujumdar, A. S.; Ray, M. B. Sonochemical decomposition of volatile and non-volatile organic compounds - a comparative study. *Water Research* **2004**, *38*, 4247-4261.

- (38) Henglein, A.; Kormann, C. Scavenging of Oh Radicals Produced in the Sonolysis of Water. *International Journal of Radiation Biology* **1985**, 48, 251-258.
- (39) Drijvers, D.; van Langenhove, H.; Beckers, M. Decomposition of phenol and trichloroethylene by the ultrasound/H<sub>2</sub>O<sub>2</sub>/CuO process. *Water Research* **1999**, 33, 1187-1194.
- (40) Bhatnagar, A.; Cheung, H. M. Sonochemical Destruction of Chlorinated-C1 and Chlorinated-C2 Volatile Organic-Compounds in Dilute Aqueous-Solution. *Environmental Science & Technology* **1994**, 28, 1481-1486.
- (41) Kotronarou, A.; Mills, G.; Hoffmann, M. R. Ultrasonic Irradiation of p-Nitrophenol in Aqueous Solution. *Journal of Physical Chemistry* **1991**, 95, 3630.
- (42) Hoffmann, M. R.; Hua, I.; Hochemer, R. Applications of Ultrasonic Irradiation for the Degradation of Chemical Contaminants in Water. *Ultrasonics Sonochemistry* **1996**, 3, 163.
- (43) Gutierrez, M.; Henglein, A. Sonolytic Decomposition of Poly(vinylpyrrolidone), Ethanol, and Tetranitromethane in Aqueous Solution. *Journal of Physical Chemistry* **1988**, 92, 2978.
- (44) Jiang, Y.; Petrier, C.; Waite, T. D. Kinetics and mechanisms of ultrasonic degradation of volatile chlorinated aromatics in aqueous solutions. *Ultrasonics Sonochemistry* **2002**, 9, 317-323.
- (45) Petrier, C.; Francony, A. Incidence of wave-frequency on the reaction rates during ultrasonic wastewater treatment. *Water Science and Technology* **1997**, 35, 175-180.
- (46) Ayyildiz, O.; Peters, R. W.; Anderson, P. R. Sonolytic degradation of halogenated organic compounds in groundwater: Mass transfer effects. *Ultrasonics Sonochemistry* **2007**, 14, 163-172.
- (47) Lide, D. *CRC Handbook of Chemistry & Physics*; 87th ed.; CRC, 2006.

- (48) Little, C.; Hepher, M. J.; El-Sharif, M. The sono-degradation of phenanthrene in an aqueous environment. *Ultrasonics* **2002**, *40*, 667-674.
- (49) Psillakis, E.; Ntelekos, A.; Mantzavinos, D.; Nikolopoulos, E.; Kalogerakis, N. Solid-phase microextraction to monitor the sonochemical degradation of polycyclic aromatic hydrocarbons in water. *J. Environ. Monit.* **2003**, *5*, 135-140.
- (50) Psillakis, E.; Goula, G.; Kalogerakis, N.; Mantzavinos, D. Degradation of polycyclic aromatic hydrocarbons in aqueous solutions by ultrasonic irradiation. *Journal of Hazardous Materials* **2004**, *108*, 95-102.
- (51) Wheat, P. E.; Tumeo, M. A. Ultrasound induced aqueous poly-cyclic aromatic hydrocarbon reactivity. *Ultrasonics Sonochemistry* **1997**, *4*, 55-59.
- (52) Zhang, G. M.; Hua, I. Cavitation chemistry of polychlorinated biphenyls: Decomposition mechanisms and rates. *Environmental Science & Technology* **2000**, *34*, 1529-1534.
- (53) Katsumata, H.; Kaneco, S.; Suzuki, T.; Ohta, K.; Yobiko, Y. Sonochemical degradation of 2,3,7,8-tetrachlorodibenzo-p-dioxins in aqueous solution with Fe(III)/UV system. *Chemosphere* **2007**, *69*, 1261-1266.
- (54) Kim, D. K.; O'Shea, K. E.; Cooper, W. J. Degradation of MTBE and related gasoline oxygenates in aqueous media by ultrasound irradiation. *Journal of Environmental Engineering-Asce* **2002**, *128*, 806-812.
- (55) Neppolian, B.; Jung, H.; Choi, H.; Lee, J. H.; Kang, J. W. Sonolytic degradation of methyl tert-butyl ether: the role of coupled fenton process and persulphate ion. *Water Research* **2002**, *36*, 4699-4708.
- (56) Petrier, C.; Jiang, Y.; Lamy, M. F. Ultrasound and environment: Sonochemical destruction of chloroaromatic derivatives. *Environmental Science & Technology* **1998**, *32*, 1316-1318.
- (57) Tauber, A.; Schuchmann, H. P.; von Sonntag, C. Sonolysis of aqueous 4-nitrophenol at low and high pH. *Ultrasonics Sonochemistry* **2000**, *7*, 45-52.

(58) Jiang, Y.; Petrier, C.; Waite, T. D. Effect of pH on the ultrasonic degradation of ionic aromatic compounds in aqueous solution. *Ultrasonics Sonochemistry* **2002**, *9*, 163-168.

(59) Wu, Z. L.; Ondruschka, B. Roles of hydrophobicity and volatility of organic substrates on sonolytic kinetics in aqueous solutions. *Journal of Physical Chemistry A* **2005**, *109*, 6521-6526.

(60) Pee, G. Y.; Rathman, J. F.; Weavers, L. K. Effects of surface active properties on the cavitation degradation of surfactant contaminants. *Industrial & Engineering Chemistry Research* **2004**, *43*, 5049-5056.

(61) Fyrrillas, M. M.; Szeri, A. J. Dissolution or Growth of Soluble Spherical Oscillating Bubbles: The Effect of Surfactants. *Journal of Fluid Mechanic* **1995**, *289*, 295-314.

(62) Hamdaoui, O.; Naffrechoux, E. An investigation of the mechanisms of ultrasonically enhanced desorption. *Aiche Journal* **2007**, *53*, 363-373.

(63) Crum, L. A. Cavitation Microjets as a Contributory Mechanism for Renal Calculi Disintegration in Eswl. *Journal of Urology* **1988**, *140*, 1587-1590.

(64) Chen, D.; Weavers, L. K.; Walker, H. W. Ultrasonic control of ceramic membrane fouling by particles: Effect of ultrasonic factors. *Ultrasonics Sonochemistry* **2006**, *13*, 379-387.

(65) Thompson, L. H.; Doraiswamy, L. K. The rate enhancing effect of ultrasound by inducing supersaturation in a solid-liquid system. *Chemical Engineering Science* **2000**, *55*, 3085-3090.

(66) Suslick, K. S. The Chemical Effects of Ultrasound. *Scientific American* **1989**, *260*, 80-86.

(67) Doktycz, S. J.; Suslick, K. S. Interparticle Collisions Driven by Ultrasound. *Science* **1990**, *247*, 1067-1069.

- (68) Leighton, T. G. *The Acoustic Bubble*; Academic Press, London., 1994.
- (69) Lu, Y. F.; Riyanto, N.; Weavers, L. K. Sonolysis of synthetic sediment particles: particle characteristics affecting particle dissolution and size reduction. *Ultrasonics Sonochemistry* **2002**, *9*, 181-188.
- (70) Fan, L.-S. *Bubble Wake Dynamics in Liquids and Liquid-Solid Suspensions*; Butterworth-Heinemann: Stoneman, MA, 1990.
- (71) Booth, J.; Compton, R. G.; Hill, E.; Marken, F.; Rebbitt, T. O. A novel approach for the quantitative kinetic study of reactions at solid/liquid interfaces in the presence of power ultrasound. *Ultrasonics Sonochemistry* **1997**, *4*, 1-7.
- (72) Verdan, S.; Burato, G.; Comet, M.; Reinert, L.; Fuzellier, H. Structural changes of metallic surfaces induced by ultrasound. *Ultrasonics Sonochemistry* **2003**, *10*, 291-295.
- (73) Hagenson, L. C.; Doraiswamy, L. K. Comparison of the effects of ultrasound and mechanical agitation on a reacting solid-liquid system. *Chemical Engineering Science* **1998**, *53*, 131-148.
- (74) Newman, A. P.; Lorimer, J. P.; Mason, T. J.; Hutt, K. R. An investigation into the ultrasonic treatment of polluted solids. *Ultrasonics Sonochemistry* **1997**, *4*, 153-156.
- (75) Meegoda, J. N.; Perera, R. Ultrasound to decontaminate heavy metals in dredged sediments. *Journal of Hazardous Materials* **2001**, *85*, 73-89.
- (76) He, Z. Q.; Traina, S. J.; Weavers, L. K. Sonolytic desorption of mercury from aluminum oxide: Effects of pH, chloride, and organic matter. *Environmental Science & Technology* **2007**, *41*, 779-784.
- (77) Meegoda, J. N.; Veerawat, K. Ultrasound to decontaminate organics in dredged sediments. *Soil & Sediment Contamination* **2002**, *11*, 91-116.

(78) Feng, D.; Aldrich, C. Sonochemical treatment of simulated soil contaminated with diesel. *Advances in Environmental Research* **2000**, *4*, 103-112.

(79) Koparal, S.; Nii, S.; Kawaizumi, F.; Takahashi, K. Use of ultrasound for tar removal from tar-contaminated sand. *Journal of Chemical Engineering of Japan* **2005**, *38*, 835-840.

(80) Collings, A. F.; Farmer, A. D.; Gwan, P. B.; Pintos, A. P. S.; Leo, C. J. Processing contaminated soils and sediments by high power ultrasound. *Minerals Engineering* **2006**, *19*, 450-453.

(81) Hamdaoui, O.; Naffrechoux, E.; Suptil, J.; Fachinger, C. Ultrasonic desorption of p-chlorophenol from granular activated carbon. *Chemical Engineering Journal* **2005**, *106*, 153-161.

(82) Cornelissen, G.; Breedveld, G. D.; Naes, K.; Oen, A. M. P.; Ruus, A. Bioaccumulation of Native Polycyclic Aromatic Hydrocarbons from Sediment by a Polychaete and a Gastropod: Freely Dissolved Concentrations and Activated Carbon Amendment. *Environmental Toxicology and Chemistry* **2006**, *25*, 2349-2355.

(83) Ghosh, U. "Rational Selection of Tailored Amendment Mixtures and Composites for In Situ Remediation of Contaminated Sediments," Strategic Environmental Research and Development Program, 2006.

(84) McLeod, P. B.; Van den Heuvel-Greve, M. J.; Luoma, S. N.; Luthy, R. G. Biological uptake of polychlorinated biphenyls by *Macoma balthica* from sediment amended with activated carbon. *Environmental Toxicology and Chemistry* **2007**, *26*, 980-987.

(85) Werner, D.; Higgins, C. P.; Luthy, R. G. The sequestration of PCBs in Lake Hartwell sediment with activated carbon. *Water Research* **2005**, *39*, 2105-2113.

(86) Zimmerman, J. R.; Werner, D.; Ghosh, U.; Millward, R. N.; Bridges, T. S.; Luthy, R. G. Effects of dose and particle size on activated carbon treatment to sequester polychlorinated biphenyls and polycyclic aromatic hydrocarbons in marine sediments. *Environmental Toxicology and Chemistry* **2005**, *24*, 1594-1601.

(87) Hwang, S.; Cutright, T. J. Biodegradability of aged pyrene and phenanthrene in a natural soil. *Chemosphere* **2002**, *47*, 891-899.

(88) Apitz, S. E.; Arias, E.; Clawson, S. A.; Lin, E. W.; Melcher, R. J.; Hemmingsen, B. B. The development of a sterile, PAH-spiked, aged marine sediment for biodegradation experiments: chemical results. *Organic Geochemistry* **1999**, *30*, 891-900.

(89) Hatzinger, P. B.; Alexander, M. Effect of Aging of Chemicals in Soil on Their Biodegradability and Extractability. *Environmental Science & Technology* **1995**, *29*, 537-545.

(90) Tang, J. X.; Carroquino, M. J.; Robertson, B. K.; Alexander, M. Combined effect of sequestration and bioremediation in reducing the bioavailability of polycyclic aromatic hydrocarbons in soil. *Environmental Science & Technology* **1998**, *32*, 3586-3590.

(91) Baldock, J. A.; Masiello, C. A.; Gelinas, Y.; Hedges, J. I. Cycling and composition of organic matter in terrestrial and marine ecosystems. *Marine Chemistry* **2004**, *92*, 39-64.

(92) Xing, B. S.; Pignatello, J. J. Dual-mode sorption of low-polarity compounds in glassy poly(vinyl chloride) and soil organic matter. *Environmental Science & Technology* **1997**, *31*, 792-799.

(93) Xing, B. S.; Pignatello, J. J.; Gigliotti, B. Competitive sorption between atrazine and other organic compounds in soils and model sorbents. *Environmental Science & Technology* **1996**, *30*, 2432-2440.

(94) Pignatello, J. J.; Xing, B. S. Mechanisms of slow sorption of organic chemicals to natural particles. *Environmental Science & Technology* **1996**, *30*, 1-11.

(95) Braida, W. J.; White, J. C.; Pignatello, J. J. Indices for bioavailability and biotransformation potential of contaminants in soils. *Environmental Toxicology and Chemistry* **2004**, *23*, 1585-1591.

(96) Xing, B. S.; Pignatello, J. J. Time-Dependent Isotherm Shape of Organic Compounds in Soil Organic Matter: Implications For Sorption Mechanism. *Environmental Toxicology and Chemistry* **1996**, *15*, 1282-1288.



- (97) Cornelissen, G.; vanNoort, P. C. M.; Govers, H. A. J. Desorption kinetics of chlorobenzenes, polycyclic aromatic hydrocarbons, and polychlorinated biphenyls: Sediment extraction with Tenax(R) and effects of contact time and solute hydrophobicity. *Environmental Toxicology and Chemistry* **1997**, *16*, 1351-1357.
- (98) Chen, W.; Cong, L.; Hu, H. L.; Zhang, P.; Li, J.; Feng, Z. Z.; Kan, A. T.; Tomson, M. B. Release of adsorbed polycyclic aromatic hydrocarbons under cosolvent treatment: Implications for availability and fate. *Environmental Toxicology and Chemistry* **2008**, *27*, 112-118.
- (99) Calderbank, A. The Occurrence and Significance of Bound Pesticide-Residues in Soil. *Reviews of Environmental Contamination and Toxicology* **1989**, *108*, 71-103.
- (100) Huang, W.; Young, T. M.; Schlautman, M. A.; Hong, Y.; Weber, W. J. A Distributed Reactivity Model for Sorption by Soils and Sediments: General Isotherm Nonlinearity and Applicability of the Dual Reactive Domain Model. *Environmental Science & Technology* **1997**, *31*, 1703-1710.
- (101) Cornelissen, G.; Gustafsson, O.; Bugeli, T. D.; Jonker, M. T. O.; Koelmans, A. A.; Van Noort, P. C. M. Extensive Sorption of Organic Compounds to Black Carbon, Coal, and Kerogen in Sediments and Soils: Mechanisms and Consequences for Distribution, Bioaccumulation, and Biodegradation. *Environmental Science & Technology* **2005**, *39*, 6881-6895.
- (102) Cornelissen, G.; Rigterink, H.; ten Hulscher, D. E. M.; Vrind, B. A.; van Noort, P. C. M. A simple Tenax (R) extraction method to determine the availability of sediment-sorbed organic compounds. *Environmental Toxicology and Chemistry* **2001**, *20*, 706-711.
- (103) Cornelissen, G.; Rigterink, H.; Ferdinandy, M. M. A.; Van Noort, P. C. M. Rapidly desorbing fractions of PAHs in contaminated sediments as a predictor of the extent of bioremediation. *Environmental Science & Technology* **1998**, *32*, 966-970.
- (104) You, J.; Landrum, P. F.; Lydy, M. J. Comparison of chemical approaches for assessing bioavailability of sediment-associated contaminants. *Environmental Science & Technology* **2006**, *40*, 6348-6353.

- (105) Semple, K. T.; Doick, K. J.; Burauel, P.; Craven, A.; Harms, H.; Jones, K. C. Defining bioavailability and bioaccessibility of contaminated soil and sediment is complicated. *Environmental Science & Technology* **2004**, *38*, 228A-231A.
- (106) Cornelissen, G.; Van Noort, P. C. M.; Parsons, J. R.; Govers, H. A. J. The temperature dependence of slow adsorption and desorption kinetics of organic compounds in sediments. *Environmental Science & Technology* **1997**, *31*, 454.
- (107) Luthy, R. D.; Aiken, G. R.; Brusseau, M. L.; Cunningham, D. S.; Gschwend, P. M.; Pignatello, J. J.; Reinert, M.; Traina, S. J.; Weber, W. J.; Westall, J. C. Sequestration of Hydrophobic Organic Contaminants by Geosorbents. *Environmental Science & Technology* **1997**, *31*, 3341.
- (108) White, J. C.; Alexander, M.; Pignatello, J. J. Enhancing the Bioavailability of Organic Compounds Sequestered in Soil and Aquifer Solids. *Environmental Toxicology and Chemistry* **1999**, *18*, 182-187.
- (109) Ghosh, U.; Talley, J. W.; Luthy, R. G. Particle-scale investigation of PAH desorption kinetics and thermodynamics from sediment. *Environmental Science & Technology* **2001**, *35*, 3468-3475.
- (110) Talley, J. W.; Ghosh, U.; Tucker, S. G.; Furey, J. S.; Luthy, R. G. Particle-scale understanding of the bioavailability of PAHs in sediment. *Environmental Science & Technology* **2002**, *36*, 477-483.
- (111) Landrum, P. F.; Eadie, B. J.; Faust, W. R. Variation in the bioavailability of polycyclic aromatic hydrocarbons to the amphipod *Diporeia* spp. with sediment aging. *Environmental Toxicology and Chemistry* **1992**, *11*, 1197-1208.
- (112) Kukkonen, J. V. K.; Landrum, P. F. Effect of particle-xenobiotic contact time on bioavailability of sediment-associated benzo(a)pyrene to benthic amphipod, *Diporeia* spp. *Aquatic Toxicology* **1998**, *42*, 229-242.
- (113) Leppanen, M. T.; Kukkonen, J. V. K. Effect of sediment-chemical contact time on availability of sediment-associated pyrene and benzo[a]pyrene to oligochaete worms and semi-permeable membrane devices. *Aquatic Toxicology* **2000**, *49*, 227-241.

(114) Reid, B. J.; Jones, K. C.; Semple, K. T. Bioavailability of persistent organic pollutants in soils and sediments—a perspective on mechanisms, consequences and assessment. *Environmental Pollution* **2000**, *108*, 103-112.

(115) Wu, S.; Gschwend, P. M. Sorption kinetics of hydrophobic compounds to natural sediments and soils. *Environmental Science & Technology* **1986**, *20*, 717-725.

(116) Sander, M.; Pignatello, J. J. On the Reversibility of Sorption to Black Carbon: Distinguishing True Hysteresis from Artificial Hysteresis Caused by Dilution of a Competing Adsorbate. *Environmental Science & Technology* **2007**, *41*, 843-849.

(117) Semple, K. T.; Doick, K. J.; Wick, L. Y.; Harms, H. Microbial interactions with organic contaminants in soil: Definitions, processes and measurement. *Environmental Pollution* **2007**, *150*, 166-176.

(118) Reid, B. J.; Stokes, J. D.; Jones, K. C.; Semple, K. T. A non-exhaustive cyclodextrin based extraction technique for the evaluation of PAH bioavailability. *Environmental Science & Technology* **2000**, *34*, 3174-3179.

(119) Kelsey, J. W.; Kottler, B. D.; Alexander, M. Selective chemical extractants to predict bioavailability of soil-aged organic chemicals. *Environmental Science & Technology* **1997**, *31*, 214-217.

(120) Kilbane, J. J. Extractability and subsequent biodegradation of PAHs from contaminated soil. *Water Air and Soil Pollution* **1998**, *104*, 285-304.

(121) Greenberg, M. S.; Burton, G. A.; Landrum, P. F.; Leppanen, M. T.; Kukkonen, J. V. K. Desorption kinetics of fluoranthene and trifluralin from Lake Huron and Lake Erie, USA, sediments. *Environmental Toxicology and Chemistry* **2005**, *24*, 31-39.

(122) You, I.; Pehkonen, S.; Landrum, P. F.; Lydy, M. J. Desorption of hydrophobic compounds from laboratory-spiked Sediments measured by tenax absorbent and matrix solid-phase microextraction. *Environmental Science & Technology* **2007**, *41*, 5672-5678.

(123) Weavers, L. K. *Advances in Sonochemistry*; Elsevier Science: Amsterdam, 2001; Vol. 6.

(124) Seymour, J. D.; Gupta, R. B. Oxidation of aqueous pollutants using ultrasound: Salt-induced enhancement. *Industrial & Engineering Chemistry Research* **1997**, *36*, 3453-3457.

(125) Weavers, L. K.; Ling, F. H.; Hoffmann, M. R. Aromatic compound degradation in water using a combination of sonolysis and ozonolysis. *Environmental Science & Technology* **1998**, *32*, 2727-2733.

(126) Algeria, A.; Lion, Y.; Kondo, T.; Riesz, P. Sonolysis of Aqueous Surfactant Solutions. Probing the Interfacial Region of Cavitation Bubbles by Spin Trapping. *Journal of Physical Chemistry* **1989**, *93*, 4908-4913.

(127) Laughrey, Z.; Bear, E.; Jones, R.; Tarr, M. A. Aqueous sonolytic decomposition of polycyclic aromatic hydrocarbons in the presence of additional dissolved species. *Ultrasonics Sonochemistry* **2001**, *8*, 353-357.

(128) Taylor, E.; Cook, B. B.; Tarr, M. A. Dissolved organic matter inhibition of sonochemical degradation of aqueous polycyclic aromatic hydrocarbons. *Ultrasonics Sonochemistry* **1999**, *6*, 175-183.

(129) Park, J. K.; Hong, S. W.; Chang, W. S. Degradation of polycyclic aromatic hydrocarbons by ultrasonic irradiation. *Environmental Technology* **2000**, *21*, 1317-1323.

(130) Mason, T. J.; Lorimer, J. P.; Bates, D. M.; Zhao, Y. Dosimetry in Sonochemistry - the Use of Aqueous Terephthalate Ion as a Fluorescence Monitor. *Ultrasonics Sonochemistry* **1994**, *1*, S91-S95.

(131) Mishin, V. A.; Thomas, P. E. Characterization of hydroxyl radical formation by microsomal enzymes using a water-soluble trap, terephthalate. *Biochemical Pharmacology* **2004**, *68*, 747-752.

(132) Tang, B.; Zhang, L.; Geng, Y. Determination of the antioxidant capacity of different food natural products with a new developed flow injection spectrofluorimetry detecting hydroxyl radicals. *Talanta* **2005**, *65*, 769-775.

(133) Millington, K. R.; Kirschenbaum, L. J. Detection of hydroxyl radicals in photoirradiated wool, cotton, nylon and polyester fabrics using a fluorescent probe. *Coloration Technology* **2002**, *118*, 6-14.

(134) Lindsey, M. E.; Tarr, M. A. Inhibition of hydroxyl radical reaction with aromatics by dissolved natural organic matter. *Environmental Science & Technology* **2000**, *34*, 444-449.

(135) Lindsey, M. E.; Tarr, M. A. Inhibited hydroxyl radical degradation of aromatic hydrocarbons in the presence of dissolved fulvic acid. *Water Research* **2000**, *34*, 2385-2389.

(136) Buxton, G. V.; Greenstock, C. L.; Helman, W. P.; Ross, A. B. Critical-Review of Rate Constants for Reactions of Hydrated Electrons, Hydrogen-Atoms and Hydroxyl Radicals ( $\cdot\text{OH}/\cdot\text{O}$ -) in Aqueous-Solution. *Journal of Physical and Chemical Reference Data* **1988**, *17*, 513-886.

(137) Humphry-Baker, R.; Gratzel, M.; Moroi, Y. Pyrene fluorescence at air/sodium dodecyl sulfate solution interface. *Langmuir* **2006**, *22*, 11205-11207.

(138) Valsaraj, K. T. Adsorption of polycyclic aromatic hydrocarbons at the air-water interface and its role in atmospheric deposition by fog droplets. *Environmental Toxicology and Chemistry* **2004**, *23*, 2318-2323.

(139) Chang, C. H.; Franses, E. I. Adsorption Dynamics of Surfactants at the Air/Water Interface - a Critical-Review of Mathematical-Models, Data, and Mechanisms. *Colloids and Surfaces a-Physicochemical and Engineering Aspects* **1995**, *100*, 1-45.

(140) Weston, D. P.; Millward, R. N.; Mayer, L. M.; Lotufo, G. "Sediment Extraction Using Deposit-Feeder Gut Fluids: A Potential Rapid Tool for Assessing Bioaccumulation Potential of Sediment-Associated Contaminants," US Army Corps of Engineers, 2002.

(141) Prabhu, A. V.; Gogate, P. R.; Pandit, A. B. Optimization of multiple-frequency sonochemical reactors. *Chemical Engineering Science* **2004**, *59*, 4991-4998.

(142) Adewuyi, Y. G.; Appaw, C. Sonochemical oxidation of carbon disulfide in aqueous solutions: Reaction kinetics and pathways. *Industrial & Engineering Chemistry Research* **2002**, *41*, 4957-4964.

(143) Sehgal, C. M.; Wang, S. Y. Threshold Intensities and Kinetics of Sonoreaction of Thymine in Aqueous-Solutions at Low Ultrasonic Intensities. *Journal of the American Chemical Society* **1981**, *103*, 6606-6611.

(144) Entezari, M. H.; Kruus, P. Effect of frequency on sonochemical reactions .2. Temperature and intensity effects. *Ultrasonics Sonochemistry* **1996**, *3*, 19-24.

(145) Petrier, C.; Lamy, M. F.; Francony, A.; Benahcene, A.; David, B.; Renaudin, V.; Gondrexon, N. Sonochemical Degradation of Phenol in Dilute Aqueous-Solutions - Comparison of the Reaction-Rates at 20-Khz and 487-Khz. *Journal of Physical Chemistry* **1994**, *98*, 10514-10520.

(146) Kidak, R.; Ince, N. H. Effects of operating parameters on sonochemical decomposition of phenol. *Journal of Hazardous Materials* **2006**, *137*, 1453-1457.

(147) Jiang, Y.; Petrier, C.; Waite, T. D. Sonolysis of 4-chlorophenol in aqueous solution: Effects of substrate concentration, aqueous temperature and ultrasonic frequency. *Ultrasonics Sonochemistry* **2006**, *13*, 415-422.

(148) Serpone, N.; Terzian, R.; Hidaka, H.; Pelizzetti, E. Ultrasonic Induced Dehalogenation and Oxidation of 2-Chlorophenol, 3-Chlorophenol, and 4-Chlorophenol in Air-Equilibrated Aqueous-Media - Similarities with Irradiated Semiconductor Particulates. *Journal of Physical Chemistry* **1994**, *98*, 2634-2640.

(149) Perry, R. H.; Green, D. W.; Maloney, J. *Perry's chemical engineers' handbook*; McGraw-Hill: New York., 1997.

(150) Kotronarou, A.; Mills, G.; Hoffmann, M. R. Decomposition of Parathion in Aqueous-Solution by Ultrasonic Irradiation. *Environmental Science & Technology* **1992**, 26, 1460-1462.

(151) Amiri, F.; Bornick, H.; Worch, E. Sorption of phenols onto sandy aquifer material: the effect of dissolved organic matter (DOM). *Water Research* **2005**, 39, 933-941.

(152) Elik, A. Ultrasonic-assisted leaching of trace metals from sediments as a function of pH. *Talanta* **2007**, 71, 790-794.

(153) Vaisanen, A.; Kiljunen, A. Ultrasound-assisted sequential extraction method for the evaluation of mobility of toxic elements in contaminated soils. *International Journal of Environmental Analytical Chemistry* **2005**, 85, 1037-1049.

(154) Li, Z.; Xu, K. F.; Li, X. B.; Xi, H. X.; Hua, B.; Li, F. S. Effect of ultrasound on desorption kinetics of phenol from polymeric resin. *Ultrasonics Sonochemistry* **2006**, 13, 225-231.

(155) Bartolome, L.; Cortazar, E.; Raposo, J. C.; Usobiaga, A.; Zuloaga, O.; Etxebarria, N.; Fernandez, L. A. Simultaneous microwave-assisted extraction of polycyclic aromatic hydrocarbons, polychlorinated biphenyls, phthalate esters and nonylphenols in sediments. *Journal of Chromatography A* **2005**, 1068, 229-236.

(156) Vessigaud, S.; Perrin-Ganier, C.; Belkessam, L.; Denys, S.; Schiavon, M. Direct link between fluoranthene biodegradation and the mobility and sequestration of its residues during aging. *Journal of Environmental Quality* **2007**, 36, 1412-1419.

(157) Pignatello, J. J. Soil organic matter as a nanoporous sorbent of organic pollutants. *Advances in Colloid Interface Science* **1998**, 76-77, 445-467.

(158) Abelman, K.; Kleinedam, S.; Knicker, H.; Grathwohl, P.; Kogel-Knabner, I. Sorption of HOC in soils with carbonaceous contamination: Influence of organic-matter composition. *Journal of Plant Nutrition and Soil Science-Zeitschrift Fur Pflanzenernahrung Und Bodenkunde* **2005**, 168, 293-306.

(159) Gaultier, J.; Farenhorst, A.; Cathcart, J.; Goddar, T. Degradation of carboxyl-C-14 2,4-D and ring-U-C-14 2,4-D in 114 agricultural soils as affected by soil organic carbon content. *Soil Biology & Biochemistry* **2008**, *40*, 217-227.

(160) Ditoro, D. M.; Zarba, C. S.; Hansen, D. J.; Berry, W. J.; Swartz, R. C.; Cowan, C. E.; Pavlou, S. P.; Allen, H. E.; Thomas, N. A.; Paquin, P. R. Technical Basis for Establishing Sediment Quality Criteria for Nonionic Organic-Chemicals Using Equilibrium Partitioning. *Environmental Toxicology and Chemistry* **1991**, *10*, 1541-1583.

(161) Thorsen, W. A.; Cope, W. G.; Shea, D. Bioavailability of PAHs: Effects of soot carbon and PAH source. *Environmental Science & Technology* **2004**, *38*, 2029-2037.

(162) Qiu, X.; Davis, J. W. Environmental bioavailability of hydrophobic organochlorines in sediment A review. *Remediation Journal* **2004**, *14*, 55-84.

(163) Parrish, Z. D.; Banks, K. M.; Schwab, A. P. Assessment of contaminant lability during phytoremediation of polycyclic aromatic hydrocarbon impacted soil. *Environmental Pollution* **2005**, *137*, 187-197.

(164) Cornelissen, G.; Gustafsson, O. Effects of added PAHs and precipitated humic acid coatings on phenanthrene sorption to environmental Black carbon. *Environmental Pollution* **2006**, *141*, 526-531.

(165) USEPA *Test Methods for Evaluating Solid Wastes. Methods 9060A: Total Organic Carbon*; 3rd ed.

(166) International Standard *Soil quality – Determination of organic and total carbon after dry combustion (elementary analysis)*. Geneva, 1995.

(167) Reichenberg, F.; Mayer, P. Two complementary sides of bioavailability: Accessibility and chemical activity of organic contaminants in sediments and soils. *Environmental Toxicology and Chemistry* **2006**, *25*, 1239-1245.

(168) Macrae, J. D.; Hall, K. J. Comparison of methods used to determine the availability of polycyclic aromatic hydrocarbons in marine sediment. *Environmental Science & Technology* **1998**, *32*, 3809-3815.



(169) Tsai, W. T. Environmental risk assessment of hydrofluoropolyethers (HFPEs). *Journal of Hazardous Materials* **2007**, *139*, 185-192.

(170) Streets, S. S.; Henderson, S. A.; Stoner, A. D.; Carlson, D. L.; Simcik, M. F.; Swackhamer, D. L. Partitioning and bioaccumulation of PBDEs and PCBs in Lake Michigan. *Environmental Science & Technology* **2006**, *40*, 7263-7269.

(171) Suslick, K. S.; Casadonte, D. J. Heterogeneous Sonocatalysis with Nickel Powder. *Journal of the American Chemical Society* **1987**, *109*, 3459-3461.

(172) Cornelissen, G.; Kukulska, Z.; Kalaitzidis, S.; Christanis, K.; Gustafsson, O. Relations between Environmental Black Carbon Sorption and Geochemical Sorbent Characteristics. *Environmental Science & Technology* **2004**, *38*, 3632.